SPIN ANGULAR MOMENTUM TRANSFER IN MAGNETIC NANOSTRUCTURE

A Dissertation

presented to

the Faculty of the Graduate School

University of Missouri-Columbia

In Partial Fulfillment

of the Requirements for the Degree

of Doctor of Philosophy

---

by

Yang, Zhaoyang

Dr. Zhang, Shufeng, Dissertation Supervisor

DECEMBER 2007

The undersigned, appointed by the Dean of the Graduate School, have examined the dissertation entitled:

SPIN ANGULAR MOMENTUM TRANSFER IN MAGNETIC NANOSTRUCTURE

presented by Yang, Zhaoyang

a candidate for the degree of Doctor of Philosophy

and hereby certify that in their opinion it is worthy of acceptance.

Dr. Zhang, Shufeng

Dr. Li, Y. Charles

Dr. Satpathy, Sashi

Dr. Ullrich, Carsten

Dr. Vignale, Giovanni

To Beibei

ACKNOWLEDGMENTS

Many have made contributions to this dissertation. I especially want to express my appreciation to my advisor, Dr. Shufeng Zhang, for his guidance, support and insightful suggestions. He taught me not only the methods to do research in physics, but also the skills to deal with any problems. The experience of working with him will be beneficial to my entire life. I owe a great deal to him.

I would like to thank Dr. Charles Li, from Department of Mathematics. In the past two years, I have learned a lot from him. He introduced a variety of mathematic concepts to me, which are extremely important to this dissertation.

I would also like to express my gratitude to Dr. Giovanni Vignale, Dr. Sashi Satpathy and Dr. Carsten Ullrich. Thanks for their helpful discussions and suggestions.

It is a great pleasure to work as a group with Dr. Yunong Qi, Dr. Zhanjie Li and Mr. Jiexuan He. My entire doctoral experience was enhanced through my friendship with them.

There is a special person who deserves my special thanks. She is my wife, Beibei Dong, who is a Ph.D. candidate in Department of Marketing at the University of Missouri-Columbia. My deepest gratitude to her for her support, encouragement and love.

Last but not least, I would like to thank my father, Changming Yang and my mother, Jinzhi Xia who brought me to this world and provided support throughout my life. I will always be in their debt.

Contents

ACKNOWLEDGEMENTS **ii**

LIST OF TABLES **vii**

LIST OF FIGURES **viii**

ABSTRACT **xiii**

CHAPTER

1 Introduction **1**

1.1 Spin Angular Momentum Transfer 1

1.2 Historical Development and Prior Work 5

1.3 Spin Transfer in Spin-Valve and MTJ 7

1.4 Spin Transfer Oscillator 9

1.5 Outline of Dissertation 10

Bibliography 12

2 Spin and Energy Transfer in Magnetic Tunnel Junctions **16**

2.1 Introduction 16

2.2 The Model of Spin Dependent Tunneling Current 17

2.3 Spin Dependent Inelastic Scattering 20

2.4 Energy Transfer Through Magnon 23
2.5 Effective Temperature 24
2.6 Energy Effect on Magnetization Switching 26
Bibliography 29

3 Magnetization Oscillations in Spin Valves 31
3.1 Experiments 31
3.2 Model 33
3.2.1 Spin Valve 33
3.2.2 Landau-Lifshitz-Gilbert Equation 35
3.3 Neutral Precessional Motions 37
3.3.1 Energy Conservation 37
3.3.2 Analytical Solution 38
3.4 Stable Precessional Motions 44
3.4.1 Limit Cycles 44
3.4.2 Transition to Limit Cycles 45
3.4.3 Determining a Limit Cycle 49
Bibliography 53

4 Synchronization in Spin Transfer Oscillators 55
4.1 Introduction 55
4.1.1 Synchronization 55
4.1.2 Synchronization in Spin Valves 56
4.2 Numerical Simulations 57
4.3 Melnikov Integral Method 64
4.3.1 Synchronization to Fundamental Frequency 64
4.3.2 Synchronization to Subharmonic Frequency 69

Bibliography 74

5 Chaos in Spin Transfer Oscillators **75**

5.1 Motivation 75

5.2 Nonlinear Equation of Motion 76

5.3 Existence of Chaos 76

5.3.1 Numerical Evidence 77

5.3.2 Melnikov Integral 80

5.3.3 Lyapunov Exponents 82

5.4 Route to Chaos 85

5.4.1 Poincaré Map 85

5.4.2 Periodic Doubling Bifurcation 87

5.4.3 Bifurcation Cascade 91

5.4.4 Feigenbaum Numbers 92

5.4.5 Chaos windows and Sharkovskii Ordering 93

5.5 Power Spectra of Chaos 93

5.6 Fluctuation 94

Bibliography 97

6 Effect of Finite Temperature **99**

6.1 Stochastic Process in Magnetization Dynamics 99

6.2 Stochastic Process of Energy 100

6.3 Fokker-Planck-Equation 102

6.4 Thermal Noise in Spin Transfer Oscillators 103

6.5 Thermal Effect on Chaos 105

Bibliography 108

7 Summary **109**

A Spin Hall Effect **112**

A.1 Intrinsic Spin Hall Effect 112

A.2 Extrinsic SHE in Rashba bands 122

Bibliography 127

VITA **129**

List of Tables

Table **page**

5.1 Feigenbaum ratio measurement. The second column is derived from Fig. 5.10; a_i is a critical value at the ith bifurcation point. 92

List of Figures

Figure **page**

1.1 A trilayer structure constituting of two ferromagnetic layers separated by a non-magnetic layer. Polarized electron passing through the ferromagnetic layer, its polarization follows the magnetization orientation. Meanwhile, a spin transfer torque exerted on the magnetization is induced by the change of spin current, which ensures the conservation of angular momentum. 3

2.1 The energy model for a MTJ. The tunneling electrons have energy higher than Fermi level of the righ electrode. They experience spin dependent inelastic scatterings due to electron-magnon interaction. Spin down electrons are scattered to lower energy level flipping to spin up and emitting magnons $\hbar\omega_q$. 18

2.2 Temperature dependence of critical current. Solid and dash lines represent the critical switching current from P to AP and from P to AP. We use $t = 0.1s$, $f_0 = 1GHz$ and assume $T_0^* = 150K$, $E_0 = 0.7eV$, $H = 0Oe$. 28

3.1 Spin Valve Model. Two ferromagnetic layers are separated by a non-magnetic layer. One of the ferromagnetic layer (fixed layer) is attached by an anti-ferromagnetic layer that fixes the orientation of the magnetization of the ferromagnetic layer through strong exchange coupling. The magnetization orientation of the other ferromagnetic layer (free layer) is free to change. 34

3.2 Neutral Orbits in $m_x - m_y$ plane. To illustrate the differences between different types of orbits, we choose an effective field $H_{eff} = 2000(Oe)$ and $4\pi M_s = 8400(Oe)$. 39

3.3 Energy Sphere. The dashed trajectory represents the separatrix which separates OOP and IP neutral orbits. 41

3.4 In-Plane Limit Cycle 46

3.5 Out-of-Plane Limit Cycle 47

3.6 Magnetization is originally located at a fixed direction where the magnetic energy is at minimum. When Increasing the dc current, stable precessional orbit is excited. This is a Hopf Bifurcation procedure. For $H_{ext} = 200\ Oe$ and $\alpha = 0.02$, Hopf Bifurcation takes place when dc current increases to around 80 Oe. 48

4.1 Synchronization Region. The topper panel shows that varying dc current, the frequency of the oscillation is locked in the synchronization region. The lower panel shows that within synchronization region, the frequency of oscillation is identical to the frequency of the ac current. Here, detune frequency is defined as the frequency difference between ac current and natural frequency; beating frequency is defined as the frequency difference between ac current and the oscillator. The parameters are: $H_{ext} = 200(Oe)$; $a_{ac} = 20(Oe)$; topper panel: $\omega_{ac} = 30GHz$; lower panel: $a_{dc} = 400(Oe)$ 59

4.2 Power spectra before and after synchronization. Natural frequency is 30GHz. After applying an ac current with amplitude 30 Oe and frequency 33GHz, the frequency peak of the spin transfer oscillator is shift to 33GHz, identical to that of ac current. 60

4.3 Phase Locking. Turning on ac current with an arbitrary phase difference between ac current and the magnetization, they will be eventually locked in their phase. 61

4.4 With the increase of the amplitude of ac current, the synchronization region will be wider. The region width is proportional to the amplitude of the ac current. 62

4.5 Driven by ac current, the spin valve oscillator can synchronized to different fractions of the frequency of the ac current 63

4.6 Synchronization in In-plan orbits. Vertical lines are predicted by Melnikov Integral. $H_{eff} = 200\ Oe$; other parameters are shown in the diagram. 68

4.7 Numerical simulations of synchronization bands. We encode the ratio of response frequency to driven frequency into different color and the lines are contour lines. In each band, $m\Omega_{STO} = n\omega_{ac}$ where m and n are integers. 70

4.8 Synchronization Bands predicted by Melnikov Integral method. Within each band, the frequencies of spin transfer oscillators are synchronized to ω, $\omega/2$ and $\omega/3$ 72

5.1 Chaos driven by large ac spin transfer torque. (a) 3D trajectory; (b) Power Spectrum of m_z; (c) Trajectory of m_x in time domain; (d) Trajectory of m_z in time domain; (e) Trajectory of m_y-m_z plane. 78

5.2 Chaos driven by small ac spin transfer torque. (a) 3D trajectory; (b) Power Spectrum of m_z; (c) Trajectory of m_x in time domain; (d) Trajectory of m_z in time domain; (e) Trajectory of m_y-m_z plane. 79

5.3 Magnetization dynamic phase diagram driven by dc and ac currents. The external field is fixed at 200 Oe and the amplitude of the ac current $a_{ac} = 20$ Oe. Three phases are: synchronization (S), modification (M) and chaos (C). The dotted line is the frequency of the limit cycle in the absence of the ac current. The analytical results from the Melnikov criterion of chaos are shown in the two nearly vertical dashed lines. Fig. 1 in [18]. Used under authors' permission. 83

5.4 Lyapunov Spectrum of the spin valve oscillator. External field is 200(Oe), ac current amplitude is 20(Oe), ac current frequency is 15GHz 84

5.5 Chaotic dynamics phase of the spin valve oscillator indicated by dark points. ac current amplitude is 20(Oe), ac current frequency is 15GHz 85

5.6 Illustration of Poincaré Map. 86

5.7 Limit Cycle (left) and Period Two Orbit (right). ac current amplitude is 20 Oe, ac current frequency is 15 GHz and external field is 200 Oe. dc currents are shown in the diagrams. 88
5.8 Period Four Orbit. ac current amplitude is 20 Oe, ac current frequency is 15 GHz and external field is 200 Oe. dc current is shown in the diagram. 89
5.9 Period Eight Orbit. ac current amplitude is 20 Oe, ac current frequency is 15 GHz and external field is 200 Oe. dc current is shown in the diagram. 90
5.10 Period Doubling Bifurcation 91
5.11 Synchronization-like chaos. Chaos that involves only one branch of orbits 95
5.12 Chaos that involves two branches of orbits 96

SPIN ANGULAR MOMENTUM TRANSFER IN MAGNETIC NANOSTRUCTURE

Zhaoyang Yang

Dr. Shufeng Zhang, Dissertation Supervisor

ABSTRACT

Spin angular momentum transfer, or spin transfer, is a short notion of the transfer of spin angular momentum between the spin polarized current and the magnetization of ferromagnetic condensates. Spin transfer effect in ferromagnetic nanostructures, such as Magnetic Tunnel Junctions (MTJ) and Spin Valves, is studied in this dissertation. Spin current generates spin transfer torque in ferromagnets, which can induce magnetization reversal, spin wave emission, as well as self-sustained magnetization precession in the presence of magnetic field.

The magnetization oscillation in spin valves is referred as the spin transfer oscillator (STO). We investigated the magnetization dynamics in STO. We applied a universal method, Melnikov Integral, to determine three different dynamical phases in STO, that is, limit cycles, synchronization and chaos. Finite temperature may have significant effect on STO dynamics. We studied the thermal effect on limit cycles and chaos.

In MTJ, in addition to spin transfer, energy transfer effect is studied on the basis of energy conservation. The effect of energy transfer on spin transfer induced magnetization switching is modeled in terms of an effective magnetic temperature.

Chapter 1

Introduction

1.1 Spin Angular Momentum Transfer

Spin angular momentum transfer, or spin transfer, is a short notion of the transfer of spin angular momentum between the spin polarized current and the magnetization of ferromagnetic condensates. Conduction electrons and magnetization are mutually dependent due to the exchange coupling between them.

One of the effects of magnetization on conduction electrons leads to the giant magnetoresistance(GMR) [1, 2]. In ferromagnetic multilayers, when magnetization configuration of the ferromagnetic layers changes from anti-parallel to parallel, the resistance drops.

Conversely, conduction electrons can also affect the magnetization. First, the magnetization of neighboring ferromagnetic layers, which are separated by a non-magnetic layer, can be indirectly coupled due to equilibrium conduction electron mediated interaction known as the RKKY interaction; this subject has been extensively studied in the last decade and we will not focus on this interlayer coupling in this thesis.

What we are interested in is how non-equilibrium conduction electrons affect the magnetization when an electrical current is turned on. An immediate consequence of the current is the generation of the Oersted magnetic field which will couple to

the magnetization through Zeeman interaction. Indeed, almost all present magnetic devices rely on the current-induced magnetic field to manipulate the states of the magnetization.

Here, we address an entirely new phenomenon, spin angular momentum transfer. In a transition ferromagnet, the current is spin-polarized due to spin-split band structure. When the magnetization varies spatially, the direction of the spin polarization of the current also varies. Based on the conservation of angular momentum, the change of spin angular momentum carried by the spin current should be compensated by the change of the magnetization. Actually, we can view the change of magnetization as an effect of a spin angular momentum transfer torque; and this torque comes from the change of the spin current.

To better understand how the magnetization is affected by conduction electrons via the spin angular momentum transfer torque, we consider a volume across the interface between the nonmagnetic layer and the ferromagnetic layer in a spin valve (see the dashed line pillbox in Fig. 1.1). Neglecting spin flipping, we can write down a continuity equation,

$$\frac{d\mathbf{m}}{dt} + \nabla \cdot \mathcal{J}^{\boldsymbol{\sigma}} = \boldsymbol{\tau}_{ext}, \tag{1.1}$$

where $\mathbf{m}$ is the spin density; $\mathcal{J}^{\boldsymbol{\sigma}}$ is the spin current density; ∇ is a spatial gradient operator; and $\boldsymbol{\tau}_{ext}$ on the right hand side is the external torque density which might be caused by external field, damping effect and *etc.* The second term on the left hand side, $\nabla \cdot \mathcal{J}^{\boldsymbol{\sigma}}$ can be viewed as a torque. Indeed, this term is defined as the spin transfer torque (STT),

$$\boldsymbol{\tau}_{st} \equiv \nabla \cdot \mathcal{J}^{\boldsymbol{\sigma}}. \tag{1.2}$$

Integrating Eq. (1.2) over the pillbox, we have

$$\mathbf{\Gamma}_{st} = (\mathcal{J}^{\boldsymbol{\sigma}}_{in} - \mathcal{J}^{\boldsymbol{\sigma}}_{out}) \cdot \mathbf{e}_x, \tag{1.3}$$

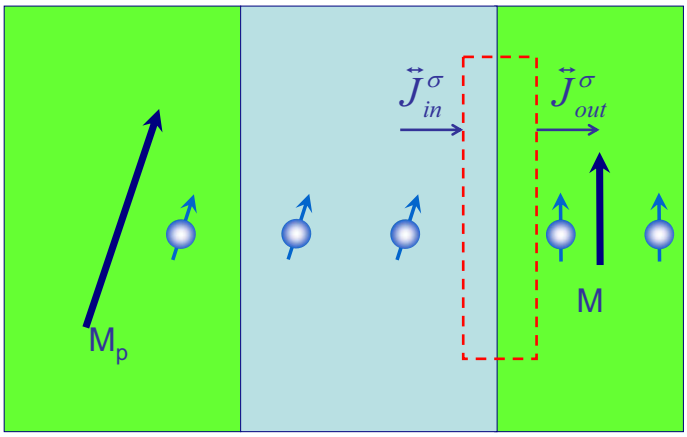

Figure 1.1: A trilayer structure constituting of two ferromagnetic layers separated by a non-magnetic layer. Polarized electron passing through the ferromagnetic layer, its polarization follows the magnetization orientation. Meanwhile, a spin transfer torque exerted on the magnetization is induced by the change of spin current, which ensures the conservation of angular momentum.

where the current flows in the direction of $\mathbf{e}_x$.

Choosing the quantization axis along the magnetization in the ferromagnet, spin-up and spin-down are two eigenstates. Transverse spin currents are composed of a combination of these two eigenstates. Since the Fermi wave vectors are different for spin-up and spin-down in ferromagnets, the phase factors for each state are different. This induces a decoherence of the precessions of these eigenstates. Thus, transverse spin current will not persist. On the other hand, longitudinal spin currents are composed of electrons in a pure eigenstate, either spin-up or spin-down. They do not have the decoherence problem and will persist.

Therefore over the pillbox in Fig. 1.1, longitudinal spin current is continuous whereas transverse ones are not. The decoherence is fast and the transverse spin currents are fully absorbed by the ferromagnetic layer within a few nanometers. Thus,

$$\mathcal{J}_{in}^{\boldsymbol{\sigma}_\parallel} \cdot \mathbf{e}_x = \mathcal{J}_{out}^{\boldsymbol{\sigma}_\parallel} \cdot \mathbf{e}_x \tag{1.4}$$

$$\mathcal{J}_{out}^{\boldsymbol{\sigma}_\perp} \cdot \mathbf{e}_x = 0. \tag{1.5}$$

Putting into Eq. (1.3),

$$\mathbf{\Gamma}_{st} = \mathcal{J}_{in}^{\boldsymbol{\sigma}_\perp} \cdot \mathbf{e}_x, \tag{1.6}$$

where $\mathcal{J}_{in}^{\boldsymbol{\sigma}_\perp}$ is the incident transverse spin current. $\mathbf{\Gamma}_{st}$ serves as an input to magnetization dynamics, and should be included in the Landau-Lifshitz-Gilbert equation,

$$\frac{d\mathbf{M}}{dt} = -\gamma \mathbf{M} \times \mathbf{H}_{eff} - \alpha\gamma \mathbf{M} \times (\mathbf{M} \times \mathbf{H}_{eff}) + \mathbf{\Gamma}_{st}. \tag{1.7}$$

Here γ is the gyromagnetic ratio; $\mathbf{H}_{eff}$ is the effective magnetic field which includes the external magnetic field, anisotropy and demagnetization field; α is the Gilbert damping constant.

The first term of Eq. (1.7) accounts for the magnetization dynamics in an effective magnetic field. It produces a steady Larmor precession. The second term, the

Gilbert damping torque will take the magnetization to an orientation so that the magnetic energy is minimized. The last term, $\mathbf{\Gamma}_{st}$, is shown to have a similar form as the damping torque (see Eq. (1.8) in next section). Under certain magnetization configuration and current direction, $\mathbf{\Gamma}_{st}$ can drive the magnetization to reverse, or generate an effect which compensates the damping effect so that steady precessional states are recovered.

Conventional method to manipulate the magnetization is to apply an external magnetic field. STT gives an innovational way to control magnetization via current. STT can induce switchings between two stable states in spin-valves or magnetic tunnel junctions(MTJ) that constitute memory devices. In magnetic random access memory (MRAM), STT may be used to write a local nanomagnetic bit without disturbing its neighboring bits. STT-induced domain wall motion could also have significant applications in memory devices. STT may enhance the performance of read head in hard-disks as well. In addition, STT may have great potential applications in on-chip microwave magnetic field generators.

1.2 Historical Development and Prior Work

GMR effect was discovered only about two decades ago. However, this discovery boosted the hard disk industry. In 2007, Albert Fert [1] and Peter Grünberg [2] received Nobel Prize for their original contributions to this discovery.

Spin transfer, the reverse effect of GMR, has a even shorter history. In 1996, J. C. Slonczewski first derived current driven spin transfer [7]. He predicted two new phenomena in a magnetic multilayer structure. One is magnetization switching driven by pulse current, the other is steady precession driven by constant current. In the same year, L. Berger also predicted that when a dc current traverses an normal-

ferromagnetic interface, coherent spin waves can be emitted and a spontaneous magnetization precession arises [4].

By assuming ballistic transport and using WKB wave functions, Slonczewski derived that STT takes the following form [7],

$$\mathbf{\Gamma}_{st} = a_j \mathbf{M}_{1,2} \times (\mathbf{M}_1 \times \mathbf{M}_2), \tag{1.8}$$

where a_j is proportional to the current and $\mathbf{M}_{1,2}$ is the magnetization of each ferromagnetic layer.

In 1998, Tsoi *et al.* [1] reported magnetic excitations resulting from injecting high-density current into a Cu/Co multilayer through point contact made of silver. Such current driven excitation only takes place in one direction of current. The threshold current has linearly dependence on applied field.

In 1999, Meyers *et al.* [6] observed magnetic excitation by passing electronic current through a bowl-shaped hole in a Silicon Nitride membrane to a Co/Cu/Co sandwich structure. In addition to magnetic excitation, they also observed current-induced hysteretic magnetic reversal.

During the same phase, STT-induced magnetic excitation has been reported by Wegrowe *et al.* in an electroplated Ni wire [7], and by Sun in manganite junctions [8].

The quantitative evidence of STT-induced magnetization reversal was finally observed in 2000, by Katine *et al.* [9]. They fabricated Co/Cu/Co spin-valve pillars with about 100 nm in diameter. By using GMR as a probe, they clearly demonstrated the linear dependence of threshold current density on the applied magnetic field, which is consistent with STT models.

Since the successful experimental verifications, extensive work have been done to develop STT model in different aspects, e.g. microscopic calculation [10–12], classical dynamics derivation [13–20], and *etc.*

It is found that magnitude of the switching current depends on the angular between magnetization [7, 8, 21]. Experiments have verified this angular dependence [22]. Furthermore, STT may comprise not only a Slonczewski term, but also a significant field-like torque. In 2002, Zhang *et al.* [23] derived this additional contribution of STT, which is in the direction of

$$\mathbf{M}_1 \times \mathbf{M}_2.$$

The superposition of the Slonczewski torque and the field-like torque has been shown experimentally by Tulapurkar *et al.* in 2005 [24].

Most recently, spin transfer was even extended to antiferromagnets. Wei *et al.* proposed a spin transfer across an interface between ferromagnetic and antiferromagnetic metals [25]. They found that the strength of the exchange bias varies due to spin transfer effect. They predicted that a spin current generates a torque on magnetic moments in the antiferromagnet.

1.3 Spin Transfer in Spin-Valve and MTJ

A spin valve consists of one thicker ferromagnetic layer (fixed layer) with a fixed magnetization and one thinner ferromagnetic layer (free layer) with a free-to-move magnetization, separated by a non-magnetic layer. When applying a current through spin valves, the nonequilibrium electrons act as intermedia to transfer angular momentum between magnetization on the two ferromagnetic layers.

When current passes through a spin valve, spin transfer can induce switching between two stable magnetic states in the free layer. Applying an external magnetic field, spin transfer may produce self-sustained magnetization precession.

A Magnetic Tunnel Junction (MTJ) has the similar structure to spin valves, with the non-magnetic separator replaced by an insulator which forms an energy barrier

between two ferromagnetic layers. The tunneling electrons experience a voltage bias between two ferromagnets.

Because of the high magnetoresistance of MTJ, it is preferable to use MTJ instead of spin valves to as storage element in high-density nonvolatile memory device such as MRAM.

The experimental confirmations of STT-induced magnetization switching in MTJ has come later than in spin valves. Recently, groups in Grandis [26–30], Cornell University [31–33] and Japan [34] have reported magnetization reversal caused by spin transfer in MTJ using MgO as insulators. By using of MgO as insulators, and introducing double fixed layer, the critical current of reversal has been significantly reduced.

Due to the existence of the voltage bias, the underlying physics of spin transfer in MTJs is much more complicated than in spin valves. One of the complications is the bias dependence of STT in MTJ. Although Tunneling magnetoresistance (TMR) has a symmetric bias dependence, STT in MTJ does not. In 2005, Slonczewski predicted the asymmetric voltage dependence of spin transfer torque in MTJ [35]. In 2006, Theodonis *et al.* reported an anomalous bias dependence of the component of STT that is parallel to the interface [36]. While the torque perpendicular to the interface exhibits a quadratic bias dependence, the parallel torque exhibits different bias dependence for different magnetization configurations, linear for parallel alignments but quadratic for antiparallel alignments.

However, in MTJ, there is an important issue accompanying the spin transfer effect, which is still unsolved: How does the energy transfer between magnets and tunneling electrons? We will address this problem in Chapter 2.

1.4 Spin Transfer Oscillator

Another promising application of STT is the spin transfer oscillator (STO). Stable precessional states can occur when the damping effect is balanced by the STT effect. These precessional states induced by dc spin current have been demonstrated by experiments recently [37–39]. The spin transfer induced precession of magnetization generates ac signal in terms of electrical current and magnetic field. Currently, GHz [38] signal with narrow linewidth [40] can be generated by nano-scale STOs which are controlled by applied magnetic field and dc current. STO offers an intriguing possibility to fabricate on-chip microwave generators.

Once a stable precessional motion occurs under certain dc current and external field, small perturbations will not change its orbit. This orbit is called a stable limit cycle. If a magnetization starts from a point not on the limit cycle, it will be attracted toward the stable limit cycle, and eventually, precess along it.

The stable limit cycles have well defined frequencies. These frequencies can be observed through the power spectra. For an STO, the measurements of these power spectra have been reported [37–41]. These frequencies vary with dc currents or external fields.

Due to the nonlinear nature of the underlying equation of motion of STO, synchronization phenomena are expected. Several Experimental observations have been reported [2, 5, 6, 43, 46], and theoretical studies have been carried out [3, 4, 7, 50–52]. These experiments and theories have been focused on two categories of synchronization. The first case is that a single STO is synchronized to an external periodic force like an ac current. This synchronization occurs when external force has a frequency that is close to the fundamental frequency of STO. The second case is that two or more STOs are self phase locking due to the *mutual synchronization* since these STOs

have similar fundamental frequencies.

The observation of the first kind of synchronization in STO was reported by Rippard *et al.* in 2005 [2]. Later, in 2006, by using a single STO, Sankey *et al.* studied the ferromagnetic resonance driven by ac current [43].

In 2005, Kaka *et al.* and Mancoff *et al.* independently reported the mutual synchronization of two coupled STOs that are fabricated by a spin-valve with double point contacts on the free layer [5, 6]. The coupling between these STOs is mainly contributed by spin wave interaction [46]. The mutual synchronization of a series of ten STOs in a circuit has been numerically simulated by Grollier *et al.* [7]. These STOs are coupled via microwave current.

STO generates microwave signal but has the drawback of low output power. By synchronized to a small ac current, output power can be increased and signal noise can be reduced. Self-phase-locking of coupled STOs generator, can further increase the output power, which can be enhanced by N^2 where N is the number of coupled STOs [7].

Intrinsic instability in STO has been studied by Li *et al.* [50]. Their numerical simulations in single domain showed that in certain ranges of magnetic field and dc current, chaotic dynamics occurs in STO. By using *Melnikov Integral*, they analytically determined chaotic regions. Strict demonstrations of chaos were given by Yang *et al.* by calculating *Lyapunov Exponents* [53].

1.5 Outline of Dissertation

In this dissertation, we investigate the spin/energy transfer in MTJ and the nonlinear dynamics of magnetization in spin valve nanostructures.

In Chapter 2, we discuss the energy transfer in MTJ. Starting from the current

model in MTJ, we analyze the contribution of transverse and longitudinal spin currents to spin transfer and energy transfer, respectively. We give a microscopic calculation on the energy transfer effect and propose an effective temperature to characterize this effect.

In Chapter 3, we investigate the magnetization dynamics of STOs. We derive the analytical solutions of the energy-conserved precessional orbits of magnetization vector and determine the stable precessional orbits.

In Chapter 4, we study the synchronization in STOs. We extend Melnikov Integral method to determine the synchronization regions for a single STO at driven ac currents.

In Chapter 5, we present the study of chaotic dynamics in STOs. We calculate Lyapunov Exponents to demonstrate the existence of chaos in STO. We investigate the route to chaos in STO and study its universality among a general class of nonlinear dynamics.

In Chapter 6, we consider the thermal effect on STO dynamics. By deriving stochastic differential equation and Fokker-Planck-Equation for magnetic energy, we confirm the dissipation-fluctuation relation. We study the thermal instability in terms of the energy deviation distribution and compare it to chaos, the intrinsic instability.

An interesting spin transport problem Spin Hall Effect is discussed in the Appendix. We propose an *intrinsic* Orbital-Angular-Momentum (OAM) Hall Effect that accompanies the *intrinsic* Spin Hall Effect. We present a Boltzmann Equation calculation of the *extrinsic* Spin Hall Effect in the presence of spin-orbit couplings.

Bibliography

[1] M. N. Baibich *et al.*, Phys. Rev. Lett. **61**, 2472 (1988).

[2] G. Binasch *et al.*, Phys. Rev. B **39**, 4828 (1989).

[3] J. C. Slonczewski, J. Magn. Magn. Mater. **159**, L1 (1996).

[4] L. Berger, Phys. Rev. B **54**, 9353 (1996).

[5] M. Tsoi *et al.*, Phys. Rev. Lett. **80**, 4281 (1998).

[6] E. B. Myers *et al.*, Science **285**, 867 (1999).

[7] J.-E. Wegrowe *et al.*, Europhys. Lett. **45** 626(1999).

[8] J. Z. Sun, J. Magn. Magn. Mater. **202**, 157 (1999).

[9] J. A. Katine *et al.*, Phys. Rev. Lett. **84**, 3149 (2000).

[10] X. Waintal *et al.*, Phys. Rev. B **62**, 12317 (2000).

[11] M. D. Stiles, A. Zangwill, Phys. Rev. B **66**, 014407 (2002).

[12] M. D. Stiles, J. Xiao, and A. Zangwill, Phys. Rev. B **69**, 054408 (2004).

[13] C. Heide, Phys. Rev. Lett. **87**, 197201 (2001).

[14] C. Heide, P. E. Zilberman, and R. J. Elliott, Phys. Rev. B **63**, 064424 (2001).

[15] J. Miltat *et al.*, J. Appl. Phys. **89**, 6982 (2001).

[16] Y. Tserkovnyak, A. Brataas, and G. E. W. Bauer, Phys. Rev. Lett. **88**, 117601 (2002).

[17] S. Zhang, and Z. Li, Phys. Rev. Lett. **93**, 127204 (2004).

[18] Z. Li, and S. Zhang, Phys. Rev. B **69**, 134416 (2004).

[19] Z. Li, J. He, and S. Zhang, Phys. Rev. B **72**, 212411 (2005).

[20] A. Brataas, Y. Tserkovnyak, and G. E. W. Bauer, Phys. Rev. B **73**, 014408 (2006).

[21] J. Z. Sun, Phys. Rev. B **62**, 570 (2000).

[22] F. B. Mancoff *et al.*, Appl. Phys. Lett. **83**, 1596 (2003).

[23] S. Zhang, P. M. Levy, and A. Fert, Phys. Rev. Lett. **88**, 236601 (2002).

[24] A. A. Tulapurkar *et al.*, Nature (London) **438**, 339 (2005).

[25] Z. Wei *et al.*, Phys. Rev. Lett. **98**, 116603 (2007)

[26] Y. Huai *et al.*, Appl. Phys. Lett. **84**, 3118 (2004).

[27] M. Pakala *et al.*, J. Appl. Phys. **98**, 056107 (2005).

[28] Y. Huai *et al.*, Appl. Phys. Lett. **87**, 222510 (2005).

[29] Z. Diao *et al.*, Appl. Phys. Lett. **87**, 232502 (2005).

[30] Z. Diao *et al.*, J. Appl. Phys. **99**, 08G510 (2006).

[31] G. D. Fuchs *et al.*, Appl. Phys. Lett. **85**, 1205 (2004).

[32] G. D. Fuchs *et al.*, Appl. Phys. Lett. **86**, 152509 (2005).

[33] G. D. Fuchs *et al.*, Phys. Rev. Lett. **96**, 186603 (2006).

[34] J. Hayakawa *et al.*, Jpn. J. Appl. Phys. **44**, L1267 (2005).

[35] J. C. Slonczewski, Phys. Rev. B **71**, 024411 (2005).

[36] I. Theodonis *et al.*, Phys. Rev. Lett. **97**, 237205 (2006).

[37] S. I. Kiselev *et al.*, Nature (London) **425**, 380 (2003).

[38] W. H. Rippard *et al.*, Phys. Rev. Lett. **92**, 027201 (2004).

[39] I. N. Krivorotov *et al.*, Science **307**, 228 (2005).

[40] W. H. Rippard *et al.*, Phys. Rev. B **70**, 100406(R) (2004).

[41] D. Houssameddine *et al.*, Nature Materials **6**, 447 (2007).

[42] W. H. Rippard *et al.*, Phys. Rev. Lett. **95**, 067203 (2005).

[43] J. C. Sankey *et al.*, Phys. Rev. Lett. **96**, 227601 (2006).

[44] S. Kaka *et al.*, Nature (London) **437**, 389 (2005) .

[45] F. B. Mancoff *et al.*, Nature (London) **437**, 393 (2005).

[46] M. R. Pufall *et al.*, Phys. Rev. Lett. **97**, 087206 (2006).

[47] J. Grollier, V. Cros, and A. Fert, Phys. Rev. B **73**, 060409(R) (2006).

[48] A. N. Slavin, and V. S. Tiberkevich, Phys. Rev. B **72**, 092407 (2005).

[49] A. N. Slavin, and V. S. Tiberkevich, Phys. Rev. B **74**, 104401 (2006)

[50] Z. Li, Y. C. Li, and S. Zhang, Phys. Rev. B **74**, 054417 (2006).

[51] J. Persson, Y. Zhou, and J. Akerman, J. Appl. Phys. **101**, 09A503 (2007).

[52] Y. Zhou, J. Persson, and J. Akerman, J. Appl. Phys. **101**, 09A510 (2007).

[53] Z. Yang, S. Zhang, and Y. Charles Li, Phys. Rev. Lett. **99**, 134101 (2007).

Chapter 2

Spin and Energy Transfer in Magnetic Tunnel Junctions

2.1 Introduction

There has been considerable interest in the phenomenon of spin-polarized current induced magnetic dynamics in magnetic multilayers and magnetic tunnel junctions (MTJ). The essential physics is the spin angular momentum transfer [1, 2]: when the spin polarized current enters a magnetic layer, the component of the spin current which is transverse to the direction of the magnetization is absorbed within a short length scale. While the spin transfer mechanism can be applied to both magnetic multilayers and MTJ, there is a key difference between these two systems. For magnetic multilayers, the spin current is carried by electrons at the Fermi level and thus the spin transfer does not involve inelastic scattering. In MTJ, however, a finite voltage bias of the order of a fraction of a volt is applied in order to provide a sufficient electric current. The tunneling electrons from the Fermi level of the emitting electrode become hot electrons for the collecting electrode. The hot electrons open additional inelastic tunneling channels which have been identified as one of the reasons for the reduction of the tunnel magnetoresistance [16]. Similarly, one expects that the inelastic scattering would also affect the current-driven magnetization

switching. Indeed, the unusual experimental observation [4–6] on the dependence of critical currents on bias asymmetry, temperature and current pulse width has not been explained satisfactorily based on the direct elastic tunneling model.

In this chapter, we intend to describe how the ferromagnetic electrode responds to the spin polarized tunneling currents at finite voltage bias by taking into account inelastic scattering processes. Specifically, the spin current in the non-collinear MTJ has four spinor matrix elements: the two off-diagonal elements represent the spin current transverse to the switching ferromagnet and the two diagonal ones are longitudinal spin currents (up and down). The ferromagnet absorbs the transverse spin current for any voltage bias, resulting in a spin torque on the ferromagnet. The absorption of the longitudinal spin current requires a finite voltage because the longitudinal spin relaxation is through the emission of magnons which costs energy (here we neglect the direct relaxation to the lattice via spin-orbit coupling). We find the energy transfer from the tunneling hot electrons to the ferromagnet can be quite substantial for a typical experimental bias. By calculating the steady-state non-equilibrium magnons emitted by the longitudinal spin current, we show that the magnetic temperature increases in the ferromagnet. When we include the spin torque and the enhanced magnetic temperature at the finite bias, we find much of the experimental observation can be satisfactorily explained.

2.2 The Model of Spin Dependent Tunneling Current

We begin our model calculation by considering an MTJ where the magnetization of two electrodes is not collinear, depicted in Fig. 2.1. The simplest connection between *spin-dependence* of the tunneling current and spin polarization of the electrodes is the Julliere model [7] where the spinor current, $\hat{j}$, is proportional to the product of

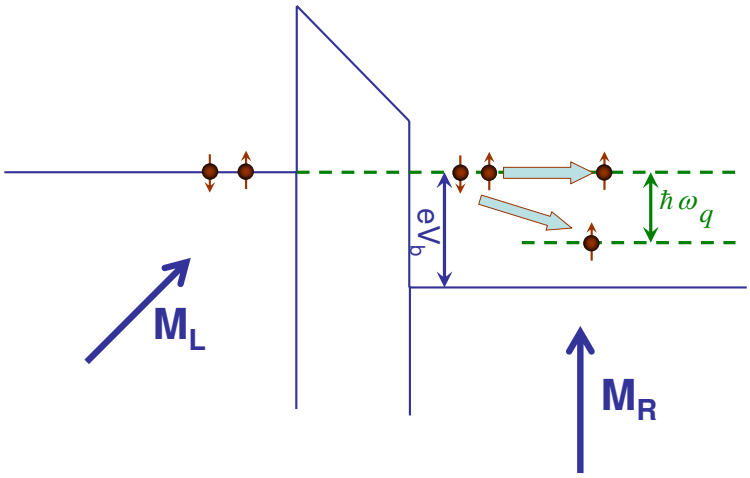

Figure 2.1: The energy model for a MTJ. The tunneling electrons have energy higher than Fermi level of the righ electrode. They experience spin dependent inelastic scatterings due to electron-magnon interaction. Spin down electrons are scattered to lower energy level flipping to spin up and emitting magnons $\hbar\omega_q$.

two spin-polarization factors of the left and right electrodes, i.e.,

$$\hat{j} = 2j_0 \hat{N}_L \hat{N}_R \tag{2.1}$$

where j_0 is the spin-independent tunneling current; $\hat{N}_i$ (i=R or L) is the spin polarization matrix which is diagonal for the quantization axis along the local magnetization.

In the representation of the quantization axis along the magnetization of each electrode, $\hat{N}_i$ can be expressed as

$$\hat{N}_i = \begin{pmatrix} \frac{1+P_i}{2} & \\ & \frac{1-P_i}{2} \end{pmatrix} \tag{2.2}$$

where P_i is the polarization. By applying the unitary rotation matrix, U,

$$U = \begin{pmatrix} \cos\frac{\theta}{2} e^{-i\frac{\phi}{2}} & \sin\frac{\theta}{2} e^{-i\frac{\phi}{2}} \\ -\sin\frac{\theta}{2} e^{i\frac{\phi}{2}} & \cos\frac{\theta}{2} e^{i\frac{\phi}{2}} \end{pmatrix}. \tag{2.3}$$

Plugging Eq. 2.3 into Eq. 2.2, then input the result into Eq. (2.1), we obtain,

$$\hat{j} = 2j_0 U \begin{pmatrix} \frac{1+P_L}{2} & \\ & \frac{1-P_L}{2} \end{pmatrix} U^\dagger \begin{pmatrix} \frac{1+P_R}{2} & \\ & \frac{1-P_R}{2} \end{pmatrix} \tag{2.4}$$

which represents the tunneling spin current spinor in the representation of the quantization axis along the magnetization of the *right* electrode.

It is noted that the present choice of the quantization axis is convenient since we consider the right electrode as a switching ferromagnet and thus "longitudinal" or "transverse" is always with respect to the magnetization of the right electrode.

The spinor current density is then

$$\hat{j} = \begin{pmatrix} j_\uparrow & j_- \\ j_+ & j_\downarrow \end{pmatrix} \tag{2.5}$$

where the two longitudinal components are

$$j_\uparrow = \frac{j_0}{2}(1+P_R)(1+P_L\cos\theta). \tag{2.6}$$

$$j_\downarrow = \frac{j_0}{2}(1-P_R)(1-P_L\cos\theta). \tag{2.7}$$

And two off-diagonal elements (taking $\phi = 0$) are

$$j_+ = -\frac{j_0}{2}(1 + P_R)P_L \sin\theta. \tag{2.8}$$

$$j_- = -\frac{j_0}{2}(1 - P_R)P_L \sin\theta. \tag{2.9}$$

The transverse spin current is thus

$$\begin{aligned} \vec{j}_T &\equiv \mathrm{Tr}_\sigma(\sigma_x \hat{j}) \\ &= -j_0 P_L \hat{M}_R \times (\hat{M}_L \times \hat{M}_R) \\ &\equiv \tau_{st} \end{aligned} \tag{2.10}$$

where $\hat{M}_i$ is the unit vector along the direction of the magnetization.

Note that the above transverse current is absorbed within 1-3 nm inside the right electrode and Eq. (2.10) is identified as the spin torque τ_{st} on the *right* electrode [8]. We immediately realize from Eq. (2.10) that the spin transfer torque is determined by the spin-polarization of the left electrode (P_L) [9] but independent of P_R as long as the right electrode is able to completely absorb the transverse spin current.

2.3 Spin Dependent Inelastic Scattering

We now proceed to discuss the role of longitudinal spin currents, $j_{\uparrow,\downarrow}$. While the total current

$$\begin{aligned} j &= j_\uparrow + j_\downarrow \\ &= j_0(1 + P_L P_R \hat{M}_L \cdot \hat{M}_R) \end{aligned} \tag{2.11}$$

determines the magnetoresistance, the spin-up and spin-down currents play different roles in terms of inelastic scattering with the magnetic electrode.

For tunneling electrons whose energies are eV_b above the Fermi level of the right electrode, as shown in Fig. 2.1, the inelastic mean free paths are much shorter for

spin-down electrons than for spin-up electrons. This is because the spin-down electron can emit spin waves (magnons) by giving up its energy while the magnon emission for spin-up electrons is prohibited due to the angular momentum conservation. Spin-up electrons can only absorb magnons, but the number of magnons at thermal equilibrium is small if the temperature is much lower than the Curie temperature. Earlier calculations [25] and experiments [11] have already showed a dramatic difference in the inelastic mean free paths for spin up and down electrons. Here we show by our explicit calculation that the spin-down electrons have the mean free path smaller or comparable to the typical experimental thickness (about 3nm) for the bias voltage of interest. Therefore, almost every spin down hot electron emits an magnon and the non-equilibrium magnons are accumulated in the ferromagnet resulting in substantial increase of the magnetic temperature, which in turn, will greatly affect the critical switching current [12–14].

The dominant inelastic magnetic scattering mechanisms of hot electrons are spin wave (magnon) emissions and Stoner excitations [25]. The latter mechanism involves excitations of electron-hole pairs in the spin-split bands. For the electron energy less than 1 eV above the Fermi level, the former mechanism dominant since the Stoner excitation requires a larger energy. Thus, we estimate the inelastic mean free path and magnon accumulation by considering the standard electron-magnon interaction Hamiltonian,

$$H_{sd} = -\sqrt{\frac{2S}{N_s}} J_{sd} \sum_{kq} c^{\dagger}_{\vec{k}-\vec{q},\uparrow} c_{\vec{k}\downarrow} (a^{\dagger}_{\vec{q}} + a_{-\vec{q}}) \tag{2.12}$$

where N_s is the number of the sites; J_{sd} is the s-d exchange constant; c_k ($c^{\dagger}_k$) is the annihilation (creation) operator for the conduction electron; $\hat{S}$ represents the local spin, and $a^{\dagger}_q$ (a_q) is the creation (annihilation) operator for magnons. The inverse mean free time for spin-down electrons, up to the second order in the coupling

constant, is thus

$$\frac{1}{\tau_\downarrow} = \frac{V}{(2\pi)^3} \int d^3q W_{\vec{k},\vec{k}-\vec{q}} \tag{2.13}$$

where

$$W_{\vec{k},\vec{k}-\vec{q}} = \frac{4\pi S}{\hbar N_s} J_{sd}^2 (1+n_q) \delta(\epsilon_k - \epsilon_{|\vec{k}-\vec{q}|} - \hbar\omega_q), \tag{2.14}$$

and $\hbar\omega_q = 2J_F S a^2 q^2$ is the magnon energy with J_F and a defined as the ferromagnetic exchange constant and the lattice constant. n_q, which is the magnon distribution, will increase from zero when $T = 0$, due to the magnon emission. However, no matter zero or finite temperature, it has negligible contributions to the mean free path and resolved energy and we simply drop it.

By approximating the velocity of tunneling electrons by the Fermi velocity v_F for a low voltage bias ($eV_b \ll \epsilon_F$), the mean free path is,

$$\lambda_\downarrow = v_F \tau_\downarrow = \frac{8\pi J_F \hbar^2}{m a J_{sd}^2} \left(\frac{\epsilon_F}{eV_b} \right). \tag{2.15}$$

A rough estimate from the above equation would produce the mean free path about 0.5nm to 3nm for a bias voltage of 0.5V; this is consistent with the estimation by using a more detailed calculation [25].

For spin-up electrons, we replace $W_{\vec{k},\vec{k}-\vec{q}}$ in Eq. (2.13) with

$$W_{\vec{k},\vec{k}+\vec{q}} = \frac{4\pi S}{\hbar N_s} J_{sd}^2 n_q \delta(\epsilon_k - \epsilon_{|\vec{k}+\vec{q}|} + \hbar\omega_q). \tag{2.16}$$

Then, the mean free path for spin-up should be

$$\lambda_\uparrow = \frac{8\pi J_F \hbar^2}{m a J_{sd}^2} \left(\frac{\epsilon_F}{k_B T} \right), \tag{2.17}$$

as long as $k_B T \ll eV_b$, $\lambda_\uparrow \gg \lambda_\downarrow$.

Therefore, spin-up electron scattering and the magnon absorption induced by it can be neglected in our calculation.

2.4 Energy Transfer Through Magnon

Next, we estimate the non-equilibrium magnon energy produced by the decay of the spin down current. Again, by using the simple electron-magnon Hamiltonian, Eq. (2.12), the rate of the nonequilibrium magnon energy emitted by the tunnel electrons is,

$$\left(\frac{\partial E}{\partial t}\right)_m = \frac{N_\downarrow V}{(2\pi)^3}\int d^3q W_{\vec{k},\vec{k}-\vec{q}}\hbar\omega_q. \tag{2.18}$$

where $N_\downarrow$ is the total number of spin down hot electrons per unit area. Since the spin down electron density, $n_\downarrow(x)$ decays exponentially inside the ferromagnet, we have

$$N_\downarrow = \int_0^d dx n_\downarrow(x) = (j_\downarrow/e)\tau_\downarrow[1-\exp(-d/\lambda_\downarrow)] \tag{2.19}$$

where $j_\downarrow$ is given by Eq. (2.7) which represents the current density at the interface between the barrier and ferromagnet. The non-equilibrium magnon energy δE is thus accumulated in the ferromagnet. If we take into account the magnon energy relaxation to the lattice via spin-orbit coupling, the net change of the magnon energy is

$$\frac{dE}{dt} = \left(\frac{\partial E}{\partial t}\right)_m - \frac{\delta E}{T_1} \tag{2.20}$$

where T_1 is the phenomenological relaxation time which has been experimentally measured for the transition metals [15]. In the steady-state,

$$dE/dt = 0.$$

By explicitly calculating Eqs. (2.18) and (2.20), we arrive at the steady-state non-equilibrium magnon energy

$$\delta E = \frac{1}{4}j_0V_b(1-e^{-\frac{d}{\lambda_\downarrow}})T_1(1-P_R)(1-P_L\cos\theta). \tag{2.21}$$

As expected, the non-equilibrium energy accumulation is proportional to the dissipative heat power j_0V_b. Therefore, our consideration is beyond the linear response for

which the current induced energy accumulation is linearly proportional to either the current density or the applied voltage but not the product of the two.

2.5 Effective Temperature

These steady-state non-equilibrium magnons effectively enhanced the temperature of the magnetization of the electrode. The initial distribution of the emitted magnons is different from the form of "thermal equilibrium". However, The characteristic time of the magnon emission is $\tau_{\downarrow} \sim 10^{-16}s$ which is much faster than the relaxation time (picoseconds) of the non-equilibrium magnons to the lattice. Therefore, it is reasonable to assume that these nonequilibrium magnons will be thermalized before they relax to the lattice. The microscopic mechanism of the magnon thermalization will involve a detail magnon-magnon interactions. For our purpose, we do not need to develop this theory but merely to observe that the characteristic time of the thermalization is $\hbar/k_BT$, which is much faster than the magnon energy relaxation. As the magnon is a Boson, the thermalization due to magnon-magnon interaction does not conserve the number of magnons. Instead, it conserves the total energy if it is faster than the energy relaxation as we have anticipated here. Thus, we can define an effective temperature T_0^* by equating the non-equilibrium magnon accumulation to the thermalized magnon energy,

$$\begin{aligned} \delta E &= \frac{d}{(2\pi)^3}\int d^3q \frac{\hbar\omega_q}{\exp\left(\hbar\omega_q/k_BT_0^*\right)-1} \\ &= \frac{3\zeta(\frac{5}{2})d(k_BT_0^*)^{\frac{5}{2}}}{16(2\pi J_F S a^2)^{\frac{3}{2}}}, \end{aligned} \tag{2.22}$$

where d is the thickness of free layer and $\zeta(\frac{5}{2}) = 1.34149$ is the Riemann Zeta function. By combining Eqs. (2.21) and (2.22), we find

$$\left(\frac{T_0^*}{T_c}\right)^{\frac{5}{2}} = c(1-P_R)(1-P_R\cos\theta)(1-e^{-d/\lambda_{\downarrow}})\frac{j_0V_ba^3T_1}{k_BT_cd} \tag{2.23}$$

where

$$c = [\pi/(S+1)]^{3/2}/6\zeta(\frac{5}{2})$$

is a numerical number and we used the mean field theory relation between J_F and the Curie temperature,

$$k_B T_c = 8S(S+1)J_F.$$

We note that the concept of the current induced magnetic temperature has been previously suggested by S. Urazhdin [16] for spin valve for a completely different reason.

The calculation of Eq. (2.23) is confined at zero temperature. At finite temperatures, there are equilibrium thermal magnons; the non-equilibrium magnon accumulation should also be thermalized with the equilibrium magnon, i.e., the effective temperature T^* is now determined by

$$\delta E(T^*) = \delta E + E_{eq}(T). \tag{2.24}$$

Then, we immediately see that the effective temperature at finite temperature T satisfies

$$T^{*\frac{5}{2}} = T_0^{*\frac{5}{2}} + T^{\frac{5}{2}}. \tag{2.25}$$

A rough estimation can be readily done for a typical MTJ. If we take the following parameters, $V_b = 1V$, $j_0 = 10^7 A/cm^2$, $P_L = P_R = 0.5$, $T_1 = 1.25 \times 10^{-12}s$ [15], $S = 1.6$, $a = 3.5\times10^{-10}m$ (for Co), $J_{sd} = 0.6eV$, $T_c = 1388K$ (for Co), $\epsilon_F = 5eV$ and $d = 2nm$. We then find that at $T = 0K$, Eq. (2.23) gives arise $T_0^* = 174K$ for $\hat{M}_L$ and $\hat{M}_R$ parallel and $T_0^* = 270K$ for antiparallel. At room temperature ($T = 300K$), the effective temperatures are $T^* = 328K$ and $T^* = 376K$ for parallel and antiparallel states respectively.

2.6 Energy Effect on Magnetization Switching

We now turn to the application of the spin and energy transfer to the current-driven magnetization switching by including the spin torque, Eq. (2.10), and the enhanced temperature, Eq. (2.23) or Eq. (2.25). First, let us examine the current directional dependence of the spin and energy transfer. In the case of electrons flowing from the fixed layer to the free layer shown in Fig. 2.1, the spin polarization factor P_L in Eq. (2.10) takes its value at the Fermi level, independent of the bias voltage, and the temperature enhancement is described by Eq. (2.23) and (2.25). In the opposite voltage polarity when electrons flow from the free layer to the fixed layer, the polarization factor P_L takes the value at eV_b above the Fermi energy, and thus the spin torque is voltage dependent in this voltage polarity; this point has been already emphysized by Slonczewski [9]. For the longitudinal current, the magnon emission now occurs at the fixed layer, i.e., *the temperature enhancement of the the free layer only occurs at one-direction of the current.* Since the current-induced magnetization switching depends on the current direction, the above asymmetries in the voltage polarity produce a profound effect: the switching from antiparallel (AP) to parallel (P) alignment of the magnetic layers leads to the enhancement of the temperature while the reversed switching is not affected by the energy transfer. To quantitatively determine the critical switching current at finite temperature, we use the model developed for the thermal assisted magnetization switching [12–14]

$$I_c = I_{c0}\left(1 - \frac{k_B T^*}{E_b(H)}\ln(t f_0)\right) \tag{2.26}$$

where t is the measuring time or the current-pulse width which can be varied from nanoseconds to a few seconds, f_0 is the attempt frequency (about several GHz), $E_b(H)$ is the energy barrier which depends on the applied magnetic field, and I_{c0} is the critical current at zero effective temperature T^*. Now, our energy transfer

mechanism produces two different temperatures. For the switching from the P to AP states, the temperature is unchanged, $T^* = T$; while for the switching from AP to P states, the energy transfer mechanism produces an enhanced temperature given by Eq. (2.25). These differences have been observed experimentally when one tries to determine $k_B T^*/E_b(H)$ using the above thermal model [5]. Specifically, since

$$E_b(H) = E_0(1 - H/H_c)^{3/2}$$

where H_c is the coercivity and thus the energy barrier is a constant for transitions between AP and P states at $H = 0$, the observed difference [5] of $E_0/k_B T^*$ must come from the different effective temperatures.

Another interesting consequence of the energy transfer is the critical current asymmetry between $I_c^{AP\to P}$ and $I_c^{P\to AP}$. The spin torque asymmetry arises due to voltage-dependence of the polarization factor P_L as pointed out by Slonczewski [9]. Other spin-flip mechanisms may also contribute to the asymmetry [17]. Our energy transfer produces a finite effective temperature even at zero temperature for the transition from AP to P states. Thus, the low temperature measurement of the critical current is not directly proportional to the intrinsic spin torque since the effective temperature is not small for a high voltage bias.

Finally we comment on the experimental extrapolation of the intrinsic spin torque by varying temperature. The common procedure relies on the linear relation between the critical current and the temperature. However, we point out that the linear relation should significantly fail at low temperatures. In Fig. 2.2, we show the relation between the critical current and the actual temperature of the device. The difference of critical currents is much larger at low temperature than at room temperature.

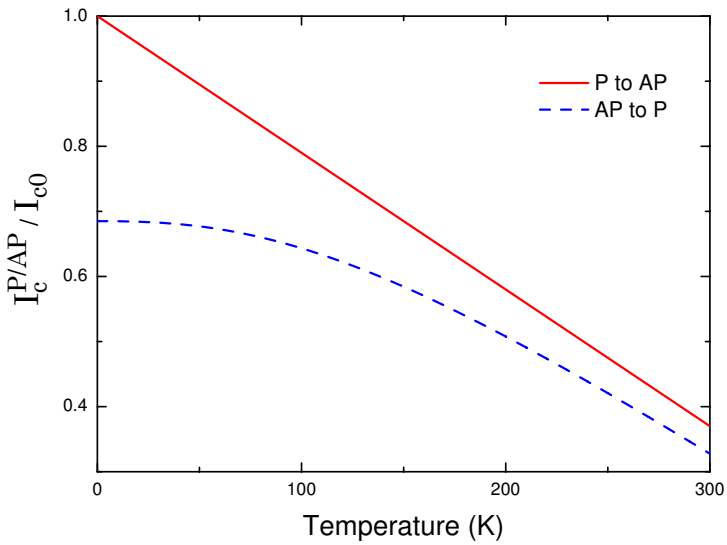

Figure 2.2: Temperature dependence of critical current. Solid and dash lines represent the critical switching current from P to AP and from P to AP. We use $t = 0.1s$, $f_0 = 1GHz$ and assume $T_0^* = 150K$, $E_0 = 0.7eV$, $H = 0Oe$.

Bibliography

[1] J. C. Slonczewski, J. Magn. Magn. Mater. **159**, L1(1996).

[2] L. Berger, Phys. Rev. B **54**, 9353(1996).

[3] S. Zhang, P. M. Levy, A. C. Marley, and S. S. P. Parkin, Phys. Rev. Lett. **79**, 3744 (1997).

[4] G.D. Fuchs *et al.*, cond-mat/0510786.

[5] J. Hayakawa *et al.*, Jpn. J. Appl. Phys. **44**, L1267(2005).

[6] Y. Huai *et al.*, Appl. Phys. Lett. **87**, 222510(2005).

[7] M. Julliere, Phys. Lett. **54A**, 225(1975); we note that one should integrate the electron energy from $E_f - eV_b$ to E_f of the left electrode. For simplicity, we neglect this energy dependence of the tunneling probability and assume that the tunneling electrons are those at the Fermi level of the left electrode.

[8] M.D. Stiles, A. Zangwill, Phys. Rev. B **66**, 014407(2002).

[9] J.C. Slonczewski, Phys. Rev. B **71**, 024411 (2005).

[10] J. Hong and D. L. Mills, Phys. Rev. B **62,** 5589(2000); **59**, 13840(1999).

[11] M. Aeschlimann *et al.*, Phys. Rev. Lett. **79**, 5158(1997).

[12] Z. Li and S. Zhang, Phys. Rev. B **69**, 134416(2004).

[13] R. H. Koch, J. A. Katine, and J. Z. Sun, Phys. Rev. Lett. **92**, 088302 (2004).

[14] D. M. Apalkov and P. B. Visscher, Phys. Rev. B **72**, 180405(R) (2005).

[15] A. G. Gurevich and G. A. Melkov, in *Magnetization Oscillations and Waves* (CRC Press, Boca Raton, FL 1996).

[16] S. Urazhdin, Phys. Rev. B **69**, 134430(2004).

[17] Z. Zhu *et al.*, Phys. Lett. A **306**, 249(2003).

Chapter 3

Magnetization Oscillations in Spin Valves

The transfer of spin angular momentum from spin current to ferromagnet provides an efficient means to manipulate the magnetization in the magnet. While Gilbert damping dissipates the energy, spin transfer torque can be either a source or a sink of energy. In the case that spin transfer torque does positive work, there is a competition between damping and spin transfer torque. When spin transfer torque overcomes damping, magnetization may be switched; if they ends up with a tie, stable precessional motion will occur.

3.1 Experiments

Current driven magnetization switching is a key concept of the spin torque magnetic random access memory. It has motivated extensive work in this field. On the other hand, due to the promising future applications in telecommunication industry, nanometer scaled magnetization oscillators have also received extensive attentions.

In 1998, Tsoi *et al.* [1] reported their measurement of resistance variation due to current-induced zero-wave-number spin waves. They injected a high density current into Co/Cu multilayers through a sharpened Ag tip point contact. The magnetization

excitation occurred only at one direction of current flow. See Fig. 1 in Ref. [1].

In 1999, Myers *et al.* [2] reported similar observations in Co/Cu sandwich structure. They produced a bowl-shaped hole in an insulating silicon nitride membrane, and applied electronic current through it. They observed peaks in differential resistance measurements when current flow is positive, but no peak when current flows in the negative direction. See Fig. 2 in Ref. [2].

These observations provided strong evidence for current driven magnetization excitation. The spin transfer torque induced magnetization oscillation is believed to be the reason of the measured variations of resistance. As we can see in the expression of spin transfer torque, spin transfer torque works against the damping in one direction of current flow, but helps damping when the current is in the opposite direction. The experimental observations and theoretical analysis are consistent.

The magnetization oscillation in spin valves (or MTJs) is governed by *nonlinear* Landau-Lifshitz-Gilbert equation. Therefore, nonlinear phenomena, such as synchronization and chaos, are expected.

The first direct measurement of synchronization (phase locking) was reported by Rippard *et al.* in 2005 [2]. Their spin transfer oscillators is synchronized to a small amplitude ac current. The synchronization band width is around several hundred megahertz.

One year later, Kaka *et al.* [4] and Mancoff *et al.* [5] reported, independently, mutual synchronization phenomenon of two magnetization oscillations in spin valves. That is, two oscillators synchronized to each other. The benefit from binding two or more oscillators are, as they reported, in two folds. First, the linewidth of the signal decreases, i.e. noise is reduced; second, the output power are increased.

The direct current driven magnetization oscillations provides an amazing opportunity to produce signal generators on a nano-scale magnetic device. The drawback

of such nano-scale oscillators, low output power (less than 1nW), can be overcome by a series of such oscillators [7]. The self phase locking of these oscillators increases the output power and reduces the signal linewidth by approximately N^2 times, where N is the number of oscillators.

3.2 Model

Magnetization dynamics is governed by Landau-Lifshitz-Gilbert Equation. In spin valves or MTJ, the absorption of transverse spin current provides the spin transfer torque. Therefore, there is an additional term, given by Slonczewski in 1996 [7], presented in Landau-Lifshitz-Gilbert Equation.

3.2.1 Spin Valve

We consider a spin valve consisted of a pinned ferromagnetic layer, a non-magnetic layer and a free ferromagnetic layer, shown in Fig. 3.1. The pinned layer is much thicker than the free layer, and the orientation of its magnetization is fixed by an attached antiferromagnetic layer. The thickness of the free layer is usually no more than a few nanometers. Its magnetization is free to rotate. The primary focus of this dissertation mostly is on the dynamics of the magnetization in the free layer.

As shown in Fig. 3.1, we define the orientation of the magnetization in the pinned layer as the $\mathbf{e}_x$, and the direction that normal to the free layer as $\mathbf{e}_z$. The magnetization in the free layer, $\mathbf{M}$, subjected into a magnetic field, is free to precess around the field. When an appropriate electrical current is applied in $\mathbf{e}_z$ or $-\mathbf{e}_z$, $\mathbf{M}$ can be switched between $\mathbf{e}_x$ and $-\mathbf{e}_x$ or precess in stable orbits.

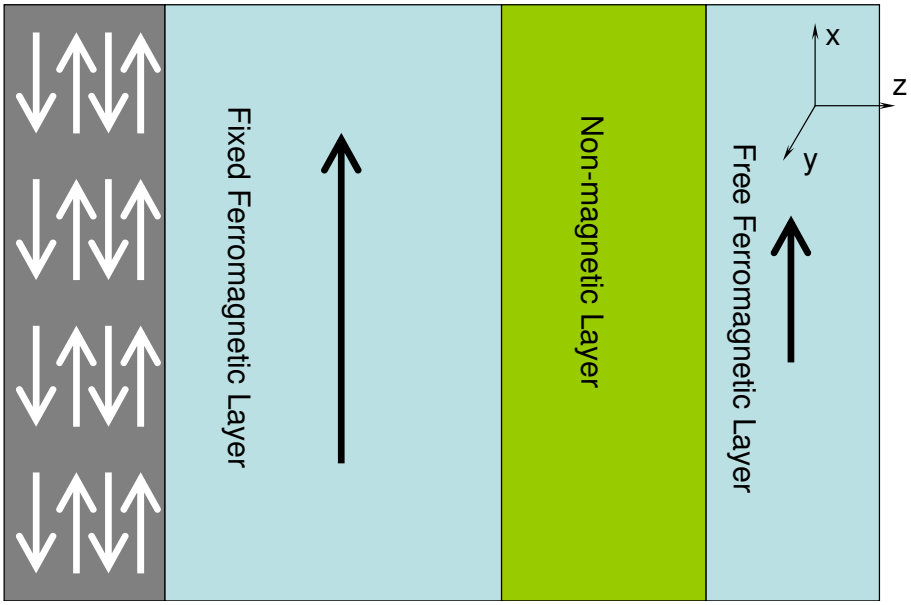

Figure 3.1: Spin Valve Model. Two ferromagnetic layers are separated by a non-magnetic layer. One of the ferromagnetic layer (fixed layer) is attached by an anti-ferromagnetic layer that fixes the orientation of the magnetization of the ferromagnetic layer through strong exchange coupling. The magnetization orientation of the other ferromagnetic layer (free layer) is free to change.

3.2.2 Landau-Lifshitz-Gilbert Equation

The equation of motion of $\mathbf{M}$ is the Landau-Lifshitz-Gilbert Equation (LLG Equation),

$$\frac{d\mathbf{M}}{dt} = -\gamma \mathbf{M} \times \mathbf{H}_{eff} + \frac{\alpha}{M_s} \mathbf{M} \times \frac{d\mathbf{M}}{dt}, \tag{3.1}$$

where M_s is the saturation magnetization; γ is the gyromagnetic ratio; $\mathbf{H}_{eff}$ is the effective field that consists of the external field, anisotropy field, exchange field and demagnetization field; the α is the Gilbert damping coefficient. The first term of the right hand side of Eq. (3.1) provides an energy conserved torque, while the second term is the Gilbert damping torque. The Gilbert damping torque drives the magneztization vector to an energy minimized orientation.

The LLG equation is indeed equivalent to Landau-Lifshitz Equation (LL Equation),

$$\frac{d\mathbf{M}}{dt} = -\frac{\gamma}{1+\alpha^2} \mathbf{M} \times \mathbf{H}_{eff} - \frac{\alpha\gamma}{(1+\alpha^2)M_s} \mathbf{M} \times (\mathbf{M} \times \mathbf{H}_{eff}). \tag{3.2}$$

When a magnetization vector is subjected to an applied magnetic field, its dynamics is determined by the LLG (or LL) equation. The final orientation of the magnetization points at the direction at which the magnetic energy is locally minimized. This is the result of the Gilbert damping.

Once an electric current is turned on, the spin transfer torque will contribute to magnetization dynamics as well. As discussed in the introduction, spin transfer torque is written as following by J. C. Slonczewski,

$$\Gamma_{STT} = \frac{\gamma a_J}{4\pi M_s} \mathbf{M} \times (\mathbf{M} \times \mathbf{e}_p), \tag{3.3}$$

where $\mathbf{e}_p$ is the orientation of the magnetization in pin layer. Notice that, current density a_J has a unit of magnetic field. For simplicity, we neglect the dependence of a_J on the angle between magnetization in different layers.

As long as the temperature is far lower than Curie temperature, the magnitude of the magnetization is fixed at M_s. For the ease of theoretical analysis and numerical simulations, one can normalize $\mathbf{M}$ by M_s and a_J, $\mathbf{H}_{eff}$ by $4\pi M_s$, i.e.

$$\mathbf{m} = \frac{\mathbf{M}}{M_s} \tag{3.4}$$

$$\beta = \frac{a_J}{4\pi M_s} \tag{3.5}$$

$$\mathbf{h}_{eff} = \frac{\mathbf{H}_{eff}}{4\pi M_s}. \tag{3.6}$$

One can further make the transformation, $\gamma t \to t$. Thus the normalized Equation of Motion is,

$$\frac{d\mathbf{m}}{dt} = -\mathbf{m} \times \mathbf{h}_{eff} + \alpha \mathbf{m} \times \frac{d\mathbf{m}}{dt} + \beta \mathbf{m} \times (\mathbf{m} \times \mathbf{e}_p). \tag{3.7}$$

Notice that Eq. (3.7) guarantees the following condition

$$|\mathbf{m}| = m_x^2 + m_y^2 + m_z^2 = 1, \tag{3.8}$$

the Eq. (3.7) is indeed a set of two dimensional coupled ordinary differential equations when both external magnetic field and β are time independent. The phase space may only contain saddle points, fixed points and *limit cycles* (to be discussed in later sections).

Before preceding to the detailed study of the dynamics, we specify all the relevant parameters we have chosen. First, we choose the magnetic field lying in the free layer plane. Although practically, the magnetic field is usually applied out of plane to achieve better observations, there is no fundamental difference if it is applied in the plane. However, choosing an in-plane magnetic field, specifically, along the same direction as the magnetization orientation of the pinned layer, will reduce the complexity of our theoretical calculation. Next, we set the anisotropy field equal to zero, in which way the external field will automatically larger than anisotropy field, which is required for self-sustained oscillation. Third, the demagnetization field is

equal to $4\pi M_z$ which is in the $\mathbf{e}_z$ direction and vertical to the free layer. Therefore, after normalization, the effective field can be expressed as,

$$\mathbf{h}_{eff} = h_e \mathbf{e}_x - m_z \mathbf{e}_z \tag{3.9}$$

3.3 Neutral Precessional Motions

The right hand side of Eq. (3.7) contains three torque terms. The simplest dynamics can be achieved by setting $\alpha = 0$ and $\beta = 0$, i.e., assuming no damping effect and no current applied.

3.3.1 Energy Conservation

As magnetization precesses, the energy may also change over time. Its time derivative can be derived by calculating the inner product of the effective magnetic field $\mathbf{h}_{eff}$ and Eq. (3.7), then take its negative value,

$$\begin{aligned} \frac{dE}{dt} &= -\mathbf{h}_{eff} \cdot \frac{d\mathbf{m}}{dt} \\ &= -\alpha \left|\mathbf{m} \times \mathbf{h}_{eff}\right|^2 + a_j (\mathbf{m} \times \mathbf{h}_{eff}) \cdot (\mathbf{m} \times \mathbf{e}_p). \end{aligned} \tag{3.10}$$

Notice that because $\mathbf{h}_{eff} \cdot (\mathbf{m} \times \mathbf{h}_{eff}) = 0$, the first term in Eq. (3.7) does not change the energy. If we set $\alpha = 0$ and $\beta = 0$, i.e. under the assumption that both damping and spin transfer torque are zero,

$$\frac{dE}{dt} = 0.$$

The energy is conserved in this system.

For an effective magnetic field given by Eq. (3.9), the magnetic energy density

$$E = -h_e m_x + \frac{1}{2} m_z^2 \tag{3.11}$$

is a constant. This is another constraint on the magnetization vector in addition to Eq. (3.8). An energy conserved magnetization trajectory is determined by the interception of these two constraints.

3.3.2 Analytical Solution

We now derive the analytical solutions of the energy conserved magnetization dynamics. The procedure is similar to what Bertotti *et al.* did in their paper published in Physica B in 2004 [8]. For a given energy, E, the trajectory is the solution of the two combined equations, Eq. (3.8) and Eq. (3.11).

Replacing m_z^2 in Eq. (3.11) by

$$m_z = 1 - m_x^2 - m_y^2, \tag{3.12}$$

we get the trajectory equation for a given energy E,

$$(m_x + h_e)^2 + m_y^2 = R^2 \tag{3.13}$$

where

$$R = \sqrt{h_e^2 - 2E + 1}.$$

This is nothing but a circle centered at $(0, \ -h_e)$ with radius R in $m_x - m_y$ plane. However, according to Eq. (3.8), $m_x^2 + m_y^2 \leq 1$, since $m_z^2 \geq 0$. Thus, the trajectory is the portion of the circle given by Eq. (3.13) inside the circle $m_x^2 + m_y^2 = 1$. These trajectories are plotted in Fig. 3.2.

When $R < 1 - h_e$, i.e. $E > h_e$, the projection of the dynamics on the $m_x - m_y$ plane is a complete circle (see Fig. 3.2). While, if $R > 1 - h_e$, i.e. $E < h_e$, the trajectory is an open circle in $m_x - m_y$ plane (see Fig. 3.2). For the former situation, the long run average of magnetization in the normal direction (m_z) is not zero. This is an out-of-plane trajectory. For the latter situation, the long run average of magnetization

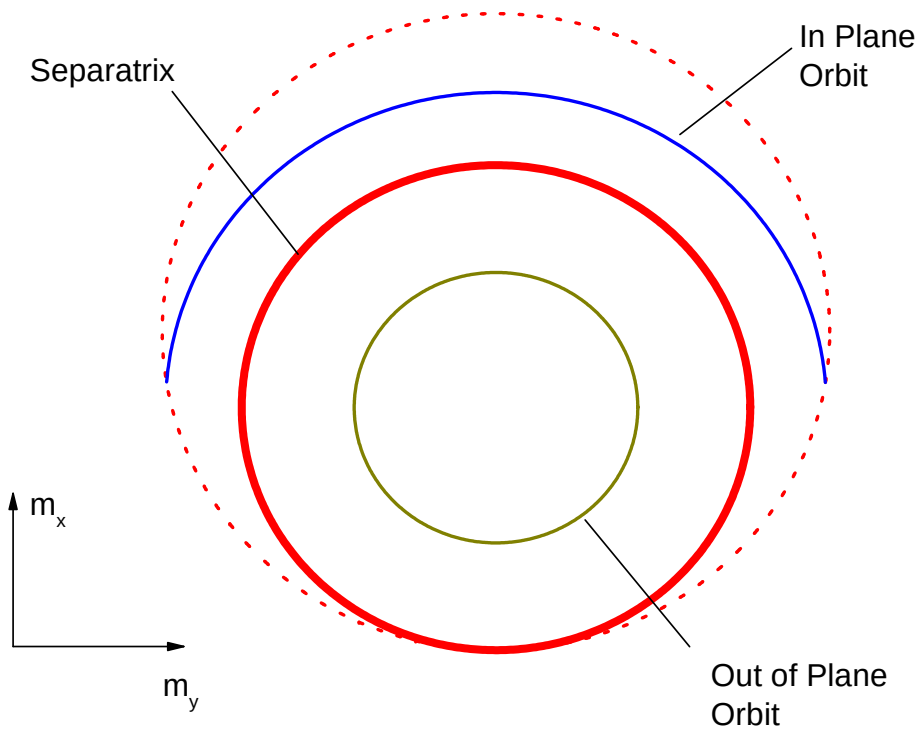

Figure 3.2: Neutral Orbits in $m_x - m_y$ plane. To illustrate the differences between different types of orbits, we choose an effective field $H_{eff} = 2000(Oe)$ and $4\pi M_s = 8400(Oe)$.

in the normal direction (m_z) is zero. Therefore it is called the in-plane motion. The *separatrix* is a special trajectory that separates the out-of-plane and in-plane trajectories in this case. The thicker solid orbit in Fig. 3.2 represents the separatrix. It appears when $R = 1 - h_e$ or say, $E = h_e$. The saparatrix touches the outer bound $m_x^2 + m_y^2 = 1$ (the dotted orbit in Fig. 3.2) at the energy saddle point ($m_x = -1,\ m_y = 0$).

Once the 2D trajectory in the $m_x - m_y$ plane is determined, the variable m_z can be reconstructed by considering Eq. (3.12). Thus, we can plot the 3D version of the energy conserved trajectories, shown in Fig. 3.3. The 3D version is also referred as an energy sphere. Every point on the energy sphere represents a fixed energy.

Notice that for a given energy that $E > h_e$, there are two degenerate out-of-plane orbits separated by the plane $m_z = 0$; however, for an energy $E < h_e$, there is only one in-plane orbit.

To obtain a solution for the energy conserved trajectory in terms of time, we first apply the following transformation according to Eq. (3.13),

$$m_x = -h_e + R\sin\theta \tag{3.14}$$

$$m_y = R\cos\theta \tag{3.15}$$

$$m_z = \pm\sqrt{2(E - h_e^2) + 2h_e R\sin\theta}. \tag{3.16}$$

Then, we need to consider the corresponding Equation of Motion, which is just Eq. (3.7) with $\alpha = 0$ and $a_j = 0$,

$$\frac{d\mathbf{m}}{dt} = -\mathbf{m} \times \mathbf{h}_{eff} \tag{3.17}$$

$$\frac{dm_x}{dt} = -m_y m_z. \tag{3.18}$$

Replace m_x, m_y and m_z by Eq. (3.14-3.16), we get a differential equation for the

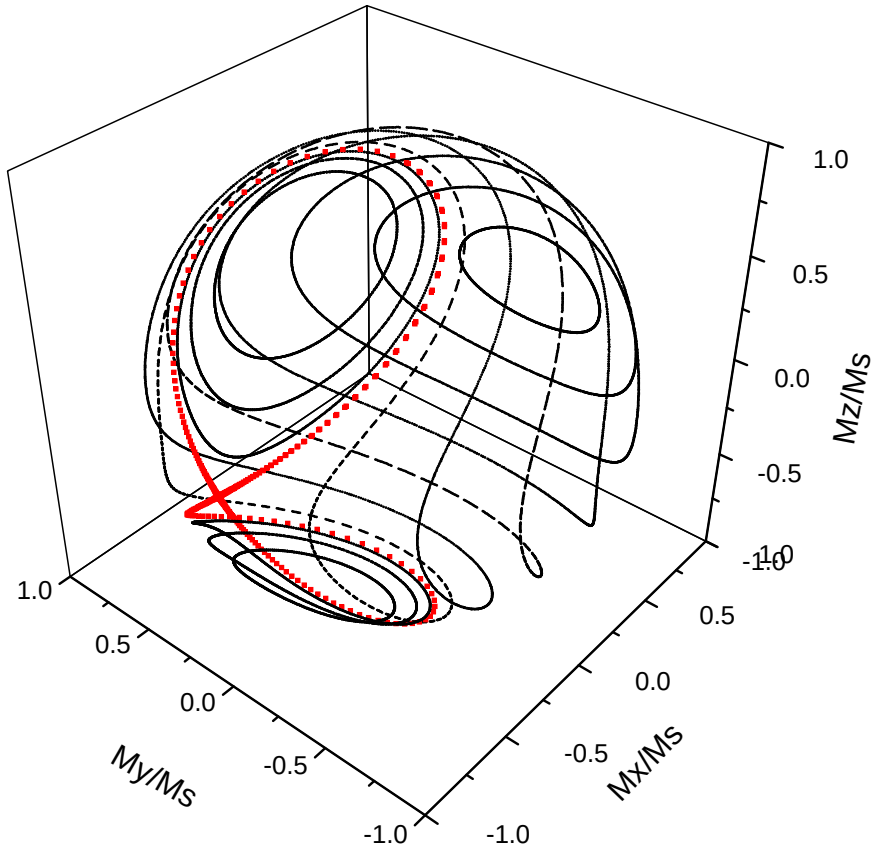

Figure 3.3: Energy Sphere. The dashed trajectory represents the separatrix which separates OOP and IP neutral orbits.

variable θ,

$$\begin{aligned} R\cos\theta\frac{d\theta}{dt} &= \pm R\cos\theta\sqrt{2(E-h_e^2)+2h_eR\sin\theta} \\ \frac{d\theta}{dt} &= \pm\sqrt{2(E-h_e^2)+2h_eR\sin\theta} \\ &= \pm\sqrt{a+b\sin\theta} \end{aligned} \tag{3.19}$$

where $a = 2(E - h_e^2)$ and $b = 2h_eR$.

Directly integrate Eq. (3.19), for $E > h_e$, $a > b$,

$$-\frac{2}{\sqrt{a+b}}F(\alpha,\ k) = \pm(t+t_0); \tag{3.20}$$

for $E > h_e$, $0 < |a| < b$,

$$-\sqrt{\frac{2}{b}}F(\beta,\ \frac{1}{k}) = \pm(t+t_0). \tag{3.21}$$

Here, F is the elliptic integral of the 1st kind [9] and the parameters are

$$\begin{aligned} \alpha &= \arcsin\sqrt{\frac{1-\sin\theta}{2}} \\ \beta &= \arcsin\sqrt{\frac{b(1-\sin\theta)}{a+b}} \\ k &= \arcsin\sqrt{\frac{2b}{a+b}} \end{aligned}$$

Notice that, the α and β here are not corresponding to damping and current density. Damping and current density are assumed to be zero here.

For Eq. (3.20),

$$\mathrm{sn}(F(\alpha,\ k)) = \pm\mathrm{sn}[\frac{\sqrt{a+b}}{2}(t+t_0)] \tag{3.22}$$

$$\sin\alpha = \pm\mathrm{sn}[\Omega_1(t+t_0)] \tag{3.23}$$

where

$$\Omega_1 = \frac{\sqrt{a+b}}{2}$$

and sn(·) is the Jacobian elliptic function [9]. Therefore,

$$\sin\theta = 1 - 2\mathrm{sn}^2[\Omega_1(t+t_0)]. \tag{3.24}$$

For Eq. (3.21),

$$\begin{aligned} \mathrm{sn}(F(\beta,\ \frac{1}{k})) &= \pm\mathrm{sn}[\sqrt{\frac{b}{2}}(t+t_0)] \qquad (3.25) \\ \sin\alpha &= \pm\mathrm{sn}[\Omega_2(t+t_0)], \qquad (3.26) \end{aligned}$$

where

$$\Omega_2 = \sqrt{\frac{b}{2}}.$$

Thus,

$$\sin\theta = 1 - \frac{a+b}{b}\mathrm{sn}^2[\Omega_2(t+t_0)]. \tag{3.27}$$

Putting back Eqs. (3.24) and (3.27) back into Eqs. (3.14-3.16), one will get the analytical solutions of the energy conserved trajectory. For OOP orbit,

$$\begin{aligned} m_x &= -h_e + R\{1 - 2\mathrm{sn}^2[\Omega_1(t+t_0)]\} \qquad (3.28) \\ m_y &= \pm R\sqrt{1 - \{1 - 2\mathrm{sn}^2[\Omega_1(t+t_0)]\}^2} \qquad (3.29) \\ m_z &= \pm\sqrt{2(E - h_e^2) + 2h_e R\{1 - 2\mathrm{sn}^2[\Omega_1(t+t_0)]\}}. \qquad (3.30) \end{aligned}$$

And for IP orbit,

$$\begin{aligned} m_x &= -h_e + R(1 - \frac{a+b}{b}\mathrm{sn}^2[\Omega_2(t+t_0)]) \qquad (3.31) \\ m_y &= \pm R\sqrt{1 - \{1 - \frac{a+b}{b}\mathrm{sn}^2[\Omega_2(t+t_0)]\}^2} \qquad (3.32) \\ m_z &= \pm\sqrt{2(E - h_e^2) + 2h_e R\{1 - \frac{a+b}{b}\mathrm{sn}^2[\Omega_2(t+t_0)]\}}. \qquad (3.33) \end{aligned}$$

These solutions are not the real trajectories for magnetization dynamics, because we have made the assumption that the damping and spin torque are zero, which does

not hold in reality. However, Melnikov Integral which can be used for determining the stable precessional orbit is based on these simplest unperturbed trajectories.

Another concern on these energy conserved trajectories is its response on perturbation. One can find these trajectories are not stable, any perturbation can kick a trajectory with certain energy to another trajectory with different energy. These precessional motions are neutral.

3.4 Stable Precessional Motions

Unlike the neutral motions, magnetization precession could be stable under the effect of appropriate damping and spin transfer torque. This is an example of so called stable limit cycles.

3.4.1 Limit Cycles

We've discussed the neutral precessional motion under the assumption that there is no damping and spin transfer torques. However, the damping is just like the friction force, which always exists. With the presence of damping effect, no neutral precessional motion will persist. If the damping is the only thing that changes the energy, the magnetization will eventually reach static equilibrium when the magnetic energy is minimized. When external forces such as an electric current is applied, they may exercise the magnetic energy, hence the magnetization will be driven toward a new direction or enter a different dynamic regime. The first dynamics beyond a fixed direction or a neutral precessional motion we will look at is the stable limit cycle.

A limit cycle is a trajectory that all neighboring trajectories approach it when $t \to \pm\infty$. For the case that the neighboring trajectories approach to the limit cycle when $t \to +\infty$, it is called an attractive or stable limit cycle. If the limit cycle is approached as $t \to -\infty$, it is a non-attractive or unstable limit cycle. Here, we are

only interested in the stable limit cycle and from now on we will ignore the word "stable" in most of situations. Fig. 3.4 and Fig. 3.5 show some examples of limit cycles in the spin valve systems.

At the first sight, the limit cycles look similar to the neutral precessional motions. However, they are different. Neutral motions are determined by its initial energy and once there is a perturbation of the energy, the trajectory is altered. While, limit cycles are usually not sensitive to the initial condition and won't be affected by small perturbations. Similar to neutral precessional motion, limit cycles do have a fixed period. As shown in the power spectra of the Fig. 3.4 and Fig. 3.5, well-defined frequency peaks exist.

3.4.2 Transition to Limit Cycles

How can a limit cycle be generated in the spin valve system? For a system that no external force exists, the magnetization stays at a fixed orientation where the energy is minimized. Now, we exert an external force, for example, we turn on an electric current. The current induced spin transfer torque has the similar form to the damping. If the current is applied in an appropriate direction, it may generate a torque against the damping. Increasing the current, after a critical point, the spin transfer torque is large enough to exercise the magnetization from its original fixed point and a balance between the damping and the spin transfer torque can be achieved. Once this balance is achieved, limit cycles appear. This transition from a fixed point to limit cycles which are actually periodic orbits is called a Hopf bifurcation. Fig. 3.6 shows a diagram of Hopf bifurcation in the spin valve system.

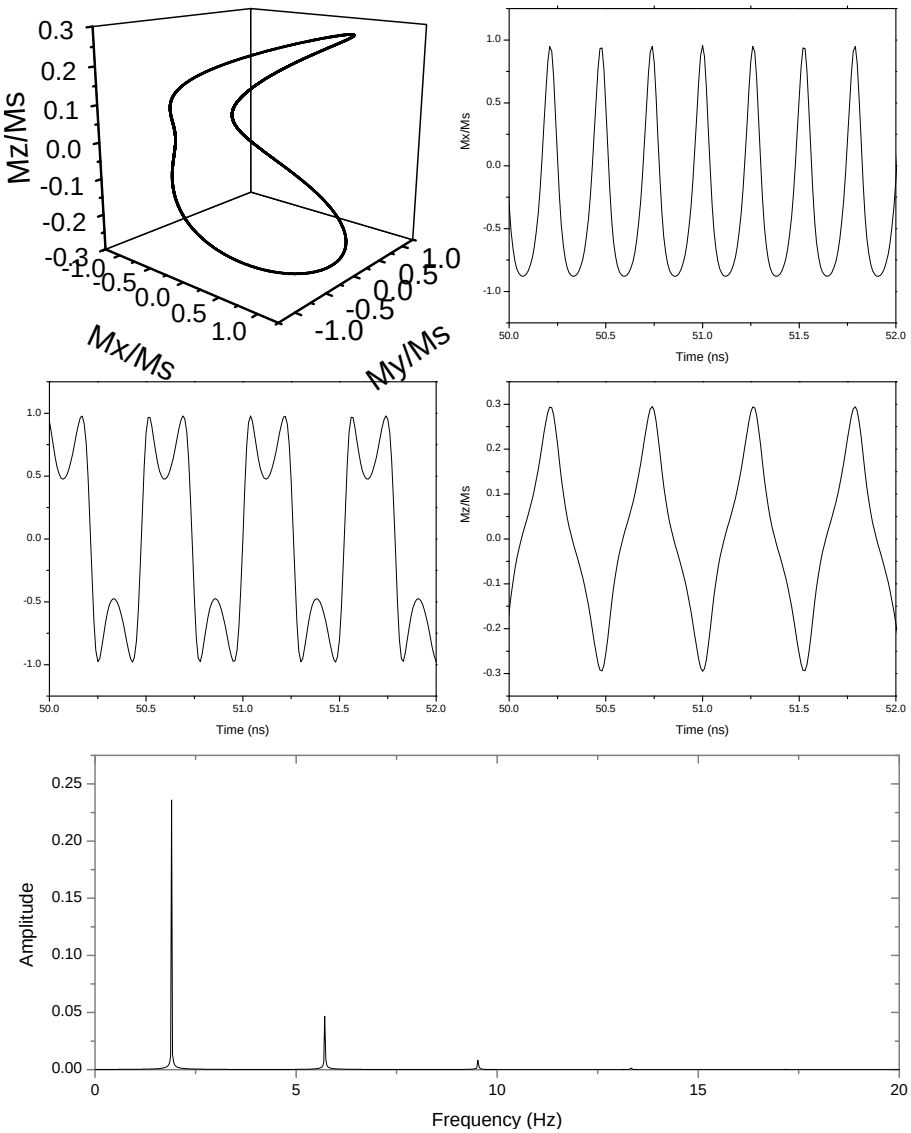

Figure 3.4: In-Plane Limit Cycle

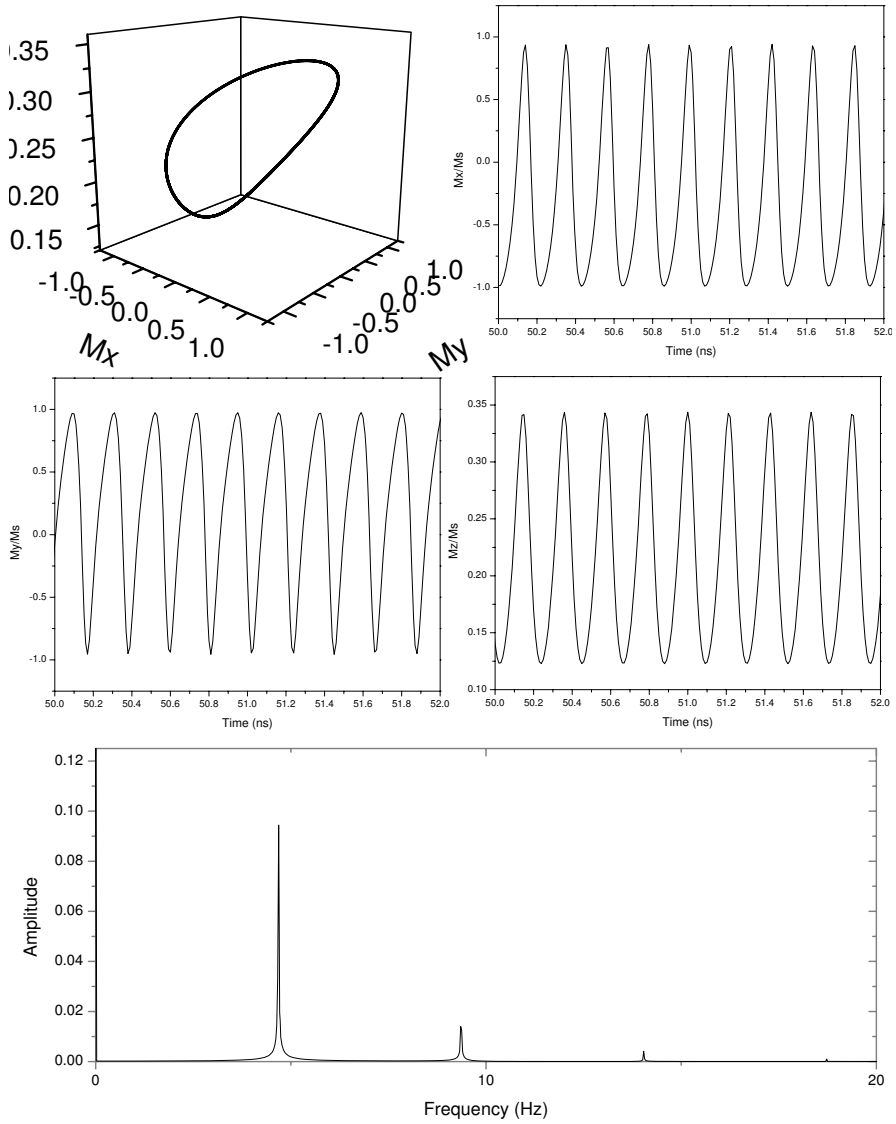

Figure 3.5: Out-of-Plane Limit Cycle

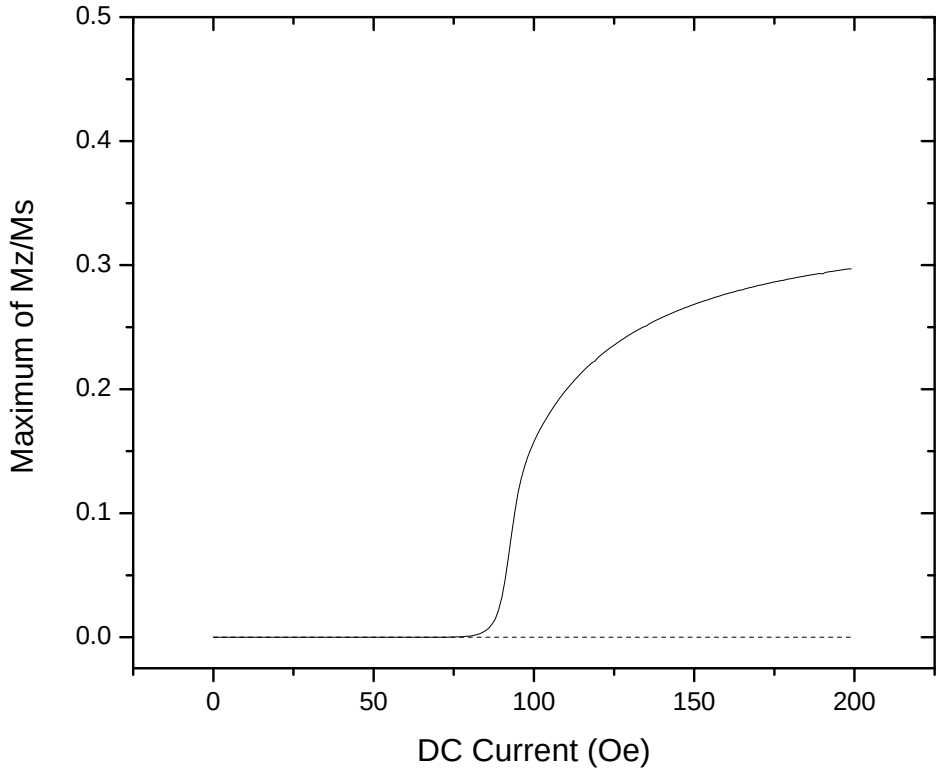

Figure 3.6: Magnetization is originally located at a fixed direction where the magnetic energy is at minimum. When Increasing the dc current, stable precessional orbit is excited. This is a Hopf Bifurcation procedure. For $H_{ext} = 200\ Oe$ and $\alpha = 0.02$, Hopf Bifurcation takes place when dc current increases to around 80 Oe.

3.4.3 Determining a Limit Cycle

The analytical solutions of neutral precessional motions have been given (see previous sections). How about limit cycles? Serpico *et al.* [8] developed a method to determine the limit cycles in spin valves by applying Melnikov Integral method.

Eq. (3.7) can be expressed as the following perturbation form,

$$\frac{d\mathbf{m}}{dt} = \mathbf{f}(\mathbf{m}) + \epsilon\mathbf{g}(\mathbf{m}) \tag{3.34}$$

where ϵ is a perturbation parameter and

$$\mathbf{f}(\mathbf{m}) = -\mathbf{m} \times \mathbf{h}_{eff},$$

$$\epsilon\mathbf{g}(\mathbf{m}) = \alpha\mathbf{m} \times \frac{d\mathbf{m}}{dt} + \beta\mathbf{m} \times (\mathbf{m} \times \mathbf{e}_p).$$

The unperturbed dynamics has been derived in the previous section. To study the dynamics in the presence of perturbation, one can construct the Melnikov integral along those unperturbed trajectories Ω,

$$M(E) = \int_\Omega \mathbf{m}_\Omega(t) \cdot (\mathbf{f} \times \mathbf{g})dt \tag{3.35}$$

where E is the energy of the unperturbed trajectories. Plugging into $\mathbf{f}$ and $\mathbf{g}$, one obtains,

$$\epsilon M(E) = \int_\Omega \left[-\alpha \left|\mathbf{m} \times \mathbf{h}_{eff}\right|^2 + \beta(\mathbf{m} \times \mathbf{h}_{eff}) \cdot (\mathbf{m} \times \mathbf{e}_p)\right] dt \tag{3.36}$$

Notice that the integrand is just time derivative of the magnetic energy density, therefore Melnikov Integral $\epsilon M(E)$ is understood as the work done by the damping and the spin transfer torque when magnetization precesses along the energy conservative orbit for exact one period.

A nonzero Melnikov Integral indicates the magnetic motion trends to deviate from the unperturbed orbit. While, if we integrate exact one period and find the Melnikov

integral is zero, the magnetic motion will not deviate at least at the point we start and stop our integral. Hence, we expect a complete trajectory with the same period as the unperturbed orbit even under perturbation.

This tentative argument can be confirmed by solid mathematical theorems (See the theorem 3 in Page 411 in Ref. [11]). When Melnikov Integral has simple zeros, that is, Melnikov Integral itself equals zero and its derivative to E is not zero, there exists limit cycles. If the derivative is positive, stable limit cycles exist. In spin valves, the stable limit cycle is the so called self sustained magnetization precessional motion.

Melnikov Integral for the system we are discussing is derived here by reproducing the similar approach Serpico *et al.* did in Ref. [8]. We first break down Eq. (3.36) into two terms,

$$\epsilon M(E) = -\alpha M_\alpha + \beta M_\beta \tag{3.37}$$

where

$$M_\alpha = \int_\Omega |\mathbf{m} \times \mathbf{h}_{eff}|^2 \, dt \tag{3.38}$$

and

$$M_\beta = \int_\Omega (\mathbf{m} \times \mathbf{h}_{eff}) \cdot (\mathbf{m} \times \mathbf{e}_p) dt. \tag{3.39}$$

M_α, M_β are expressed as,

$$M_\alpha = h_e^2 I_a + I_b + 2h_e I_c \tag{3.40}$$

$$M_\beta = h_e I_a + I_c \tag{3.41}$$

where

$$I_a = \int_\Omega (1 - m_x^2) dt \tag{3.42}$$

$$I_b = \int_\Omega m_z^2 (1 - m_z^2) dt \tag{3.43}$$

$$I_c = \int_\Omega (m_x m_z^2) dt \tag{3.44}$$

Now, we can plug the exact solutions of m_x, m_y and m_z (Eq. (3.28-3.33)) into above equations to evaluate Melnikov Integral. However, to avoid the complex forms of expansions of the Jacobian Elliptic functions in the exact result, we can plug in Eq. (3.14-3.16) and consider the following approximations for OOP orbits,

$$\int_\Omega \sin\theta dt = 0 \tag{3.45}$$

$$\int_\Omega \sin^2\theta dt = \frac{1}{2}. \tag{3.46}$$

Also notice that for small h_e, we neglect the terms containing h_e^2. Therefore,

$$I_a = \frac{1}{2}(1+2E)T_\Omega \tag{3.47}$$

$$I_b = E(1-2E)T_\Omega \tag{3.48}$$

$$I_c = h_e(1-2E)T_\Omega, \tag{3.49}$$

where T_Ω is the period of the orbit. For OOP orbits, it can be derived as,

$$T_\Omega = \int_\Omega dt \tag{3.50}$$

$$= \int_\Omega \frac{1}{\sqrt{a+b\sin\theta}} d\theta \tag{3.51}$$

$$= \frac{4K(k)}{\sqrt{a+b}}. \tag{3.52}$$

where $K(k)$ is the complete Elliptic function of the first kind.

Replace I_a, I_b and I_c in Eq. (3.40) and Eq. (3.41) by Eq. (3.47-3.49),

$$M_\alpha = 2E(1-2E)T_\Omega \tag{3.53}$$

$$M_\beta = h_e(\frac{3}{2}-3E)T_\Omega. \tag{3.54}$$

One condition for the existence of stable limit cycle is

$$\epsilon M(E) = 0,$$

thus,

$$\alpha M_\alpha = \beta M_\beta \tag{3.55}$$

$$\alpha[2E(1-2E)]T_\Omega = \beta h_e(\frac{3}{2} - 3E)T_\Omega. \tag{3.56}$$

Therefore, the solution is,

$$E = \frac{3\beta}{4\alpha} h_e.$$

That is to say, Melnikov Integral along the orbit of energy $\frac{3\beta}{4\alpha} h_e$ may have simple zero, and limit cycle can establish. Other conditions fixed, the orbit is determined by the DC current. The energy of the orbit is approximately proportional to the DC current.

Bibliography

[1] M. Tsoi, A. G. M. Jansen, J. Bass, W.-C. Chiang, M. Seck, V. Tsoi, and P. Wyder, Phys. Rev. Lett. **80**, 004281 (1998).

[2] E. B. Myers, D. C. Ralph, J. A. Katine, R. N. Louie, and R. A. Buhrman, Science **285**, 867(1999).

[3] W. H. Rippard, M. R. Pufall, S. Kaka, T. J. Silva, S. E. Russek, and J. A. Katine, Phys. Rev. Lett. **95**, 067203(2005).

[4] S. Kaka, M. R. Pufall, W. H. Rippard, T. J. Silva, S. E. Russek, J. A. Katine, Nature (London) **437**, 389(2006).

[5] F. B. Mancoff, N. D. Rizzo, B. N. Engel, S. Tehrani, Nature (London) **437**, 393(2006).

[6] J. Grollier, V. Cros, and A. Fert, Phys. Rev. B **73**, 060409(R) (2006).

[7] J. C. Slonczewski, J. Magn. Magn. Mater. **159**, L1(1996).

[8] G. Bertotti, I. D. Mayergoyz and C. Serpico, Physica B**343**, 325(2004).

[9] I. S. Gradshteyn and I. M. Ryzhik, *Table of Integrals, Series and Products*, (Oxford : Academic, 2007).

[10] C. Serpico, M. d'Aquino, G. Bertotti, and I. D. Mayergoyz, J. Magn. Magn. Mater. **290-291**, 502(2005).

[11] L. Perko, *Differential Equations and Dynamical Systems*, (Springer, New York, 1996).

Chapter 4

Synchronization in Spin Transfer Oscillators

Synchronization describes a fixed phase relation between the response and driven dynamics. The relation can be simply equality or in general, a rational multiple relation. It is a key feature of nonlinear dynamics. Due to the nonlinearity of Landau-Lifishitz-Gilbert equation, the magnetization oscillations also have this property.

4.1 Introduction

4.1.1 Synchronization

Synchronization is understood as an "adjustment of rhythms of oscillating objects due to their weak interaction" [1]. The rhythm is usually characterized as period of frequency. Thus, quantitatively, synchronization leads to frequency locking of different oscillating objects.

As early as in the seventeenth century, Huygens found the oscillations of two pendulum clocks that were hanging on a common support coincided with the pendula moving in opposite directions. This is probably the first study of synchronization.

In Huygens' system, two pendulum clocks synchronized; this is recognized as mutual synchronization. However, the oscillating objects are not necessarily to be

the same type. As long as they have interactions, synchronization can take place. For example, an oscillating object can be synchronized to a periodic external force.

4.1.2 Synchronization in Spin Valves

In the last chapter, we have looked into the magnetization dynamics. Governed by Landau-Lifshitz-Gilbert equation, in the presence of spin transfer torque, magnetization vector can have a self-sustained oscillation. Applying a periodic external force such as an ac current, the spin transfer torque will have an ac component. Affected by the oscillating spin transfer torque, magnetization oscillation may be synchronized to the its frequency which is equal to the frequency of the ac current.

Experimental Observation of the external force driven synchronization in spin valve system was first reported by Rippard *et.al.* in 2005 [2]. The theoretical study was carried out via phase dynamics [3, 4]. We will show an alternative approach later in this chapter to study the synchronization.

Mutual synchronization in spin valves was observed by two unrelated experimental groups independently [5, 6]. Numerical simulations were done to study a series of spin valve oscillators [7]. In these studies, two or more spin valve oscillators have interactions to each other. Unlike the external force synchronization, this synchronization is due to the mutual effect; oscillator A impacts oscillator B, and at the same time, oscillator B impacts oscillator A as well. In the previous case, ac current, which can be regarded as an oscillator, impacts the magnetization oscillators. However, on the contrary, the ac current will not be affected by magnetization oscillation, so that it is a one-way effect. We will focus on the ac current driven synchronization phenomena in this dissertation.

4.2 Numerical Simulations

To numerically simulate the synchronization to ac current in spin valve systems, we first establish a limit cycle. Starting from an arbitrary point other than stable point or saddle point on the sphere $|m| = 1$, choosing an appropriate set of parameters, applying regular ODE algorithm, the limit cycle is usually achieved after several nanoseconds.

Once this self sustained magnetization oscillation becomes stable, we determine its natural frequency by measuring the inverse of the average of time intervals between succussive minima of m_x. Then, we turn on an ac current, which induces an ac component of spin transfer torque. The frequency is chosen to be close to the measured natural frequency; the amplitude is small, usually less then one-tenth of the dc component of the spin transfer torque.

When the limit cycle is not close to the separatrix, one can find the magnetization oscillation will adjust its phase automatically so that its frequency tends to be the same as the frequency of ac current. Compared to this synchronization phenomenon, when no ac current is turned on, the frequency of limit cycle varies almost linearly with the dc current. In the presence of the ac current, the frequency of magnetization oscillation is a strongly nonlinear function of dc current. In a certain range of dc current, the frequency is fixed and equal to the frequency of the ac current. The experimental observations of synchronization are usually presented in this way, e.g., Fig. 1(b) in Ref. [2]. In the next section, we will use Melnikov Integral method to determine the synchronization region.

In the Fig. 4.1, we show the synchronization region in two different representations. The topper panel describes the relation between response frequency and a parameter of the magnetic system, the dc current; the lower panel presents the difference between

the response frequency and the natural frequency of the oscillator (beating frequency) as a function of the difference between the frequency of ac current and the natural frequency (detune frequency).

There are two assumptions here. First, the amplitude of ac current is relatively small. Second, limit cycles are not close enough to separatrix. If the real condition is deviated from these assumptions, either with a large ac current amplitude, or with a trajectory close to separatrix, chaos may occur. Discussion on chaotic dynamics will be deferred to next chapter.

At zero temperature, simulations suggest that when synchronization occurs, the oscillation has a well defined frequency, which is identical to the frequency of the external ac current. In the power spectrum (see Fig. 4.2), the frequency peak shift from the natural frequency to the frequency of the ac current. From the time domain illustration, Fig. 4.3, one can see that the phase shift between ac current and the magnetization is automatically adjusted to be fixed.

Simulation also suggests that the larger the amplitude of ac current is, the wider the synchronization region. The relation of synchronization region width and ac current amplitude is numerically determined (See Fig. 4.4). An analytically proof is provided in the next section.

The synchronization occurs as well when ac current has a frequency close to the subharmonic frequency of the magnetization oscillation. When the external frequency is close to $\frac{m}{n}$ times of the natural frequency, the magnetization oscillation is synchronized to $\frac{n}{m}$ of the external frequency, see Fig. 4.5. This issue will be also discussed in the next section.

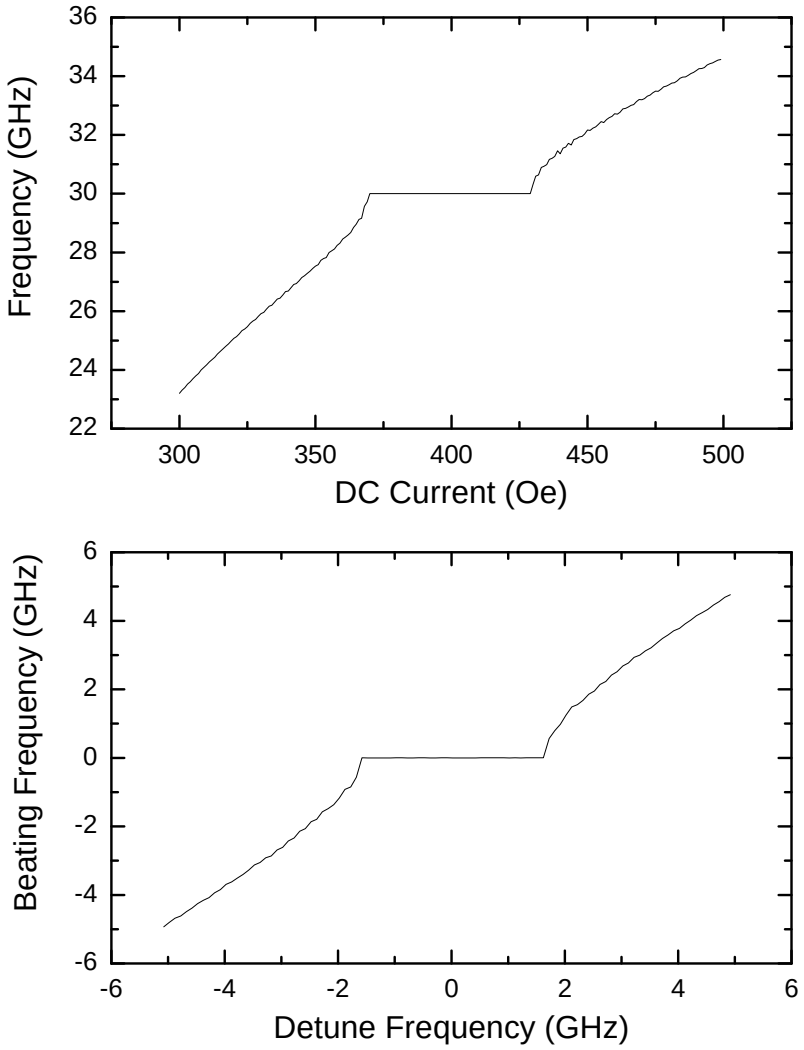

Figure 4.1: Synchronization Region. The topper panel shows that varying dc current, the frequency of the oscillation is locked in the synchronization region. The lower panel shows that within synchronization region, the frequency of oscillation is identical to the frequency of the ac current. Here, detune frequency is defined as the frequency difference between ac current and natural frequency; beating frequency is defined as the frequency difference between ac current and the oscillator. The parameters are: $H_{ext} = 200(Oe)$; $a_{ac} = 20(Oe)$; topper panel: $\omega_{ac} = 30GHz$; lower panel: $a_{dc} = 400(Oe)$

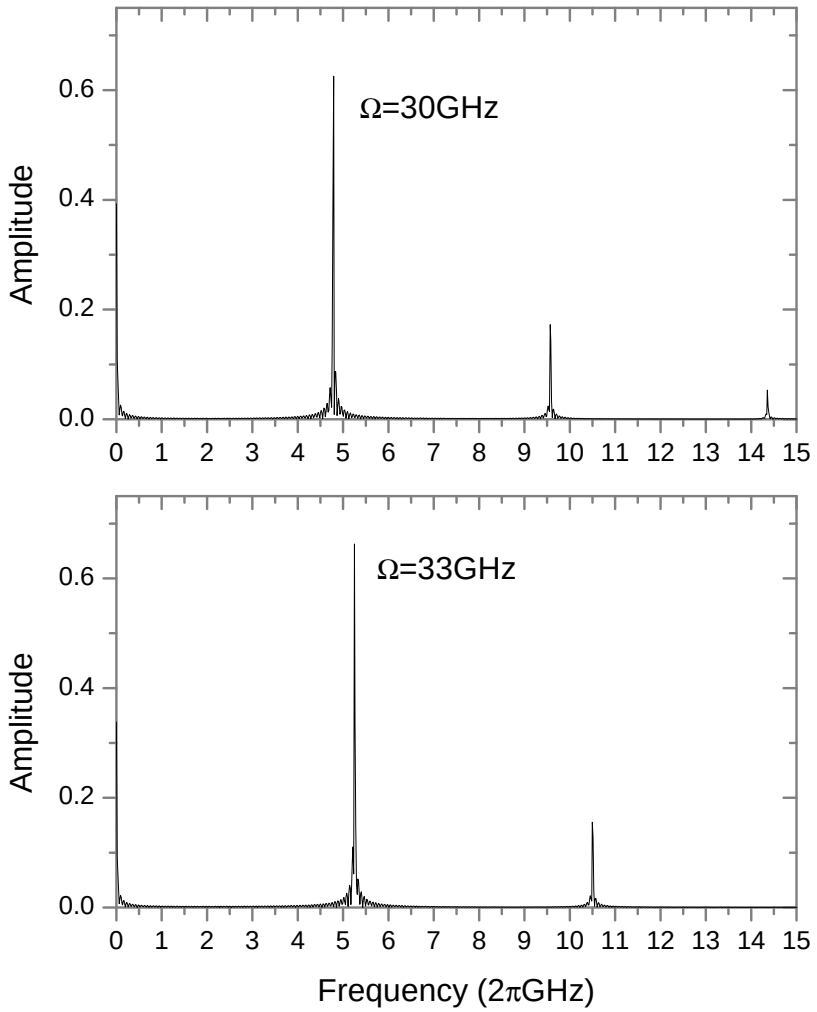

Figure 4.2: Power spectra before and after synchronization. Natural frequency is 30GHz. After applying an ac current with amplitude 30 Oe and frequency 33GHz, the frequency peak of the spin transfer oscillator is shift to 33GHz, identical to that of ac current.

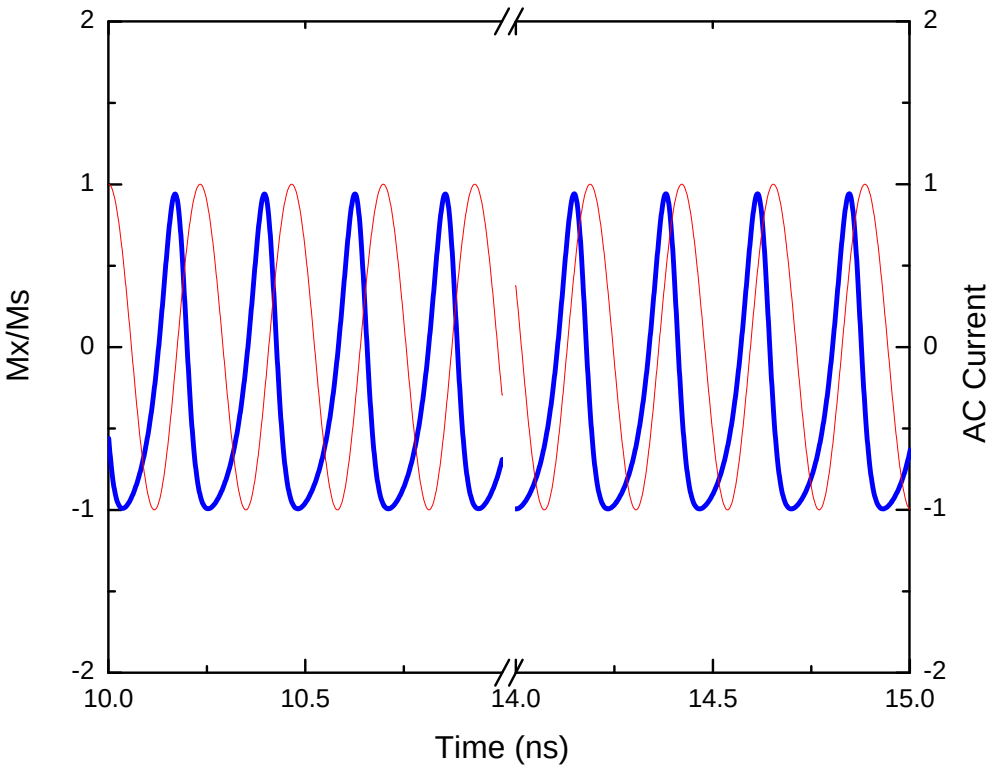

Figure 4.3: Phase Locking. Turning on ac current with an arbitrary phase difference between ac current and the magnetization, they will be eventually locked in their phase.

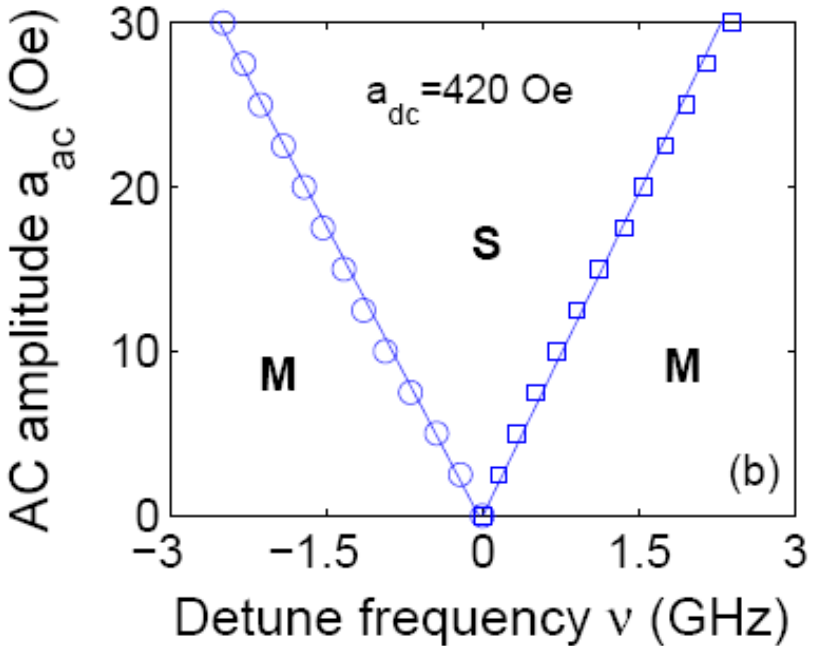

Figure 4.4: With the increase of the amplitude of ac current, the synchronization region will be wider. The region width is proportional to the amplitude of the ac current.

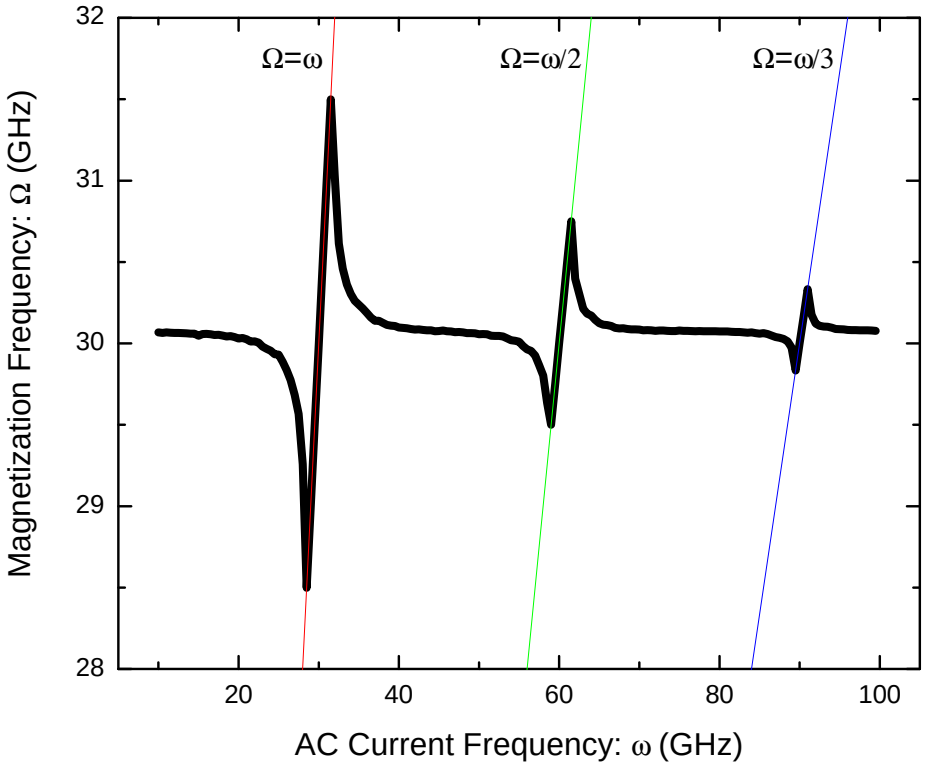

Figure 4.5: Driven by ac current, the spin valve oscillator can synchronized to different fractions of the frequency of the ac current

4.3 Melnikov Integral Method

The regular theoretical approach to these nonlinear dynamics could be phase dynamics [3, 4]. Here, we seek an alternative approach. We extend the Melnikov Integral method used for determining limit cycles (see previous chapter or Ref. [8]) to the synchronization phenomena.

4.3.1 Synchronization to Fundamental Frequency

In the last chapter, we discussed how to apply Melnikov Integral to determine limit cycles in spin valve oscillators. When Melnikov Integral itself is zero and its derivative to the orbit energy is negative (simple zero), there exists a limit cycle. That is to say, the simple zero of Melnikov Integral indicates a complete trajectory. For limit cycles, both external field and electrical current are fixed. Now, we include an ac current with a small amplitude. Since its amplitude is small, we can regard the ac current as an additional perturbation to the Melnikov Integral.

Just like what we did in determining the limit cycle, we calculate the work done by the damping and the spin transfer torque along an energy conserved trajectory loop, which has a frequency of Ω_0. If the damping and time-invariant component of spin transfer torque give a simple zero in Melnikov Integral, we claim a limit cycle. In addition, the time-dependent component of spin transfer torque, whose frequency is set to Ω_0, gives an extra amount in Melnikov Integral. If it is zero, the trajectory still completes after its originally period, i.e., its frequency is Ω_0. However, in general, this extra contribution to Melnikov Integral could be non-zero. Therefore, the trajectory is not complete, and the energy has a positive or negative shift after the loop integral. We argue that, this shift can be compensated by change in the fixed component of spin transfer torque, that is, the change of the dc current.

As long as the ac current perturbation to the Melnikov Integral can be offset by changes in dc current contribution, the trajectory is complete after the same period as the energy conserved orbit. The trajectory therefore still has a frequency of Ω_0, which is the same as that of the ac current, i.e. the spin valve oscillator is synchronized to the ac current. Thus we can now theoretically predict the range of dc current, in which the trajectory precesses at a fixed frequency.

As we just mentioned above, we assume the frequency of the ac current identical to that of the energy conserved precessional orbit, along which we conduct the Melnikov Integral, i.e. $\omega = \Omega_0 = \frac{2\pi}{T_\Omega}$. We express the Melnikov Integral in this case as following,

$$M = -\alpha M_\alpha + \beta M_\beta + \beta_{ac} M_{ac} \tag{4.1}$$

where M_α and M_β are the same as those in the last chapter; β_{ac} is the normalized amplitude of ac current; and

$$M_{ac} = \int_0^{T_\Omega} \cos(\omega t + \phi_0)[(\mathbf{m} \times \mathbf{h}_{eff}) \cdot (\mathbf{m} \times \hat{e}_p)]dt.$$

Notice that there is an arbitrary phase ϕ_0 in the ac current $\beta_{ac}\cos(\omega t + \phi_0)$. If we choose this phase appropriately, the third term in Eq. (4.1) can be just zero. In this case, ac current has no effect on the Melnikov Integral. The trajectory has the same frequency as that of the integral orbit, which is Ω_0. If the phase is chosen so that the third term in Eq. (4.1) is not zero, one can change the dc current correspondingly to bring the value of Eq. (4.1) back to zero. Thus the frequency of trajectory is still Ω_0.

One can it reversely. Based on an established stable limit cycle, which has a simple zero Melnikov Integral, if the dc current is changed, in the absence of ac current, the net change of Melnikov Integral leads to a change its energy stage, and the frequency of the trajectory is changed. On the other hand, in the presence of ac current, the trajectory will adjust its phase by itself so that the change in Melnikov

Integral generated by the change of dc current is balanced by the contribution of the ac current, that is, the amount of the third term in Eq. (4.1).

Therefore, there exits a range of dc current, within which ac current can adjust its phase to bring the Melnikov Integral back to zero. This range is nothing but the synchronization region. Thus, to determine the synchronization region, we just need to calculate the largest adjustment the ac current can make to Melnikov Integral.

Following this procedure, we break the dc current torque into two terms $\beta = \beta_0 + \delta\beta$, where β_0 makes $-\alpha M_\alpha + \beta_0 M_\beta$ simple zero as we have discussed in limit cycles case. Thus, Eq. (4.1) reduces to,

$$M = \delta\beta M_\beta + \beta_{ac} M_{ac}. \tag{4.2}$$

Using the notations

$$M_1 = \int_0^T \cos\omega t[(\mathbf{m} \times \mathbf{H}_{eff}) \cdot (\mathbf{m} \times \hat{e}_p)]dt,$$

and

$$M_2 = \int_0^T \sin\omega t[(\mathbf{m} \times \mathbf{H}_{eff}) \cdot (\mathbf{m} \times \hat{e}_p)]dt,$$

for simple zero of Melnikov Integral,

$$\delta\beta M_\beta + \beta_{ac}\cos\phi_0 M_1 - \beta_{ac}\sin\phi_0 M_2 = 0. \tag{4.3}$$

Because ϕ_0 is an arbitary phase, the above equation has infinite many solutions. Setting

$$\begin{aligned} \cos\psi_0 &= \frac{M_1}{\sqrt{M_1^2 + M_2^2}} \\ \sin\psi_0 &= \frac{M_2}{\sqrt{M_1^2 + M_2^2}}, \end{aligned} \tag{4.4}$$

we have

$$|\cos(\omega t_0 + \psi_0)| = \left| \frac{\delta\beta M_\beta}{\beta_{ac}\sqrt{M_1^2 + M_2^2}} \right| \leq 1.$$

Thus, as long as

$$-\left|\frac{\beta_{ac}\sqrt{M_1^2+M_2^2}}{M_\beta}\right| \leq \delta\beta \leq \left|\frac{\beta_{ac}\sqrt{M_1^2+M_2^2}}{M_\beta}\right|, \tag{4.5}$$

there exist simple zero of Melnikov Integral. In other words, when

$$\beta_0 - \left|\frac{\beta_{ac}\sqrt{M_1^2+M_2^2}}{M_\beta}\right| \leq \beta \leq \beta_0 + \left|\frac{\beta_{ac}\sqrt{M_1^2+M_2^2}}{M_\beta}\right|, \tag{4.6}$$

adjusting ϕ_0 appropriately, the magnetization trajectory will complete one period as ac current completes exact one period. Therefore, the frequency of the spin valve oscillator is identical to ω, the frequency of the ac current.

The above range is the synchronization range for dc current. Fig. 4.6 compares numerical simulation of synchronization and the synchronization range determined by Melnikov Integral.

Taking a closer look at M_{ac}, $U(t) = (\mathbf{m} \times \mathbf{H}_{eff}) \cdot (\mathbf{m} \times \hat{e}_p)$ is a periodic function with period T_Ω, where $\mathbf{m} = \mathbf{m}(t)$ is a precessional orbit. Choosing the arbitrary ϕ_0 appropriately, $U(t)$ has the form of

$$\sum_{n=0}^{\infty} a_n \cos(n\omega t)$$

Therefore, $M_2 = 0$, and

$$\begin{aligned} M_1 &= a_1 \sum_{n=0}^{\infty} \int_0^{T_\Omega} \cos(\omega t)\cos(n\omega t)dt \\ &= a_1 \int_0^T \cos^2(\omega t)dt = \frac{1}{2}a_1 T = \frac{\pi a_1}{\omega}. \end{aligned}$$

Putting them into Eq. (4.5) or (4.3), a simpler requirement for $\delta\beta$

$$-\frac{\pi\beta_{ac}}{\omega}\left|\frac{a_1}{M_\beta}\right| < \delta\beta < \frac{\pi\beta_{ac}}{\omega}\left|\frac{a_1}{M_\beta}\right|. \tag{4.7}$$

From this relation, it is clear that the width of synchronization band are proportional to amplitude of ac current and inversely proportional to frequency of ac current. The

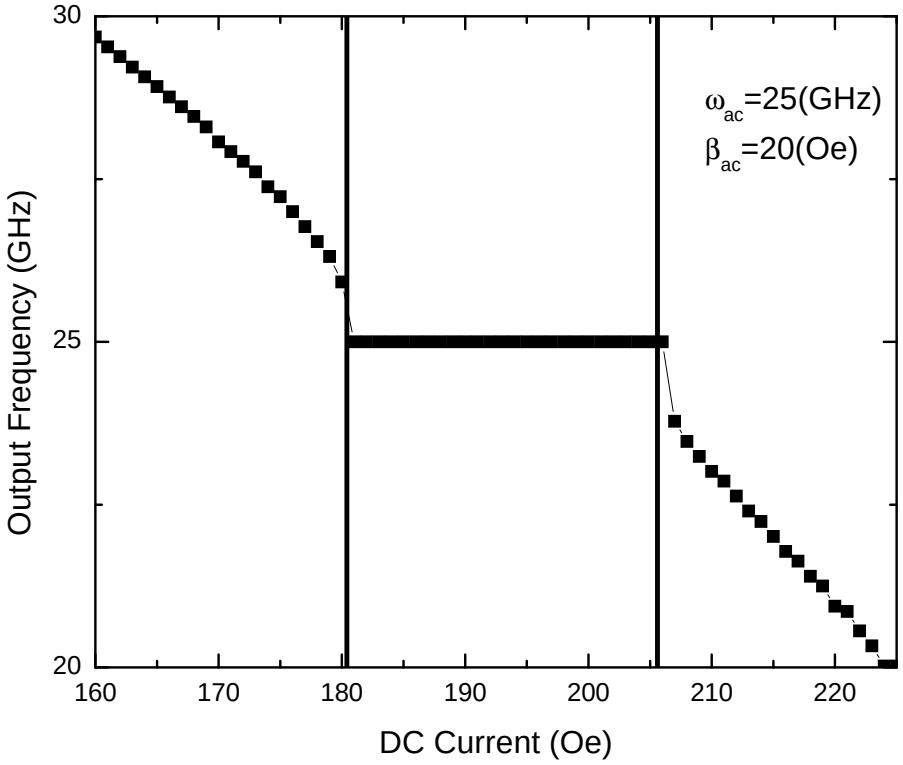

Figure 4.6: Synchronization in In-plan orbits. Vertical lines are predicted by Melnikov Integral. $H_{eff} = 200\ Oe$; other parameters are shown in the diagram.

former relation has already been revealed by Eq. (4.5) and shown in Fig. 4.4. The latter relation can be verified by numerical simulation of the synchronization phase diagram (see Fig. 4.7), which will be shown in next chapter.

We have considered the synchronization of spin valve oscillators to a simplest external periodic force, ac current. In coupled spin valve oscillators, each oscillator drives an oscillating signal, which can be treated as periodic external force for other oscillators. Another complication is that this effect is a mutual effect, that is one oscillator generates signals but meanwhile it receives signals from other oscillators. We may view the case we discussed in this section as a one-way effect and those mutual synchronization as two-way effect.

4.3.2 Synchronization to Subharmonic Frequency

As mentioned previously, it is not necessary that ac frequency ω is close to the natural frequency of spin valve oscillators Ω_0. Whenever $\frac{\omega}{\Omega_0}$ is rational, one may have an opportunity to observe synchronization phenomena. Suppose $n\omega$ is close to $m\Omega_0$ where both m and n are positive integers, the response oscillator may oscillate exact n periods when the driven force oscillates m periods. Thus, one observes

$$nT_{STO} = mT_{ac}$$

or

$$m\Omega_{STO} = n\omega_{ac}$$

where the T_{STO} and Ω_{STO} are the period and frequency of the spin transfer oscillator in response of the driven ac current; the T_{ac} and ω_{ac} are the period and frequency of the ac current. The phase diagram of these general synchronization is shown in Fig. 4.7.

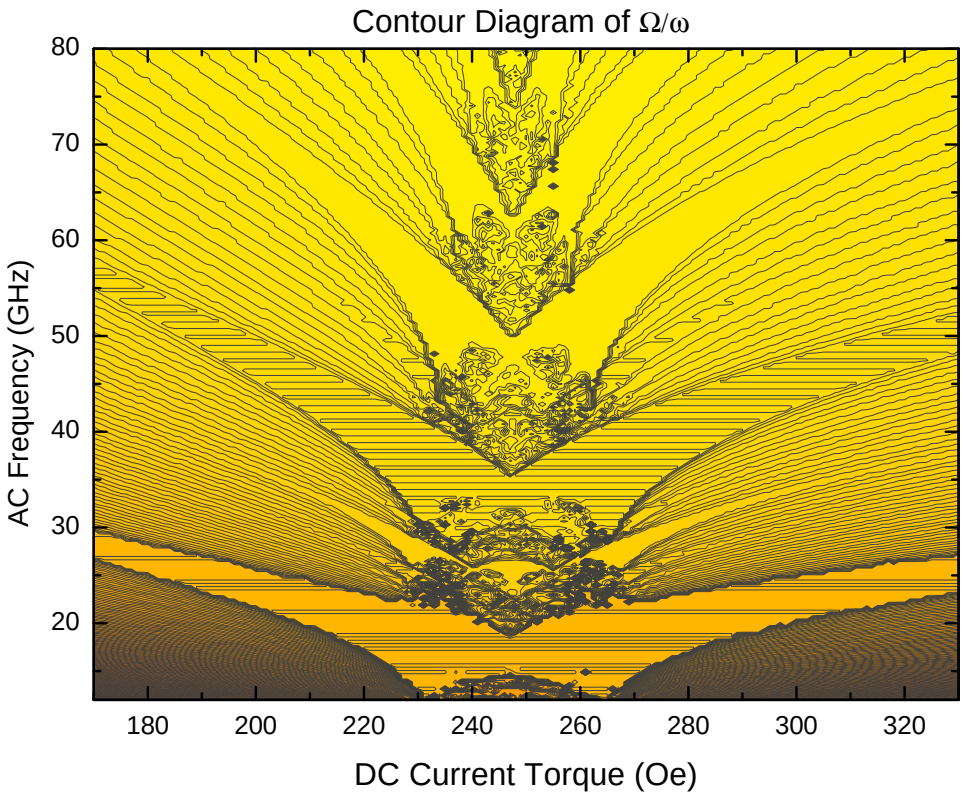

Figure 4.7: Numerical simulations of synchronization bands. We encode the ratio of response frequency to driven frequency into different color and the lines are contour lines. In each band, $m\Omega_{STO} = n\omega_{ac}$ where m and n are integers.

The synchronization region for this general case can also be determined by constructing Melnikov Integral. Again, one can start from a established stable limit cycle with a frequency of Ω_0, which has a simple zero Melnikov Integral. Turning on a small amplitude ac current with a frequency of $\frac{m}{n}\Omega_0$, we modify M_1 and M_2 as,

$$M_1 = \int_0^{nT_0} \cos(\frac{m}{n}\omega t)[(\mathbf{m} \times \mathbf{h}_{eff}) \cdot (\mathbf{m} \times \hat{e}_p)]dt$$

and

$$M_2 = \int_0^{nT_0} \sin(\frac{m}{n}\omega t)[(\mathbf{m} \times \mathbf{H}_{eff}) \cdot (\mathbf{m} \times \hat{e}_p)]dt.$$

Then, calculate the maximum deviation of Melnikov Integral made by changes of dc current that can be compensated by ac current due to the phase shift. Thus, the synchronization region is determined in a range of dc current.

Notice that, in the expressions of M_1 and M_2, there is another thing different from previous subsection. When construct Melnikov Integral, one need to integral over nT_0 instead of T_0, the natural period of the spin valve oscillators. Suppose $m\Omega_0 = n\omega$, considering $T_0 = \frac{2\pi}{\Omega_0}$ and $T_{ac} = \frac{2\pi}{\omega}$, one easily gets $mT_{ac} = nT_0$. That is to say, once synchronization happens, the time interval of n periods of spin valve oscillators matches the time interval of m periods of ac current.

Fig. 4.8 shows several synchronization bands determined by Melnikov Integral which are consistent with the direct simulation result shown in Fig. 4.7. Within each synchronization band, spin valve oscillators are synchronized to a different fraction of the driven frequencies.

We noticed that all of the synchronization bands overlap in a vertical stripe. Within this stripe, at a certain set of parameters, since the synchronization bands overlap, a spin valve oscillator may be "synchronized" to infinitely many different fractions of the driven frequency. That is, the spin valve oscillator actually can not determine a fixed frequency. This corresponds to chaos. We will discuss chaos in spin

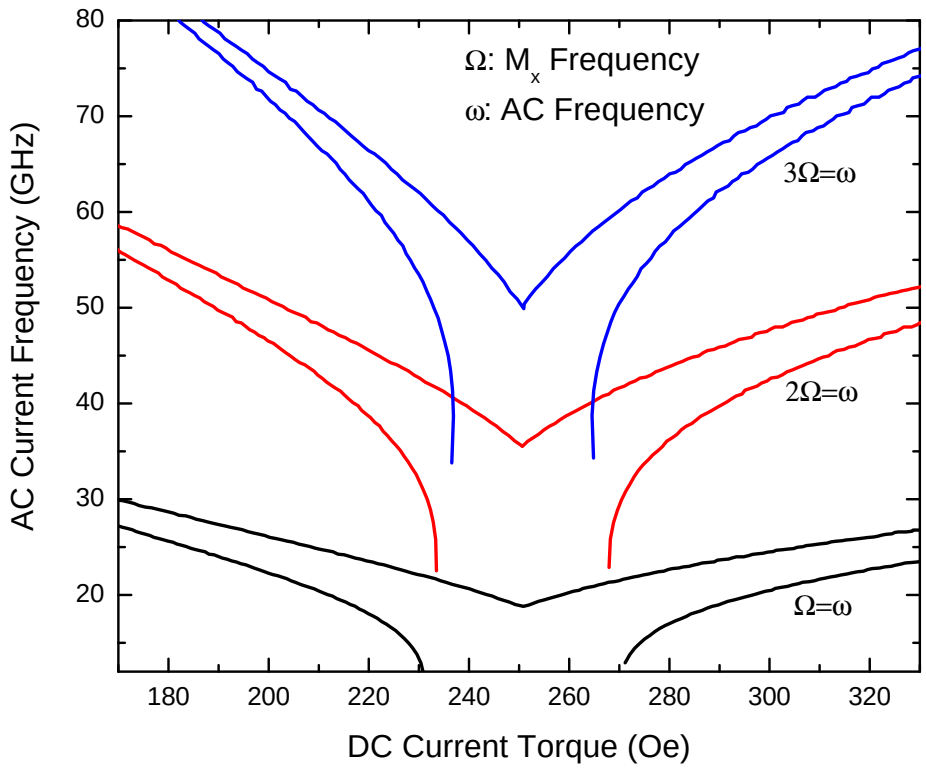

Figure 4.8: Synchronization Bands predicted by Melnikov Integral method. Within each band, the frequencies of spin transfer oscillators are synchronized to ω, $\omega/2$ and $\omega/3$

transfer oscillators in the next chapter.

Bibliography

[1] A. Pikovsky, M. Rosenblum, and J. Kurths, *Synchronization: A Universal Concept in Nonlinear Sciences* (Cambridge University Press, Cambridge, 2001).

[2] W. H. Rippard, M. R. Pufall, S. Kaka, T. J. Silva, S. E. Russek, and J. A. Katine, Phys. Rev. Lett. **95**, 067203 (2005).

[3] A. N. Slavin, and V. S. Tiberkevich, Phys. Rev. B **72**, 092407 (2005).

[4] A. N. Slavin, and V. S. Tiberkevich, Phys. Rev. B **74**, 104401 (2006)

[5] S. Kaka, M. R. Pufall, W. H. Rippard, T. J. Silva, S. E. Russek, and J. A. Katine, Nature (London) **437**, 389 (2005) .

[6] F. B. Mancoff, N. D. Rizzo, B. N. Engel, and S. Tehrani, Nature (London) **437**, 393 (2005) .

[7] J. Grollier, V. Cros, and A. Fert, Phys. Rev. B **73**, 060409(R) (2006).

[8] C. Serpico, M. d'Aquino, G. Bertotti, and I. D. Mayergoyz, J. Magn. Magn. Mater. **290-291**, 502(2005).

Chapter 5

Chaos in Spin Transfer Oscillators

Chaos is essentially an intrinsically unstable trajectory. We are unable to predict the future state of a chaotic system. Much attention has been paid to chaos through out mathematics, physics and engineering societies. There are a couple physics systems such as the Josephson junction that may behave chaotically. The spin transfer induced magnetization oscillation can also be chaotic. In this chapter, we investigate chaos in spin valve oscillators.

5.1 Motivation

Among many well-studied non-linear oscillators driven by external forces, only a handful oscillators have technological applications [1, 2]. The recently discovered current-driven magnetization oscillators with tunable microwave frequencies in spin valves are very desirable for magnetic storage devices and for telecommunications. Up until now, theoretical and experimental studies of the oscillator have been carried out only for the simplest cases where the dynamics of the oscillator is either in a self-sustained steady-state precessional motion (limit cycle) [3–8] or in synchronization with other oscillator(s) [9–13]. Since the equation that governs the oscillator is highly non-linear, it would be fundamentally interesting to map out the full dynamics for experimen-

tally relevant parameters. In particular, a thorough study of chaotic dynamics will elucidate how the current-driven oscillator responds to an external perturbation.

5.2 Nonlinear Equation of Motion

Nonlinear differential equations usually have irregular behaviors like synchronization and chaos. Nonlinearities are the crucial points to generate these behaviors. The Landau-Lifshitz-Gilbert Equation

$$\frac{d\mathbf{m}}{dt} = \mathbf{m} \times \mathbf{h}_{eff} + \alpha \mathbf{m} \times \frac{d\mathbf{m}}{dt} + a_j \mathbf{m} \times (\mathbf{m} \times \mathbf{e}_p), \tag{5.1}$$

which governs the magnetization dynamics in spin transfer oscillators, is also a set of nonlinear differential equations. It's natural to expect spin transfer oscillators have those nonlinear behaviors. It is true, but only when time-dependent external forces are applied to the system. The reason why we need external forces is that LLG equation is essentially a 2D differential equation set when both external field and spin torque driven by current are not time-dependent. The magnetization are oscillating in the 3D space, however, since the temperature is usually far from Curie temperature, the magnitude of the magnetization is fixed. This constrain reduces the system to 2D.

It is believed that in a 2D nonlinear system, there is no possibility that chaos can exist. Therefore, to study chaos in spin valve oscillators, we have to turn on ac currents or ac fields. Both ac currents and ac fields generate an explicit time variable in Eq. (5.1). Thus, the system is extended to 3D, and chaos becomes possible.

5.3 Existence of Chaos

In what circumstance chaos can take place in spin valve oscillators? After showing the numerical examples of chaos in spin valve oscillation, we use Melnikov Integral

to predict the region that chaos could happen, and Lyapunov Exponents to reveal where chaos really is.

5.3.1 Numerical Evidence

Based on a regular dynamics such as a limit cycle, chaos can be generated by changing the system parameters. Since introducing ac current makes it possible to observe interesting nonlinear features, a straightforward means to generate chaos is increasing the ac current amplitude. When the amplitude is comparable to dc current, it can no longer be treated as a perturbation and synchronization phenomena is replaced by chaotic dynamics. Fig. 5.1 shows chaos driven by large amplitude ac current for a spin valve oscillator.

One usually observes chaos by increasing parameters of a regular nonlinear dynamics. Large ac current driven chaos is just a particular case. Indeed, the ac current pass through the device will not be so high. The device will probably be burnt before chaos can be seen by increasing the ac amplitude because the frequency of ac current is about gigahertz. In the last chapter, we mentioned that in a vertical stripe, the spin valve oscillation does not have a fixed frequency. This may indicate the existence of chaos. As we will show later, chaos appears in a certain region of dc current (within the vertical stripe) with a fixed amplitude ac current.

That is, one can adjust the dc current instead of the ac current to generate chaotic dynamics in spin valve oscillators. Fig. 5.2 shows chaos in this case. By sweeping dc current from low to high (or from high to low), one can find spin valve oscillation behaves regularly (synchronization) then chaotic then back to regularly. Notice that in this case, ac current amplitude is very small.

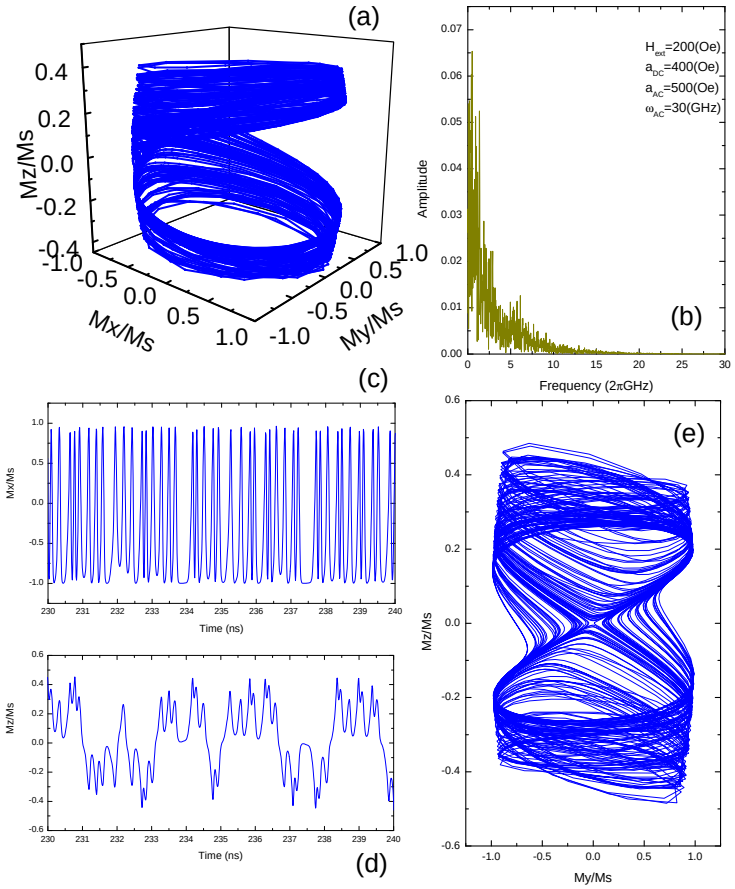

Figure 5.1: Chaos driven by large ac spin transfer torque. (a) 3D trajectory; (b) Power Spectrum of m_z; (c) Trajectory of m_x in time domain; (d) Trajectory of m_z in time domain; (e) Trajectory of m_y-m_z plane.

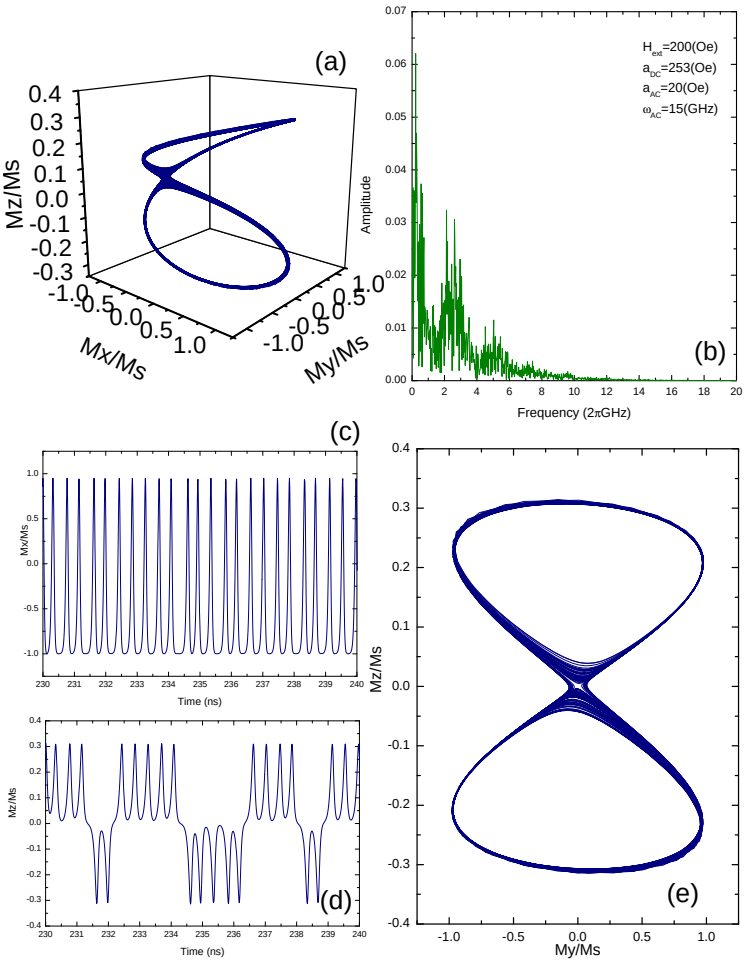

Figure 5.2: Chaos driven by small ac spin transfer torque. (a) 3D trajectory; (b) Power Spectrum of m_z; (c) Trajectory of m_x in time domain; (d) Trajectory of m_z in time domain; (e) Trajectory of m_y-m_z plane.

5.3.2 Melnikov Integral

Melnikov Integral provides an approach to determine the synchronization region. We have discussed it for spin valve oscillators in the previous chapter. Now, we apply this technique to determine the chaos region. This time the integral is taken along separatrix. Separatrix is a special orbit that passes the saddle point. On the separatrix, the trajectory has the same energy as saddle point energy; On the energy sphere, separatrix separates out-of-plane and in-plane energy orbits. One crucial property for separatrix is that its period is infinite. Similar to the determining the synchronization, if we can get simple zeros after integrating along the separatrix, we may "synchronize" to separatrix. Therefore the trajectory should also have an infinite period.

Melnikov theorem says, simple zeros of Melnikov Integral along separatrx indicates existence of homoclinic orbit; around homoclinic orbit, chaos exists.

To take the integral along the separatrix, we need to know the equation of it. For the spin valve oscillator model that we investigated in the last chapter, the separatrix is derived as following.

Calculating separatrices connected to a saddle point ($m_x = -1, m_y = 0, m_z = 0$), one can obtain a pair of homoclinic orbits in the parameter range of $h_k < h_e < h_k + 1$ (Homoclinic orbit theorem [14]),

$$m_x = M_0 - 1 \tag{5.2}$$

$$m_y = \pm\sqrt{M_0[2(h_k + 1 - h_e) - (h_k + 1)M_0]} \tag{5.3}$$

$$m_z = \pm\sqrt{M_0[2(h_e - h_k) + h_k M_0]} \tag{5.4}$$

where

$$M_0 = \frac{4C_1 e^{-\tau}}{(e^{-\tau} - C_2)^2 - 4C_1 C_3} \tag{5.5}$$

$$\tau = \sqrt{C_1}(t_1 + t_0), t_1 = 4\pi M_s \gamma t \tag{5.6}$$

$$C_1 = 4(h_e - h_k)(h_k + 1 - h_e), \tag{5.7}$$

$$C_2 = 2[h_k(h_k + 1 - h_e) - (h_e - h_k)(h_k + 1)], \tag{5.8}$$

$$C_3 = -h_k(h_k + 1) \tag{5.9}$$

in which t_0 is a real parameter. It is found that the pair of homoclinic orbits are asymptotic to the saddle point when $t \to \pm\infty$.

Now, we construct Melnikov Integral along this trajectory.

$$G = E_0 + \frac{h_k - h_e}{2}(m_x^2 + m_y^2 + m_z^2) \tag{5.10}$$

The Melnikov integral is given by

$$U = -\alpha U_1 + \beta_1 U_2 + \beta_2 \cos(\frac{\omega t_0}{4\pi M_s \gamma})U_3 + \beta_2 \sin(\frac{\omega t_0}{4\pi M_s \gamma})U_4 \tag{5.11}$$

where

$$U_1 = \int_{-\infty}^{+\infty} \boldsymbol{\nabla} G \cdot [\mathbf{m} \times (\mathbf{m} \times \mathbf{H}_{eff})] d\tau$$

$$U_2 = \int_{-\infty}^{+\infty} \boldsymbol{\nabla} G \cdot [\mathbf{m} \times (\mathbf{m} \times \mathbf{e}_x)] d\tau$$

$$U_3 = -\int_{-\infty}^{+\infty} \cos \frac{\omega\tau}{4\pi M_s \gamma \sqrt{C_1}} \boldsymbol{\nabla} G \cdot [\mathbf{m} \times (\mathbf{m} \times \mathbf{e}_x)] d\tau$$

$$U_4 = -\int_{-\infty}^{+\infty} \sin \frac{\omega\tau}{4\pi M_s \gamma \sqrt{C_1}} \boldsymbol{\nabla} G \cdot [\mathbf{m} \times (\mathbf{m} \times \mathbf{e}_x)] d\tau$$

are evaluated along the homoclinic orbits Eq. (3).

In general, the simple zero of the Melnikov integral implies the existence of a homoclinic orbit. Around the homoclinic orbit, chaos is often generated (Chaos theorem [14, 15]).

Setting $U = 0$, one obtains that

$$\cos(\frac{\omega t_0}{4\pi M_s \gamma} - \psi) = \frac{\alpha U_1 - \beta_1 U_2}{\beta_2 \sqrt{U_3^2 + U_4^2}} \tag{5.12}$$

where

$$\cos\psi = \frac{U_3}{\sqrt{U_3^2 + U_4^2}}, \sin\psi = \frac{U_4}{\sqrt{U_3^2 + U_4^2}} \tag{5.13}$$

thus as long as

$$|\alpha U_1 - \beta_1 U_2| \leq |\beta_2|\sqrt{U_3^2 + U_4^2} \tag{5.14}$$

U has zeros. Direct calculation shows that the zeros of U lie in the vertical band region in Fig. 1. The existence of a pair of transversal homoclinic orbits follows from standard arguments [15] for parameters near the zeros of U. Then the existence of chaos can be rigorously proved in a neighborhood of the pair of homoclinic orbits via a shadowing lemma [14, 15].

We can see that, there is an undetermined initial phase in the Melnikov Integral approach. This phase make it impossible to get exact solutions for simple zeros. We can only predict a region, in which, chaos can exist, see Fig. 5.3 To precisely determine where is chaos in the phase diagram, we need the help of Lyapunov exponents.

5.3.3 Lyapunov Exponents

The unpredictability of chaos is due to the sensitivity to initial conditions. Two trajectories of a system that initially close will diverge exponentially. Lyapunov exponents provides a measurement of this stability. It can be expressed as the following mathematical form,

$$\lambda_i = \lim_{t\to\infty} \frac{1}{t} \ln \frac{\|\delta m_t^i\|}{\|\delta m_0^i\|} \tag{5.15}$$

where λ_i is the ith Lyapunov exponent and $\|\delta m_t^i\|$ is the separation between the trajectories of the ith orthogonal axis at time t. One may choose the initial points in a small sphere. With the evolution of the dynamics, the sphere becomes an ellipsoid. The ith axis corresponds to the ith axis of the ellipsoid. See Ref. [16, 17] for more general explanation. When $\lambda_i > 0$, the distance between two arbitrarily close points

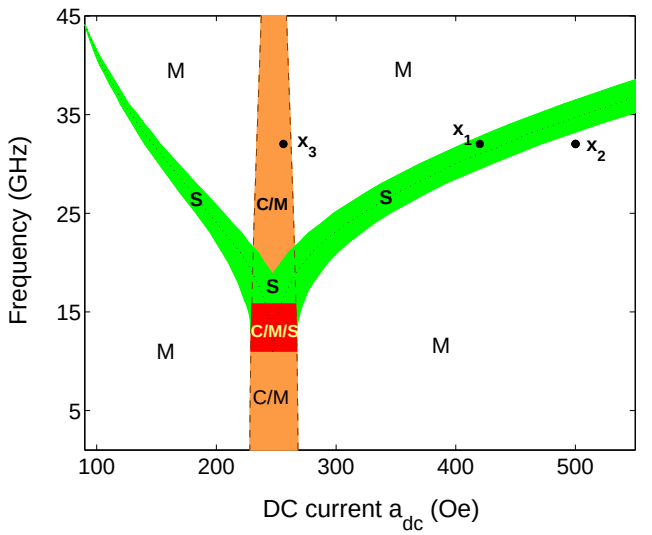

Fig.1

Figure 5.3: Magnetization dynamic phase diagram driven by dc and ac currents. The external field is fixed at 200 Oe and the amplitude of the ac current $a_{ac} = 20$ Oe. Three phases are: synchronization (S), modification (M) and chaos (C). The dotted line is the frequency of the limit cycle in the absence of the ac current. The analytical results from the Melnikov criterion of chaos are shown in the two nearly vertical dashed lines. Fig. 1 in [18]. Used under authors' permission.

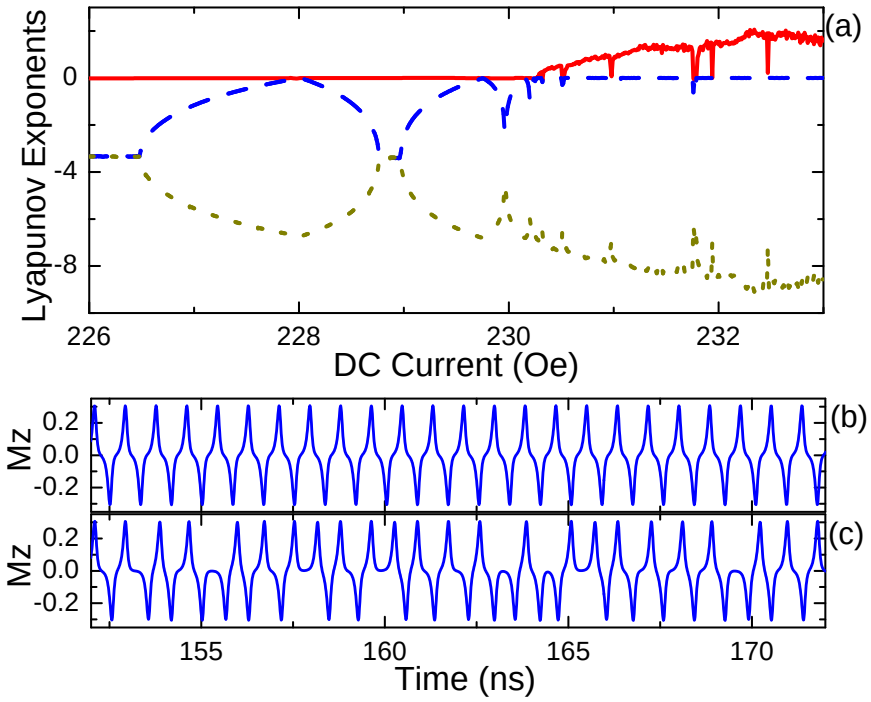

Figure 5.4: Lyapunov Spectrum of the spin valve oscillator. External field is 200(Oe), ac current amplitude is 20(Oe), ac current frequency is 15GHz

will increase exponentially along the i-axis at a large t [17].

For a bounded dynamic system, any positive Lyapunov exponent indicates chaos. We use this property of chaos to map out the chaotic phase in phase diagram. Insert a figure containing the boundary of chaos, chaos point indicated by positive Lyapunov exponent.

Lyapunov exponents are numerically computed for spin valve oscillators and Fig. 5.4(a) shows an example of the Lyapunov spectra, where the largest exponent is shown in red solid line and the other two are in dashed and dotted lines. When a_j is smaller than the critical value $230.03(Oe)$, all three Lyapunov exponents are non-positive and thus the dynamics are non-chaotic, see Fig. 5.4(b). When a_j becomes larger than $230.03(Oe)$, the largest Lyapunov exponents become positive, and thus chaos appears

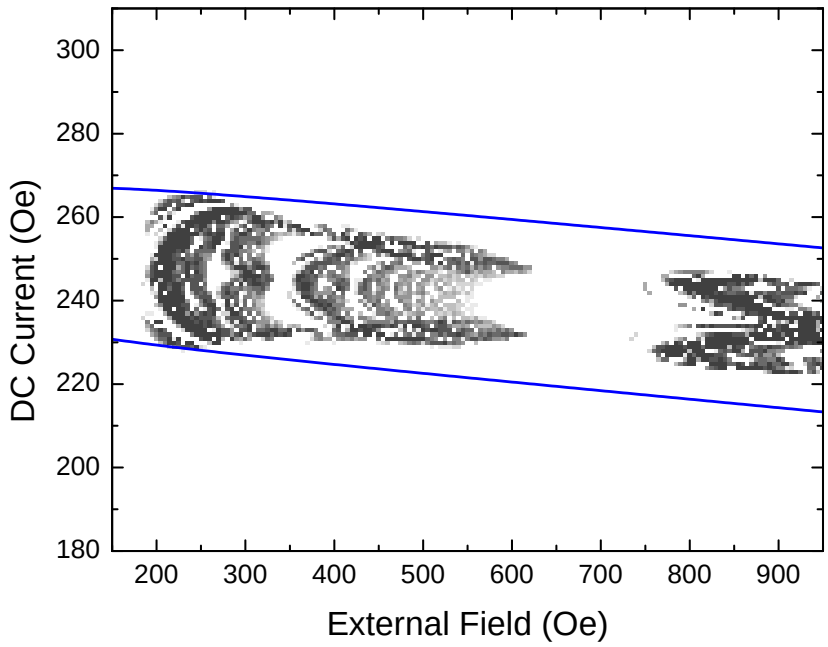

Figure 5.5: Chaotic dynamics phase of the spin valve oscillator indicated by dark points. ac current amplitude is 20(Oe), ac current frequency is 15GHz

[Fig. 5.4(c)].

By varying the parameters of the dc current and the external field, we have mapped out the parameters that give arise at least one positive Lyapunov exponent, shown as the dark area in Fig. 5.5.

5.4 Route to Chaos

5.4.1 Poincaré Map

Complex chaotic systems usually embed simpler maps. The analysis of chaos can much simplified by extracting maps from its original continuous dynamics.

For a continuous dynamical system that evolves in time space and has the dimension larger than two, one can construct a two-dimensional Poincaré map. Usually,

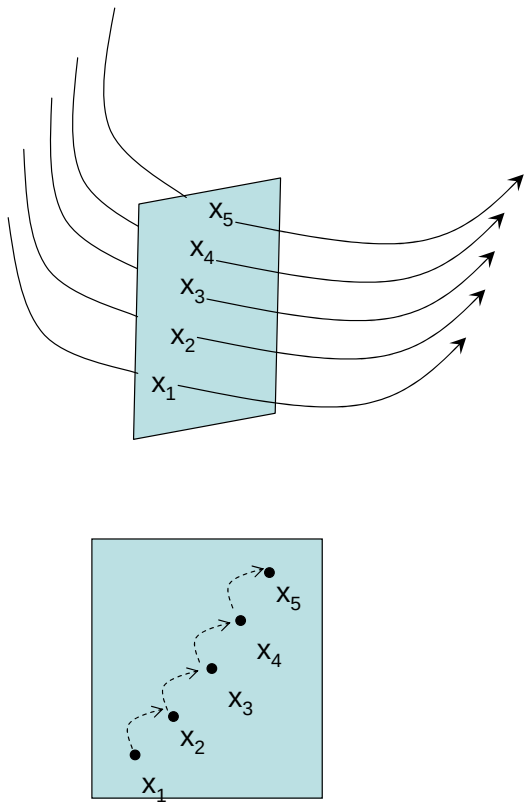

Figure 5.6: Illustration of Poincaré Map.

a section of surface is selected so that the trajectory crosses the section successively after some time intervals. Thus, the continuous time dynamics becomes a discrete time map. The time series t_i is defined as the time when the trajectory intersects the selected section, where i is non-negative integer. The intersection coordinates are measured and assigned to the corresponding time t_i, expressed as $\mathbf{x}_i = \mathbf{x}(t_i)$. Now, one obtains a discrete map because the following value of $\mathbf{x}_i$, $\mathbf{x}_{i+1}$ is determined by $\mathbf{x}_i$, or say, $\mathbf{x}_{i+1} = \mathbf{F}(\mathbf{x}_i)$.

To investigate the route to chaos in spin valve systems, we applied the Poincaré map. In spin valve oscillators, it is difficult to choose a simple Poincaré section because a simple section can hardly intersect both out-of-plane and in-plane orbits

simultaneously. To avoid this difficulty, we measure the trajectory points every time a local minimum of m_x is reached. Therefore, at the infinite time sequence ...t_i, t_{i+1}, t_{i+2}, ... when local minimum of m_x is reached, the magnetization vector is measured and assigned to that time point. Thus, we obtain a sequence of $\mathbf{m_i}$ is recorded and a map function $\mathbf{m}_i + 1 = \mathbf{F}(\mathbf{m}_i)$ is constructed.

5.4.2 Periodic Doubling Bifurcation

By either increasing the ac current amplitude or sweeping dc current from non-chaotic region to chaotic region, the trajectory of spin valve oscillators experiences a process called periodic doubling bifurcation.

Unlike the Hopf bifurcation we mentioned in the route to limit cycles, a limit cycle is already established in this case. As we move close to chaos by changing the parameter, the complete limit cycle will not come back to its original point after one period. Instead, the trajectory has to wait for another period to be completed. The trajectory is now called period two orbit. And the change from a one-period limit cycle to a period two orbit is referred as a period doubling bifurcation.

Moving closer to chaos, after another period doubling bifurcation, the trajectory will not be completed until four original periods. Then it's called period four orbit. Continuously changing the parameter, a sequence of period doubling bifurcations are observed. Correspondingly, period 2^n orbit, where n is non-negative integers appears. When n approaches ∞, the trajectory becomes chaos.

Period 2^n orbits with increasing n are shown Fig. 5.7 to Fig. 5.9, which represent the route of period doubling bifurcation to chaos for spin valve oscillators.

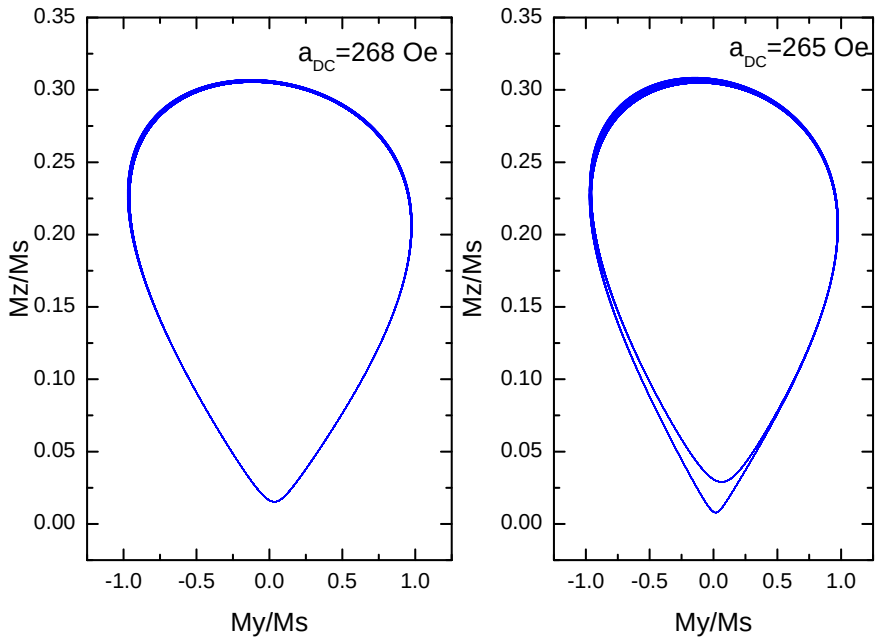

Figure 5.7: Limit Cycle (left) and Period Two Orbit (right). ac current amplitude is 20 Oe, ac current frequency is 15 GHz and external field is 200 Oe. dc currents are shown in the diagrams.

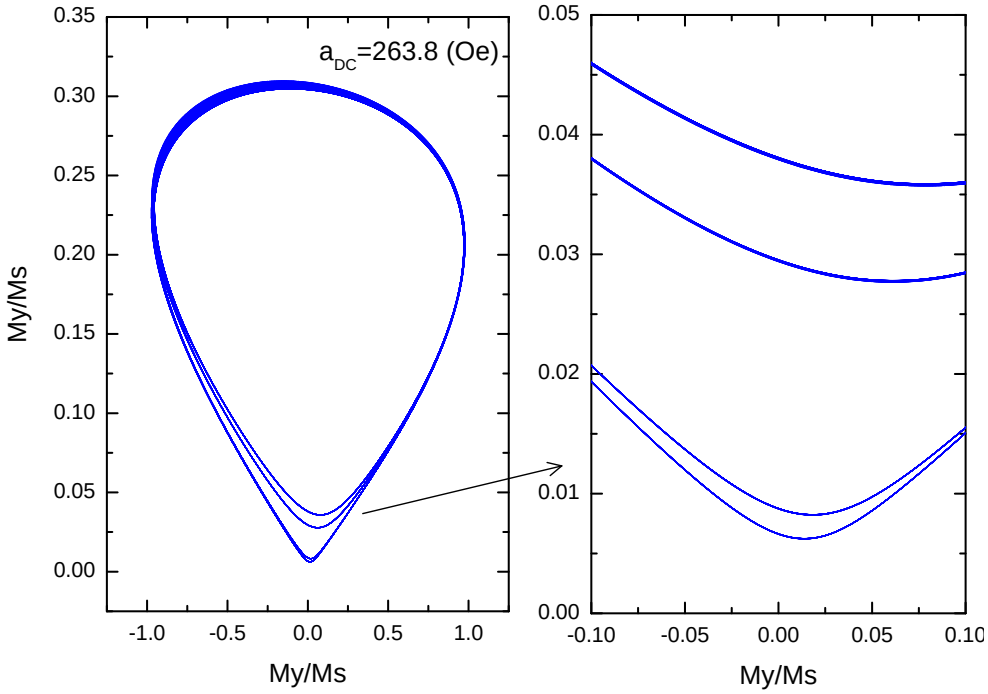

Figure 5.8: Period Four Orbit. ac current amplitude is 20 Oe, ac current frequency is 15 GHz and external field is 200 Oe. dc current is shown in the diagram.

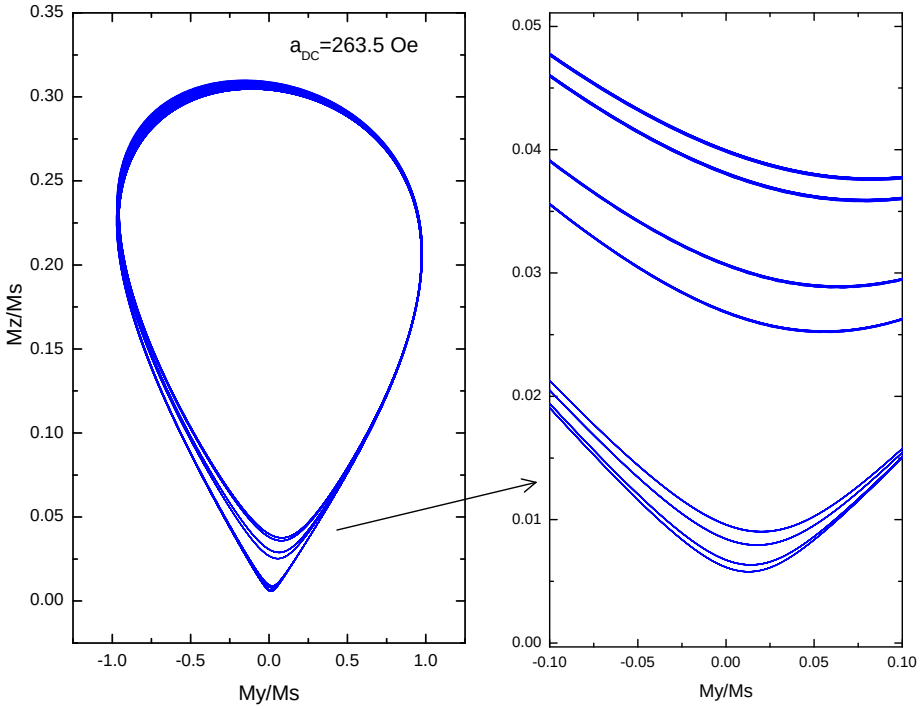

Figure 5.9: Period Eight Orbit. ac current amplitude is 20 Oe, ac current frequency is 15 GHz and external field is 200 Oe. dc current is shown in the diagram.

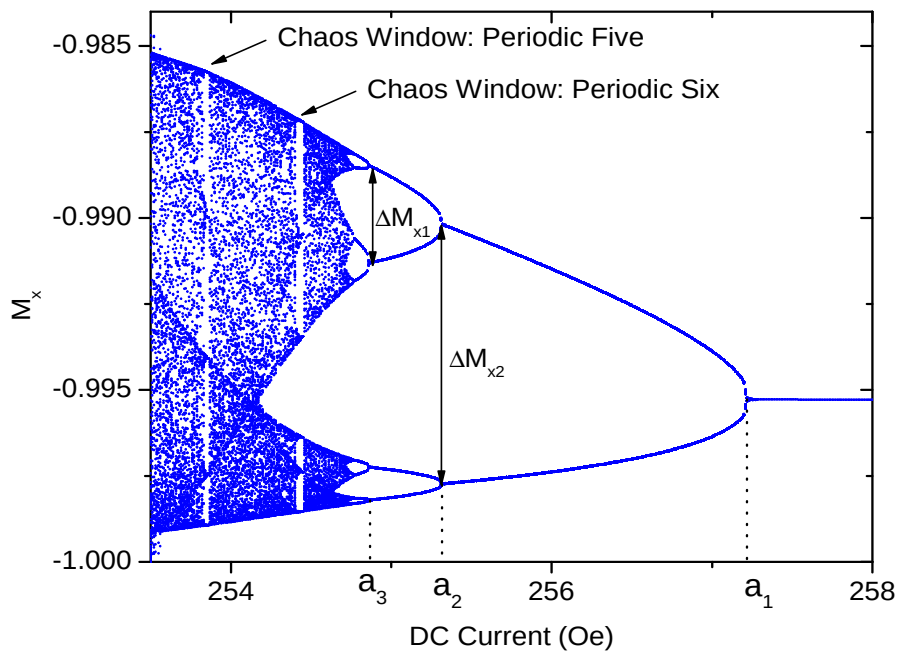

Figure 5.10: Period Doubling Bifurcation

5.4.3 Bifurcation Cascade

A better way to investigate period doubling bifurcation is via Poincaré map. Use the approach we mentioned previously to study the Poincaré map in spin valve oscillators. We obtain the Bifurcation Cascade shown in Fig. 5.10.

In Fig. 5.10, we clearly see that, in synchronization region, the map point is one fixed point, although it will move due to the change of parameter; After a critical parameter, two fixed points appears in the cascade diagram, and this fork structure represents a period doubling bifurcation. Another bifurcation gives four fixed points recorded on the diagram. One finds the period doubling bifurcations take place faster and faster, as the system is getting closer and closer to chaos. Eventually, there are infinitely many points recorded. That corresponds to chaos. The rescaling ratios of the fork size appear universal among different systems. Feigenbaum demonstrated

i	a_i	$a_i - a_{i+1}$	δ_i
1	257.2500	-1.9300	4.289
2	255.3200	-0.4500	4.356
3	254.8700	-0.1033	4.472
4	254.7667	-0.0231	4.529
5	254.7436	-0.0051	4.636
6	254.7385	-0.0011	
7	254.7374		

Table 5.1: Feigenbaum ratio measurement. The second column is derived from Fig. 5.10; a_i is a critical value at the ith bifurcation point.

this universality. And the two ratios regarding the fork size and critical parameters are referred as Feigenbaum numbers. [19]

5.4.4 Feigenbaum Numbers

There are two Feigenbaum Numbers. The first Feigenbaum number is defined as

$$\delta_i = \frac{a_i - a_{i+1}}{a_{i+1} - a_{i+2}} \tag{5.16}$$

where a_i is the value of the parameter at the ith bifurcation point.

The Feigenbaum ratio is approaching to a universal number within the dynamical systems that have the same order of nonlinearity. For a system with a nonlinearity of two, the number is 4.6692... To see if spin valve oscillators belong to the same universal quadratic class, we evaluate the Feigenbaum ratio shown in the Table 5.4.4.

There is a second Feigenbaum ratio that denotes the rescaling ratio of the bifurcation forks. For example, from first two bifurcation in Fig. 5.10, we measured $|\alpha| = |\Delta M_{x1}/\Delta M_{x2}| = 2.68$. Analytically, $|\alpha| = 2.5029\ldots$ [19], for a quadratic non-linear system [20].

We find that the measured ratios agree with the universal Feigenbaum numbers exceedingly well. This indicates that our system indeed belongs to a quadratic non-linear class. In another word, the nonlinearity of spin valve system is two.

5.4.5 Chaos windows and Sharkovskii Ordering

We noticed that in the Lyapunov spectra, in the chaos region, there are some small parameter intervals where Lyapunov Exponents drop equal or below zero. These intervals are chaos windows. One can also find them on the bifurcation cascade diagram.

In Fig. 5.10, we see periodic seven and periodic five chaos window. Within these chaos windows, the system is not a chaotic system since they don't have a nonzero Lyapunov Exponent. Instead, their trajectories are period five or period seven regular orbits, i.e., trajectories will be complete after five or seven loops.

These chaos windows provide another demonstration of the existence of chaos by the Sharkovskii ordering theorem [21]. According to this theorem, the system will experience period one orbit (regular limit cycle), period two orbit ... period 2^n orbit ... chaos...period seven orbit, period six orbit, period five orbit and period three orbit. If one of these periodic orbit is observed those kinds of orbit before the observed one have already taken place. For example, if one observes period eight orbit, he can conclude the system has experienced period one to period four orbit. Now, we observed period five orbit, all the orbit before that in the Sharkovskii sequence have appeared. Therefore, chaos must have occurred before we saw period five orbit.

5.5 Power Spectra of Chaos

A highly interesting feature is the two distinct magnetization trajectories during the transition to chaos. In the first case, the bifurcation occurs only at the out-of-plane orbits shown in Fig. 5.11. Although the bifurcation on this single orbit also leads to chaos because the largest calculated Lyapunov exponent is positive, the power spectrum displays a well defined peak. The peak position corresponds to the inverse

of the average time for the magnetization to complete one loop (since the loop never closes, we define a one-loop when the trajectory returns to the point nearest to the starting point of the loop). Thus, the presence of the narrow peak indicates a quasi-periodic motion of the magnetization in chaotic dynamics. It would be erroneous if one automatically assumes the dynamics is synchronization when the experimental power spectrum is highly peaked. Synchronization refers to the phase-locking between the external and natural frequencies but the positive Lyapunov exponent excludes the possibility of the phase-locking. The second chaotic motion involves both out-of-plane and in-plane orbits, as seen in Fig. 5.12. In this case, the power spectra display typical noise, i.e., broadly distributed spectra. The magnetization jumps between out-of-plane and in-plane orbits are completely random; it is an intrinsic stochastic process driven by a deterministic external perturbation. This stochastic jumping leads to a much stronger noise in the power spectra. On the other hand, it is necessary that trajectories are within the vicinity of the separatrix of two different orbits so that the stochastic magnetization jump can take place under small perturbations. Since the separatrix has an infinite period, the trajectory close to it must have a nearly zero frequency as seen in left panel of Fig. 5.12.

5.6 Fluctuation

The synchronization-like chaotic power spectra imply that quasi-periodicity can be observed in chaos if the trajectory is not near the separatrix. It is the stochastic jump of the trajectory in the vicinity of the separatrix that reduces the periodicity. The reduction of the periodicity due to stochastic jumps could also occur when the thermal fluctuations exist because the thermal fluctuations are stochastic, known as a Wiener process. In general, there exists a bifurcation gap [22] where the thermal

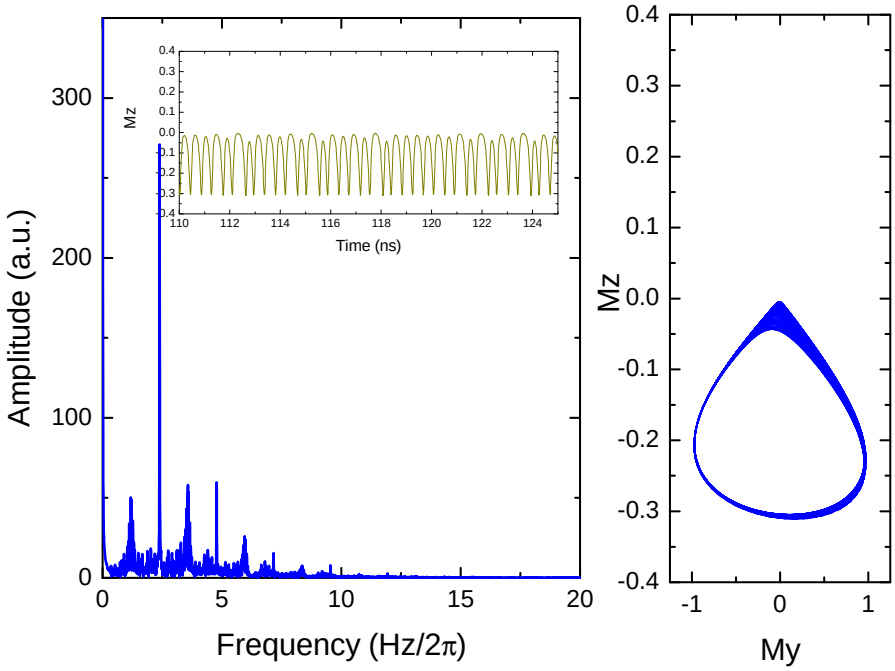

Figure 5.11: Synchronization-like chaos. Chaos that involves only one branch of orbits

fluctuations limit the observation of 2^n orbits in the bifurcation diagram to a finite number $n < n_0$. The stronger the fluctuations are, the smaller n_0 is. Consequently, the thermal fluctuations make the Lyapunov spectra smoother in Fig. 2 and chaos windows invisible in Fig. 3. We emphasize that although the thermal fluctuations lead to noise in the power spectra and the possible random jumps between two orbits, it is not associated with the bifurcation and thus there are no universal Feigenbaum numbers. Experimentally, one can distinguish chaotic dynamics generated by the deterministic perturbation (ac current) and by the thermal fluctuations. For example, when the parameter, e.g. dc current in our study, is varied, the current driven power spectrum should evolve from non-chaotic dynamics to chaos and back to non-chaos.

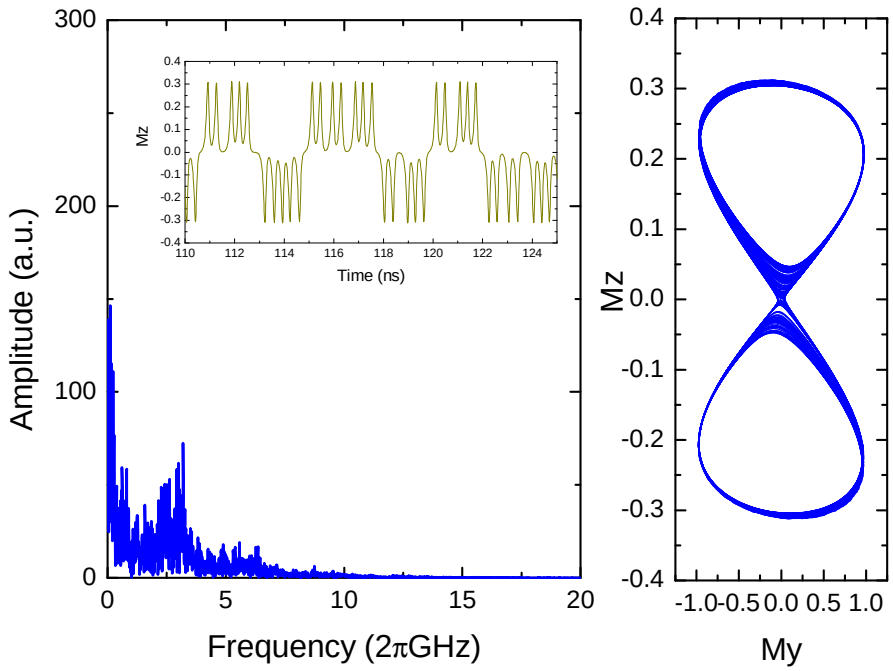

Figure 5.12: Chaos that involves two branches of orbits

Bibliography

[1] A. Pikovsky, M. Rosenblum, and J. Kurths, *Synchronization: A Universal Concept in Nonlinear Sciences* (Cambridge University Press, Cambridge, 2001).

[2] M. I. Rabinovich and D. I. Trubetskov, *Oscillations and Waves in Linear and Nonlinear Systems* (Kluwer, Dordrecht, 1989).

[3] J. C. Slonczewski, J. Magn. Magn. Mater. **159**, 1(1996); **195**, 261 (1999).

[4] J. Z. Sun, Phys. Rev. B **62**, 570 (2000).

[5] G. Bertotti, C. Serpico, I. D. Mayergoyz, A. Magni, M. d'Aquino, and R. Bonin, Phys. Rev. Lett. **94**, 127206 (2005).

[6] S. I. Kiselev, J. C. Sankey, I. N. Krivorotov, N. C. Emley, R. J. Schoelkopf, R. A. Buhrman, and D. C. Ralph, Nature (London) **425**, 380(2003).

[7] I. N. Krivorotov, N. C. Emley, J. C. Sankey, S. I. Kiselev, D. C. Ralph, and R. A. Buhrman, Science **307**, 228(2005).

[8] Z. Li and S. Zhang, Phys. Rev. B **68**, 024404 (2003).

[9] W. H. Rippard, M. R. Pufall, S. Kaka, T. J. Silva, S. E. Russek, and J. A. Katine, Phys. Rev. Lett. **95**, 067203 (2005).

[10] S. Kaka, M. R. Pufall, W. H. Rippard, T. J. Silva, S. E. Russek, and J. A. Katine, Nature (London) **437**, 389 (2005) .

[11] F. B. Mancoff, N. D. Rizzo, B. N. Engel, and S. Tehrani, Nature (London) **437**, 393 (2005) .

[12] J. Grollier, V. Cros, and A. Fert, Phys. Rev. B **73**, 060409(R) (2006).

[13] A. N. Slavin and V. S. Tiberkevich, Phys. Rev. B **72**, 092407 (2005).

[14] K. Palmer, Dynamics Reported **1**, 265 (1988).

[15] Y. Li, *Chaos in Partial Differential Equations* (International Press, 2004).

[16] K. T. Alligood, T. D. Sauer, and J. A. Yorke, *Chaos: An Introduction to Dynamical Systems* (Springer, New York, 1997).

[17] J. M. González-Miranda, *Synchronization and Control of Chaos: An Introduction for Scientists and Engineers* (Imperial College Press, London, 2004).

[18] Z. Li, Y. C. Li, and S. Zhang, Phys. Rev. B **74**, 054417 (2006).

[19] M. J. Feigenbaum, J. Stat. Phys **19**, 25(1978).

[20] J. P. Van Der Weele, H. W. Capel and R. Kluiving, Physica **145A**, 425 (1987).

[21] E. Ott, *Chaos in Dynamical Systems* (Cambridge University Press, New York, 2002).

[22] J. P. Crutchfield, J. D. Farmer and B. A. Huberman, Phys. Rep. **92**, 45 (1982)

Chapter 6

Effect of Finite Temperature

The magnetization dynamics discussed in previous chapters are subject to the zero temperature restriction. However, the real device works at room temperature. Even though in experimental labs, low temperature is accessible, we can not overlook the fact that the electrical current will increase the temperature of the device. Finite Temperature introduces instability of magnetization [1]. Thermal effect agitates the magnetization switching [2–5]. On the other hand, the thermal effect explains the large variation of linewidths in spin transfer oscillators. [6].

In this chapter, we investigate the thermal effect of magnetization, especially for the cases when self-sustained oscillations have been established under zero temperature. We will also consider the thermal effect on chaotic dynamics in spin transfer oscillators.

6.1 Stochastic Process in Magnetization Dynamics

Following the treatment of Brown [7], the thermal effect on magnetization dynamics is interpreted by a three dimensional isotropic random field $\mathbf{h}(t)$ that has the following

properties. First, the process $\mathbf{h}(t)$ is stationary. Second, its statistical average is zero,

$$< h_i(t) >= 0, \tag{6.1}$$

where i represents x, y or z direction. Third, the correlation function can be written as,

$$< h_i(t)h_j(t+\tau) >= \mu\delta_{ij}\delta(\tau). \tag{6.2}$$

Because $\mathbf{h}(t)$ is stationary, μ is a constant. According to these assumptions, the distribution of $h_i(t)$ is $N(0,\ \sigma^2)$ at time t. Therefore, a three dimensional Wiener process can be constructed

$$\sigma d\mathbf{W}(t) = \mathbf{h}(t)dt \tag{6.3}$$

where $\sigma^2 = \mu$.

Now, thermal agitated Landau-Lifshitz-Gilbert equation can be expressed as

$$\frac{d\mathbf{M}}{dt} = -\gamma\mathbf{M}\times(\mathbf{H}_{eff}+\mathbf{h}(t)) - \frac{\alpha}{M_s}\mathbf{M}\times\frac{d\mathbf{M}}{dt} + \frac{\gamma a_J}{4\pi M_s}\mathbf{M}\times(\mathbf{M}\times\mathbf{e}_p) \tag{6.4}$$

It can be converted into,

$$d\mathbf{M} = \dot{\mathbf{M}}_{det}dt + \sigma\gamma\mathbf{M}\times d\mathbf{W} \tag{6.5}$$

where

$$\dot{\mathbf{M}}_{det} = -\gamma\mathbf{M}\times\mathbf{H}_{eff} + \frac{\alpha}{M_s}\mathbf{M}\times\frac{d\mathbf{M}}{dt} + \frac{\gamma a_J}{4\pi M_s}\mathbf{M}\times(\mathbf{M}\times\mathbf{e}_p) \tag{6.6}$$

which is just the determinative Landau-Lifshitz-Gilbert equation.

6.2 Stochastic Process of Energy

From the stochastic differential equation of magnetization, Eq. (6.5), we derive the stochastic differential equation for the free energy density of the magnetization by considering

$$dE = -\mathbf{H}_{eff}\cdot d\mathbf{M} \tag{6.7}$$

Plug Eq. (6.5) into the above equation, one gets

$$\begin{aligned} dE &= -\frac{\alpha\gamma}{M_s}|\mathbf{M}\times\mathbf{H}_{eff}|^2 dt \\ &\quad +\frac{\gamma a_J}{4\pi M_s}(\mathbf{M}\times\mathbf{H}_{eff})\cdot(\mathbf{M}\times\mathbf{e}_p)dt \\ &\quad +\gamma\sigma(\mathbf{M}\times\mathbf{H}_{eff})\cdot d\mathbf{W} \end{aligned} \tag{6.8}$$

Notice that Stratonovich calculus instead of Ito calculus is used here, so that chain rules hold.

Since each component of $d\mathbf{W}$ can be written as

$$dW_i = \epsilon_i\sqrt{dt},$$

where ϵ_i is normally distributed with mean 0 and variance 1, the last term in Eq. (6.8) becomes,

$$\gamma\sigma\sum_{i=x,y,z}(\mathbf{M}\times\mathbf{H}_{eff})_i\epsilon_i\sqrt{dt}$$

which is indeed a summation of three independent normal distributions. The result distribution has the mean equal to the sum of means of the three distributions and the variance equal to sum of variances of the three distributions. The variance of

$$\sum_{i=x,y,z}(\mathbf{M}\times\mathbf{H}_{eff})_i\epsilon_i$$

is

$$\begin{aligned} &\sum_{i=x,y,z}(\mathbf{M}\times\mathbf{H}_{eff})_i^2 \\ =\quad & |\mathbf{M}\times\mathbf{H}_{eff}|^2. \end{aligned} \tag{6.9}$$

Therefore,

$$\begin{aligned} &\gamma\sigma(\mathbf{M}\times\mathbf{H}_{eff})\cdot d\mathbf{W} \\ =\quad & \gamma\sigma|\mathbf{M}\times\mathbf{H}_{eff}|dW \end{aligned} \tag{6.10}$$

where $dW = \epsilon\sqrt{dt}$ is simply a one-dimensional Wiener Process. Combining the drift term in Eq. (6.8), the stochastic differential equation of the energy of magnetization is,

$$dE = -\frac{\alpha\gamma}{M_s}|\mathbf{M}\times\mathbf{H}_{eff}|^2 dt + \frac{\gamma a_J}{4\pi M_s}(\mathbf{M}\times\mathbf{H}_{eff})\cdot(\mathbf{M}\times\mathbf{e}_p)dt + \gamma\sigma|\mathbf{M}\times\mathbf{H}_{eff}|dW \quad (6.11)$$

The first two terms are simply the determinative drift term of the energy, which we use to calculate Melnikov Integral in previous chapters. The last term accounts for the thermal effect.

Now, instead of dealing with a three-dimensional stochastic process on magnetization dynamics, we have obtained a simpler one-dimensional stochastic process on the magnetic energy.

6.3 Fokker-Planck-Equation

From Eq. (6.8), one can see that the drift vector and the diffusion tensor are simply,

$$-\frac{\alpha\gamma}{M_s}|\mathbf{M}\times\mathbf{H}_{eff}|^2 + \frac{\gamma a_J}{4\pi M_s}(\mathbf{M}\times\mathbf{H}_{eff})\cdot(\mathbf{M}\times\mathbf{e}_p),$$

and

$$\gamma^2\sigma^2|\mathbf{M}\times\mathbf{H}_{eff}|^2,$$

respectively.

Thus, we derived the Fokker-Planck-Equation as following,

$$\begin{aligned}\frac{\partial P(E,t)}{\partial t} &= \frac{\partial}{\partial E}\{[\frac{\alpha\gamma}{M_s}|\mathbf{M}\times\mathbf{H}_{eff}|^2 - \frac{\gamma a_J}{4\pi M_s}(\mathbf{M}\times\mathbf{H}_{eff})\cdot(\mathbf{M}\times\mathbf{e}_p)]P(E,t)\} \\ &\quad \frac{1}{2}\frac{\partial^2}{\partial E^2}[\sigma^2\gamma^2|\mathbf{M}\times\mathbf{H}_{eff}|^2 P(E,t)] \qquad (6.12)\end{aligned}$$

The function $P(E,t)$ represents the probability that at time t, magnetic energy is E.

For stationary state,

$$\frac{\partial P(E,t)}{\partial t} = 0.$$

Setting $a_J = 0$, i.e. current is zero, one has the following relationship of $P(E,t)$,

$$\frac{\partial}{\partial E}[\frac{\alpha\gamma}{M_s}|\mathbf{M}\times\mathbf{H}_{eff}|^2 P(E,t)] = -\frac{1}{2}\frac{\partial^2}{\partial E^2}[\sigma^2\gamma^2|\mathbf{M}\times\mathbf{H}_{eff}|^2 P(E,t)] \tag{6.13}$$

Testing the trial solution,

$$P = A_0 e^{-\frac{V(E-E_0)}{k_B T}},$$

where V is the volume, we get

$$\frac{\alpha\gamma}{M_s}(\frac{V}{k_B T}) = \frac{1}{2}\sigma^2\gamma^2(\frac{V}{k_B T})^2.$$

Therefore,

$$\sigma^2 = \frac{2\alpha k_B T}{\gamma M_s V}. \tag{6.14}$$

This result is so called dissipation-fluctuation relation in literatures.

6.4 Thermal Noise in Spin Transfer Oscillators

As we discussed in previous chapter, Melnikov Integral which is essentially the net work done by damping torque and spin transfer torque after one period of magnetization oscillation, is zero for the self-sustained oscillation. However, we have assumed the temperature is zero. When temperature is higher than zero, the net work done by both torques after one period of oscillation may be non-zero.

The thermal effect induces stochastic processes for magnetization and its energy, as we can see in Eq. (6.5) and Eq. (6.11). These stochastic processes make the Melnikov Integral deviating from zero. The first two terms in Eq. (6.11) are drift terms, and the integral of them for one period of oscillation gives the usual Melnikov Integral, which is zero for self-sustained oscillations. But the integral of the third term is not determinative. Its result is a random variable and indicates a non-zero net work done by damping and spin transfer torque.

In another word, after one period of oscillation, the energy may not come back to it original level. Instead, the energy after one period will constitute a distribution which is centered at the energy one period earlier, and has a certain variance. To determine this variance, we need integral the variance of dE.

The variance of Eq. (6.11) is

$$\gamma\sigma|\mathbf{M}\times\mathbf{H}_{eff}|^2,$$

so that the variance of the energy deviation after one period is,

$$Var(\Delta E_{th}) = \int_\Omega \gamma^2\sigma^2|\mathbf{M}\times\mathbf{H}_{eff}|^2 dt \tag{6.15}$$

Plugging Eq. (6.14),

$$Var(\Delta E_{th}) = \frac{2k_BT\alpha\gamma}{M_sV}\int_\Omega |\mathbf{M}\times\mathbf{H}_{eff}|^2 dt. \tag{6.16}$$

Notice that the integral in the above equation is nothing but the work done by damping torque in one period of oscillation. Thus, the variance of the energy deviation is determined by the temperature, which is obviously, and the work done by damping. For self-sustained oscillations, the work done by damping torque is the same as the work done by the spin transfer torque. That is to say, the variance of the energy deviation distribution can be understood as a function of spin transfer torque instead of the damping torque.

The existence of the energy deviation can also be interpreted as the thermal effect kicking the trajectory to another orbit which has different energy. Trajectories that have different energies have different frequency. Since thermal effect induces a distribution of energy deviation, the frequency of the trajectory will also has a distribution. This is shown as a broadening of the frequency peak in the power spectrum.

For trajectories that are close to separatrix, the thermal effect may kick the trajectory to separatrix, or from one branch of orbit (OOP/IP) to the other (IP/OOP).

In terms of the energy, the closer the center of the energy distribution is to the energy of separatrix, the higher the probability of the trajectory precess around separatrix. Since the separatrix has a zero frequency, the noise will be enhanced in the power spectrum around zero frequency. It is the thermal effect that generate the broaden distribution of energy, which further enhance the noise in power spectra.

6.5 Thermal Effect on Chaos

When ac current is turned on, at the neighborhood of the separatrix, chaos may appear. Chaos also induces noise in power spectra. However, the mechanisms are different from thermal noise. The underlying equation for chaos and thermal effect are different. One is a determinative process, the other is a stochastic one.

Chaos induced noise only appears when trajectories are near the separatrix; it is not necessary for thermal noise. However, since thermal effect generates a distribution of energies or say a distribution of trajectories, a trajectory that is initially out of chaotic region may be kicked into this region. In other words, the thermal effect blurs the boundary of chaotic region.

In the previous chapter, our numerical results have shown that a well defined frequency peak may persist in the power spectrum of chaos. In the presence of finite temperature, this peak is suppressed.

At zero temperature, "Synchronization-like" chaos only appears within a small region of DC current. A change around 1 Oe of dc current suppresses the peak in the power spectrum of chaos. This is because trajectories get closer to separatrix, and jump between OOP branch and IP branch. From the Melnikov Integral, we can calculate how much energy change will be driven by the 1 Oe dc current change. We use ΔE_{dc} to represent this energy change. On the other hand, the thermal effect

will generate an energy deviation distribution. If the distribution is wide enough compared to ΔE_{dc}, the peak in chaos will disappear. Thus, we may calculate the ratio

$$\frac{\Delta E_{dc}}{\sqrt{Var(\Delta E_{th})}}$$

and compare it to 1. If $\frac{\Delta E_{dc}}{\sqrt{Var(\Delta E_{th})}} \gg 1$, the thermal effect will not affect the "synchronization-like" chaos significantly; if $\frac{\Delta E_{dc}}{\sqrt{Var(\Delta E_{th})}} \ll 1$, the thermal effect will generate large enough energy deviation and kill the phenomena of "synchronization-like" chaos.

Because of the simple zero of limit cycle, the integral in Eq. (6.16), which is the work done by damping torque, can be replaced by the integral that represents the work done by spin transfer torque,

$$Var(\Delta E_{th}) = \frac{2k_B T a_J \gamma}{V} M_s^2 M_\beta \tag{6.17}$$

where M_β is defined by Eq. (3.41). And

$$\Delta E_{dc} = \gamma \Delta a_J M_s^2 M_\beta \tag{6.18}$$

Therefore

$$\frac{\Delta E_{dc}}{\sqrt{Var(\Delta E_{th})}} = \Delta a_J M_s \sqrt{\frac{\gamma V M_\beta}{2k_B T a_J}} \tag{6.19}$$

For small $\mathbf{H}_{ext}$, using the approximated result Eq. (3.54),

$$\frac{\Delta E_{dc}}{\sqrt{Var(\Delta E_{th})}} = \Delta a_J M_s \sqrt{\frac{\gamma V h_e (\frac{3}{2} - 3E) T_\Omega}{2k_B T a_J}} \tag{6.20}$$

where T_Ω is known as the period of the limit cycle which is expressed by Eq. (3.52). Since chaotic trajectory is close to separatrix, their energy E has to be close to $-h_e$, the energy of the saddle point. Thus,

$$\frac{\Delta E_{dc}}{\sqrt{Var(\Delta E_{th})}} = \Delta a_J M_s (1 - h_e) \sqrt{\frac{3\gamma V h_e T_\Omega}{4k_B T a_J}} \tag{6.21}$$

Consider the following parameters,

$$\begin{aligned} M_s &= 800\ Oe \\ h_e &= \frac{200\ Oe}{4\pi M_s} \\ a_J &= 262.5\ Oe \\ \Delta a_J &= 1.5\ Oe. \end{aligned}$$

The period of the limit cycle T_Ω is of the order of $10^{-10}s$. So that

$$\frac{\Delta E_{dc}}{\sqrt{Var(\Delta E_{th})}} \sim \sqrt{\frac{V}{T}} \times 10^9 \tag{6.22}$$

For $V = 10^4 nm^3$, at room temperature,

$$\frac{\Delta E_{dc}}{\sqrt{Var(\Delta E_{th})}} \sim 10^{-4}.$$

To make the ratio close to 1, one has to drop the temperature to as low as $10^{-5}K$, which is not possible in any experimental condition. Therefore, the power spectrum of chaos in real experiments will always show wide spread noise without "synchronization-like" peak.

Bibliography

[1] Z. Li, J. He, and S. Zhang, Phys. Rev. B, **72**, 212411(2005).

[2] E. B. Myers, F. J. Albert, J. C. Sankey, E. Bonet, R. A. Buhrman, and D. C. Ralph, Phys. Rev. Lett. **89**, 196801 (2002)

[3] I. N. Krivorotov, N. C. Emley, A. G. F. Garcia, J. C. Sankey, S. I. Kiselev, D. C. Ralph, and R. A. Buhrman, Phys. Rev. Lett. **93**, 166603 (2004).

[4] Z. Li, and S. Zhang, Phys. Rev. B, **69**, 134416(2004).

[5] D. M. Apalkov, and P. B. Visscher, Phys. Rev. B, **72**, 180405(R)(2005).

[6] S. E. Russek, S. Kaka, W. H. Rippard, M. R. Pufall, and T. J. Silva, Phys. Rev. B **71**, 104425(2005).

[7] W. F. Brown, Phys. Rev. **130**, 1677(1963).

Chapter 7

Summary

In this dissertation, we presented the studies on different phenomena related to spin angular momentum transfer effect.

The first phenomenon is the energy transfer effect associated with spin transfer effect in Magnetic Tunnel Junctions. Starting from Jüllier model of tunneling current, we derived the formula of transverse and longitudinal spin currents, which are contributed to spin transfer effect and energy transfer effect, respectively. Based on sd exchange model, we investigated the microscopic mechanism of energy transfer in MTJ induced by spin dependent inelastic scattering of the longitudinal spin current. We used an effective temperature to characterize the energy transfer effect and applied this model to thermal assisted magnetization switching effect.

We then studied the magnetization dynamics in spin valve systems. We showed the derivation of the analytic solutions of an artificial neutral precession of magnetization. We calculate the Melnikov Integral to present the establishment of stable self-sustained precession.

We extended the Melnikov Integral method to determine the synchronization phenomena in spin valves when a small ac current is turned on. We found this method can effectively predict the synchronization region even in more general cases.

Melnikov Integral method can also used to determine chaotic region in the phase

diagram of the magnetization dynamics of spin valve. However, since there exists an arbitrary phase term in the simple zero solution of Melnikov Integral, we can't exactly predict at which condition chaos will appear. To overcome this problem, we apply Lyapunov exponents calculations. Since the positive Lyapunov exponent indicates chaos, we map out the detail phase diagram within the chaos region.

To understand the route to chaos, we implemented Poincaré Map. Period doubling bifurcation was captured and two universal Feigenbaum constants was demonstrated by measuring the change of scaling of bifurcation cascade. In the cascade diagram, regular attractors such period-five, period-seven trajectories were seen in chaotic region. These are called chaos windows.

We analyzed the power spectrum of chaos based on numerical simulation of the magnetization dynamics. Numerical simulation suggests there are two types of power spectrum for chaos. One has broadened noise without frequency peak, the other shows a "synchronization-like" frequency peak.

However, considering the finite temperature effect, the thermal noise will be large enough to smooth out the peaks in chaotic power spectrum. The estimation of thermal effect is based on the Melnikov Integral calculation of energy change between two types of chaos and the calculation of energy deviation distribution due to temperature effects.

In the appendix, we present another interesting topic that attracted much attention in the past years, the spin Hall effect. We will discuss a general formula for transport coefficients. Then we apply it to spin Hall effect for a Rashba Hamiltonin and distinguish the extrinsic spin Hall current and intrinsic spin Hall current. On the other hand we calculate the transport coefficient for Orbit-Angular-Momentum using the same formula. We argue that the intrinsic spin Hall current is always compensated by an equal-magnitude but negative intrinsic Orbit-Angular-Momentum current. We

then investigate the extrinsic spin Hall effect in the presence of Rashba spin-orbit coupling bands by using Boltzmann Equation. It is found that the extrinsic spin Hall current is depressed by the spin-orbit coupling bands unless there exist magnetic scattering.

Appendix A

Spin Hall Effect

A.1 Intrinsic Spin Hall Effect

Recently, there are emerging *theoretical* interests on the spin Hall effect in a spin-orbit coupled system [1–14]. The spin Hall effect refers to a non-zero *spin* current in the direction transverse to the direction of the applied electric field. Earlier studies had been focused on an extrinsic effect [15, 16], namely, when conduction electrons scatter off an impurity with the spin-orbit interaction, the electrons tend to deflect to the left (right) more than to the right (left) for a given spin orientation of the electrons. Thus the impurity is the prerequisite in the extrinsic spin Hall effect. Recently, the spin Hall effect has been extended to semiconductor heterostructures where the spin-orbit coupled *bands* are important. It has been shown that the spin current exists in the absence of impurities, termed as the intrinsic or dissipationless spin Hall effect (ISHE) in order to distinguish the impurity-driven extrinsic spin Hall effect (ESHE) mentioned above. In general, the magnitude of ISHE is two to three orders larger than that of ESHE; this immediately generates an explosive interest in theoretical research on the ISHE since the spin current is regarded as one of the key variables in spintronics application.

However, the spin current generated via ISHE is fundamentally different from

conventional spin-polarized transport in many ways. First, the spin current is carried by the entire spin-orbit coupled Fermi sea, not just electrons or holes at the Fermi level [1, 4]. Second, ISHE exists even for an equilibrium system (without external electric fields) [5] and ISHE is closely related to the dielectric response function that characterizes the electronic deformation [6]. Most recently, it is proposed that the intrinsic spin Hall effect exists even in insulators [17]. The above unconventional properties cast serious doubts on experimental relevance of the intrinsic spin current. It has been already alerted by Rashba [5, 6] that the ISHE may not be a transport phenomenon. Due to the ill-defined nature of the spin current in the spin-orbit coupled Hamiltonian, theories utilizing different approaches produce contradicting results: some predicted a zero spin Hall current in the presence of an arbitrary weak disorder and some claimed a universal spin conductivity at weak disorder. In this letter, we do not try to resolve the above theoretical debate, instead we reveal the spurious nature of the intrinsic spin Hall effect and discuss its experimental consequences. We first define generalized intrinsic and extrinsic transport coefficients from the semiclassical transport equation. We show that the intrinsic spin current is always accompanied by an equal but opposite orbital-angular-momentum (OAM) current for a spin orbit coupled system. Thus, the intrinsic magnetization current which is the sum of the spin current and the orbital angular momentum current is identically zero. Next, we construct the equation of motion for the spin density in the presence of the intrinsic and extrinsic mechanisms. We find that the intrinsic spin current is exactly canceled by a spin torque and thus the spin accumulation at the edge of the sample is solely determined by the extrinsic spin current. The above results make us conclude that the intrinsic spin current has *no experimental consequences* in terms of the spin transport measurement for an arbitrary strength of the intrinsic Hall conductivity. Therefore, the intrinsic spin current is a pure theoretical object, at least, in the limit of the

semiclassical picture of the spin transport. Finally, we brief comment on the most recent experimental results [18].

Let us consider a spin-dependent Hamiltonian

$$H = -\frac{\hbar^2}{2m}\nabla^2 + V(\mathbf{r}, \boldsymbol{\sigma}) + eEx + V_i(\mathbf{r}, \boldsymbol{\sigma}) \tag{A.1}$$

where the second term represents a periodic spin-orbit potential, the third term is the interaction with a DC electric field E in the x-direction, and the last term is the impurity potential that may or may not depend on spin. Now let us consider how an arbitrary dynamic variable $\hat{G}$ responds to the electric field. A standard semiclassical version of the linear response function $\mathcal{J}(\mathbf{r})$ is

$$\mathcal{J}(\mathbf{r}) = \sum_{\mathbf{k}\lambda} G_{\mathbf{k}\lambda} f(\epsilon_{\mathbf{k}\lambda}, \mathbf{r}) \tag{A.2}$$

where $\hat{G}$ can be any dynamic variable such as the current density, the spin current density, the magnetic moment, etc., $G_{\mathbf{k}\lambda} = \int d\mathbf{r}\Psi^{+}_{\mathbf{k}\lambda}(\mathbf{r})\hat{\mathbf{G}}\boldsymbol{\Psi}_{\mathbf{k}\lambda}(\mathbf{r}) \equiv < \boldsymbol{\Psi}_{\mathbf{k}\lambda}|\hat{\mathbf{G}}|\boldsymbol{\Psi}_{\mathbf{k}\lambda} >$ is the expectation value for the eigenstate $\Psi_{\mathbf{k}\lambda}(\mathbf{r})$ (Bloch states) determined by the first three terms in Eq. (1), $\lambda = \pm 1$ represents the index of the spin sub-band, and $f(\epsilon_{\mathbf{k}\lambda}, \mathbf{r})$ is the distribution function that depends on the detail of the scattering potential $V_i(\mathbf{r}, \sigma)$, the last term of Eq. (1). The dependence of $\mathcal{J}(\mathbf{r})$ on the electric field enters in two places: the wavefunctions and the distribution function. We may expand them up to the first order in the electric field. The wavefunction is written as,

$$\Psi_{\mathbf{k}\lambda}(\mathbf{r}) = \Psi^{(0)}_{\mathbf{k}\lambda}(\mathbf{r}) + \Psi^{(1)}_{\mathbf{k}\lambda}(\mathbf{r}) \tag{A.3}$$

where $\Psi^{(0)}_{\mathbf{k}\lambda}(\mathbf{r})$ is the unperturbed electronic structure determined by the first two terms in Eq. (1), and

$$\Psi^{(1)}_{\mathbf{k}\lambda}(\mathbf{r}) = \sum_{\mathbf{k}'\lambda' \neq \mathbf{k}\lambda} \frac{< \Psi^{(0)}_{\mathbf{k}'\lambda'}|eEx|\Psi^{(0)}_{\mathbf{k}\lambda} >}{\epsilon_{\mathbf{k}\lambda} - \epsilon_{\mathbf{k}'\lambda'}} \Psi^{(0)}_{\mathbf{k}'\lambda'}(\mathbf{r}), \tag{A.4}$$

is the first order perturbation to the third term in Eq. (1). Similarly, we write the distribution function in terms of the equilibrium and non-equilibrium parts,

$$f(\epsilon_{\mathbf{k}\lambda}, \mathbf{r}) = f^0(\epsilon_{\mathbf{k}\lambda}) + \left(-\frac{\partial f^0}{\partial \epsilon_{\mathbf{k}\lambda}}\right) g(\mathbf{k}\lambda, \mathbf{r}) \tag{A.5}$$

where f^0 is the equilibrium distribution function and the non-equilibrium function $g(\mathbf{k}\lambda, \mathbf{r})$ is proportional to the electric field. By placing Eqs. (3) and (5) into Eq. (2) and keeping only the first order term in the electric field, we have $\mathcal{J}(\mathbf{r}) \equiv \mathcal{J}_{int} + \mathcal{J}_{ext}$ where

$$\mathcal{J}_{int} = 2\mathrm{Re} \sum_{\mathbf{k}\lambda} < \Psi^{(0)}_{\mathbf{k}\lambda} | \hat{G} | \Psi^{(1)}_{\mathbf{k}\lambda} > f^0(\epsilon_{\mathbf{k}\lambda}) \tag{A.6}$$

is defined as the intrinsic linear response and Re stands for the real part, and

$$\mathcal{J}_{ext} = \sum_{\mathbf{k}\lambda} < \Psi^{(0)}_{\mathbf{k}\lambda} | \hat{G} | \Psi^{(0)}_{\mathbf{k}\lambda} > \left(-\frac{\partial f^0}{\partial \epsilon_{\mathbf{k}\lambda}}\right) g(\mathbf{k}\lambda, \mathbf{r}) \tag{A.7}$$

is called the extrinsic linear response. The above distinction between intrinsic and extrinsic contributions to the transport properties has been already introduced by a number of groups, in particular, by Jungwirth *et al.* [19] in their study of the anomalous Hall effect in itinerant ferromagnets. Equation (6) shows that the intrinsic linear response coefficient is not related to the transport phenomenon since $\mathcal{J}_{int}$ is determined by the equilibrium distribution function and the *local electronic structure*. Thus, there are no transport length scales such as the mean free path or spin diffusion length in $\mathcal{J}_{int}$. The extrinsic linear response, $\mathcal{J}_{ext}$, is a true transport quantity because it is directly proportional to the non-equilibrium distribution function that is determined by various scattering mechanisms. At low temperature, the factor of $\partial f^0 / \partial \epsilon_{\mathbf{k}\lambda}$ limits the transport states to the Fermi level. Comparing Eq. (6) and Eq. (7), we realize that the intrinsic effect is simple and easy to calculate while the extrinsic effect is much more complicated. As long as we know the Bloch states $\Psi^{(0)}_{\mathbf{k}\lambda}$, the intrinsic transport coefficient can be straight-forwardly evaluated since f^0 is known.

The extrinsic transport coefficient not only depends on the Bloch states, but also on the non-equilibrium distribution function that is usually the center of the relevant physics. Here, however, we should concentrate on the easy problem: calculation of the intrinsic transport from Eq. (6) by using a model Hamiltonian.

We choose a Rashba Hamiltonian to illustrate the physics of the intrinsic transport properties. A similar calculation can also be performed for a Luttinger Hamiltonian [20]. For the Rashba Hamiltonian, the second term of Eq. (1) is $V(\mathbf{r},\sigma) = (\alpha/\hbar)\boldsymbol{\sigma}\cdot(\mathbf{p}\times\hat{\mathbf{z}})$ where $\mathbf{p}$ is the momentum in xy plane, $\boldsymbol{\sigma}$ is the Pauli matrix and α is the coupling constant. Before we calculate the spin and the OAM Hall currents from Eq. (6), we list the wavefunction and the dispersion relation of the Rashba Hamiltonian so that one can easily follow our derivation at each step

$$\Psi^{(0)}_{\mathbf{k}\lambda}(\mathbf{r}) = \frac{e^{i\mathbf{k}\cdot\mathbf{r}}}{\sqrt{2A}}\begin{pmatrix} 1 \\ -i\lambda(k_x+ik_y)k^{-1} \end{pmatrix} \tag{A.8}$$

where A is the area of the 2-dimensional electron gas, and

$$\epsilon_{\mathbf{k}\lambda} = \frac{\hbar^2k^2}{2m} + \lambda\alpha k \tag{A.9}$$

where $k = |\mathbf{k}| = \sqrt{k_x^2+k_y^2}$. By placing above two equations into (4), we have [5]

$$\Psi^{(1)}_{\mathbf{k}\lambda}(\mathbf{r}) = -\frac{\lambda eEk_y}{4\alpha k^3}\Psi^{(0)}_{\mathbf{k}-\lambda}(\mathbf{r}). \tag{A.10}$$

In obtaining the above result, we have used $< \Psi^{(0)}_{\mathbf{k}'\lambda'}|x|\Psi^{(0)}_{\mathbf{k}\lambda} >= -\frac{\lambda\lambda'}{2}\delta_{\mathbf{k}\mathbf{k}'}\frac{k_y}{k^2}$.

We now proceed to calculate the spin Hall current by taking the operator $\hat{G} = (1/2)[s_zv_y + v_ys_z]$ where $s_z = (\hbar/2)\sigma_z$ is the z-component of the spin operator and v_y is the y-component of the velocity. By placing the above definition along with Eqs. (8) and (10), and by taking the distribution function a step function at zero temperature, we obtain the intrinsic spin Hall current from Eq. (6),

$$\mathcal{J}^{spin}_{int} = \frac{e}{8\pi}E; \tag{A.11}$$

where we have assumed that the Fermi energy is larger than the spin-orbit coupling energy so that both spin sub-bands cross the Fermi level. Equation (11) represents the universal spin conductivity ($e/8\pi$) obtained by many groups [1, 4].

Our central question is: what is the physical meaning of this spin current derived from the equilibrium distribution function? To see clearly what this spin current represents, we recall that the spin is not a conserved quantity in a spin-orbit coupled system. If one is interested in the *magnetization current* or the total angular momentum current, one should also include the OAM Hall current. The OAM Hall current can be similarly calculated by introducing an operator for the OAM Hall current

$$\hat{G} = \frac{1}{2}\left[(\mathbf{r}\times\mathbf{p})_z v_y + v_y(\mathbf{r}\times\mathbf{p})_z\right] \tag{A.12}$$

where $(\mathbf{r}\times\mathbf{p})_z = xp_y - yp_x$ is z-component of the OAM. The same straightforward evaluation of Eq. (6) leads to

$$J_{int}^{orbit} = -\frac{e}{8\pi}E. \tag{A.13}$$

Thus the OAM current is exactly equal and opposite to the spin current. This result is not surprising at all: the total angular momentum (z-component), spin plus orbital, is conserved for the Rashba Hamiltonian and thus we can choose the Bloch states that are simultaneous eigenstates of the total angular momentum and the Hamiltonian. In fact, one can directly show that the total angular momentum current vanishes if we use $[s_z + L_z, H] = 0$ to the Rashba Hamiltonian.

Having discussed that the intrinsic spin current is always accompanied with the OAM current in a bulk spin-orbit coupled material, our next question is whether the intrinsic spin current can produce a spin accumulation at the edge of the sample? To answer this question, we recall the basic idea of the spin accumulation for the extrinsic spin current. When an extrinsic spin current spatially varies, non-equilibrium spins will be accumulated so that the spin-diffusion is balanced by the spin-drift cur-

rent. Equivalently, the spin accumulation results in the chemical potential splitting between two spin sub-bands and a voltage can be measured experimentally when the sample is attached to a ferromagnetic lead [16]. Mathematically, the non-equilibrium spin-dependent chemical potential or spin accumulation is the average of the *non-equilibrium distribution function* [21]. For the intrinsic spin Hall current, the distribution is an equilibrium distribution and one would expect that the concept of the spin-dependent chemical potential breaks down. Indeed, we show next that the the intrinsic spin Hall current does not lead to spin accumulations at the sample edge and across an interface.

To calculate the spin accumulation or the position-dependent spin density $\mathbf{S}(\mathbf{r}, t)$ at the edge of the sample or across an interface, one relies on the semiclassical equation of motion that can be generally written as

$$\frac{\partial \mathbf{S}(\mathbf{r}, t)}{\partial t} + \boldsymbol{\nabla} \cdot [\mathbf{J}_{int} + \mathbf{J}_{ext}] = \boldsymbol{\tau} + \boldsymbol{\tau}_{ext} + \left(\frac{\partial \mathbf{S}}{\partial t}\right)_{colli} \tag{A.14}$$

where $\mathbf{J}_{int}$ and $\mathbf{J}_{ext}$ are the intrinsic and extrinsic spin current densities, $\boldsymbol{\tau}$ and $\boldsymbol{\tau}_{ext}$ are the intrinsic and extrinsic spin torques due to non-commutivity of the Hamiltonian with the spin operator, i.e., the spin torque is calculated by replacing $\hat{G}$ by $[\mathbf{s}, H]/i\hbar$ in Eqs. (6) and (7), and the last term in Eq. (14) is a collision term that is to relax the nonequilibrium distribution function to an equilibrium one. To explicitly obtain the spin accumulation $\mathbf{S}(\mathbf{r}, t)$ in a closed form, it is necessary to use a wave-package description so that the position-dependence can be readily included. Culcer *et al.* [2] have already formulated that the spin torque can be written as two terms. In our notation, we find the expression for the intrinsic spin torque is $\boldsymbol{\tau} = \boldsymbol{\tau}_0 + \boldsymbol{\tau}_1$ where

$$\boldsymbol{\tau}_0 = \sum_{\mathbf{k}\lambda} < \mathbf{k}\lambda | \frac{1}{i\hbar}[\mathbf{s}, H] | \mathbf{k}\lambda > f^0(\mathbf{k}\lambda, \mathbf{r}) \tag{A.15}$$

and

$$\boldsymbol{\tau}_1 = -\boldsymbol{\nabla} \cdot \sum_{\mathbf{k}\lambda} < \mathbf{k}\lambda | \frac{1}{i\hbar}[\mathbf{s}, H]\mathbf{r} | \mathbf{k}\lambda > f^0(\mathbf{k}\lambda, \mathbf{r}) \tag{A.16}$$

where the symmetrization of the product of $[\mathbf{s}, H]$ and $\mathbf{r}$ is implied. We emphasize that $\boldsymbol{\tau}_1$ comes from the position-dependence of the center of the wave-packet. By using the fact that the wavefunction is an eigenstate of the Hamiltonian, $H|\mathbf{k}\lambda >= E_{\mathbf{k}\lambda}|\mathbf{k}\lambda >$, we immediately see that the expectation value of $[\mathbf{s}, H]$ is zero, i.e., $\boldsymbol{\tau}_0 = 0$. To calculate $\boldsymbol{\tau}_1$, we use the commuting relation $[H, \mathbf{r}] = -i\hbar\mathbf{v} + i\alpha(\mathbf{e}_z \times \boldsymbol{\sigma})$, where $\mathbf{v}$ is the velocity operator. After a straight-forward algebra simplification, we have found [22]

$$\boldsymbol{\tau} = \boldsymbol{\nabla} \cdot \sum_{\mathbf{k}\lambda} < \mathbf{k}\lambda | \frac{\mathbf{vs} + \mathbf{sv}}{2} | \mathbf{k}\lambda > f^0(\mathbf{k}\lambda, \mathbf{r}) \equiv \boldsymbol{\nabla} \cdot \mathbf{J}_{int}. \tag{A.17}$$

Therefore, the intrinsic spin torque exactly equals the divergence of the intrinsic spin current. The equation of motion, Eq. (14), now becomes

$$\frac{\partial \mathbf{S}(\mathbf{r}, t)}{\partial t} + \boldsymbol{\nabla} \cdot \mathbf{J}_{ext} = \boldsymbol{\tau}_{ext} + \left(\frac{\partial \mathbf{S}}{\partial t}\right)_{colli}. \tag{A.18}$$

We conclude that the intrinsic spin current does not enter into the play in the equation of motion. The spin accumulation $\mathbf{S}(\mathbf{r}, t)$ is solely determined by the extrinsic part of the current density $\mathbf{j}_{ext}$, the spin torque $\boldsymbol{\tau}_{ext}$, and the spin relaxation in the collision term.

We now return to our central issue on the problem, namely, whether the intrinsic spin Hall conductivity can be measured via conventional meanings of the spin transport. Since the spin current is not directly measurable, two schemes are usually employed: one is the realization of measuring the electric field induced by the *magnetization current* [24] and the other is the spin accumulation at the sample of the edge or across an interface [23]. We should discuss them separately below.

If there is a net magnetization current in a bulk material, a circular electric field outside the sample will be induced. This phenomenon is analogous to the magnetic

field induced by a charge current, known as Biot-Savart law or Ampere's law. For example, it was proposed that a spin current generated via spin waves propagation through a nanowire can be detected by an induced electric field just outside the nanowire [24, 25]. However, the above proposal is applied to the case where the OAM current is absent. In the present case, the OAM current is exactly opposite to the spin current so that the net magnetization current is zero. Therefore, we conclude that there is no electric field associated with the intrinsic spin current.

The more efficient method to detect the spin current is by measuring the spin accumulation due to spatial variation of the spin current, e.g., the Johnson-Silsbee's experiment [23]. Based on the equation of motion given by Eq. (18), the divergent of the *extrinsic but not intrinsic* spin currents can lead to a buildup of spin accumulation. To determine the spin accumulation, one usually makes a relaxation-time approximation so that the collision term in Eq. (18) is modeled by $-\mathbf{S}/\tau_{sf}$. Since the intrinsic spin current does not contribute to the equation of motion for the spin accumulation, the measurement based on the detection of the spin accumulation will produce a null contribution from the spin Hall effect, no matter how large the intrinsic spin current is.

Two experimental groups have recently observed the spin Hall effect by detecting spin accumulation at the edges of the samples [18]. Kato *et al.* argued that the effect is extrinsic based on their experimental results that the spin accumulation is independent of the strain direction, while Wunderlich *et al* claimed that their observed effect is intrinsic based on the assumption that the impurity scattering is weaker than the spin-orbit coupling in their samples (clean limit). We point our here that the clean limit in the experiment does not imply the spin accumulation from the intrinsic origin. Instead, our analysis has shown that no matter how large is the intrinsic spin current, the observed effect has to be an extrinsic origin because the spin accumulation

is independent of the intrinsic spin current.

We finally draw a picture on why the intrinsic spin Hall fails to produce experimental consequences. Consider a contact between a Rashba material and a non-magnetic material with no spin-orbit coupling. The spin current, as well as the orbital angular momentum current, would exist in the the Rashba material. However, the spin current drops to zero across the interface of the non-magnetic material, i.e., the spin current is not continuous; this is because the spin torque produces a mechanism to transfer the spin current to the orbital angular momentum current or vice versus. As a result, when the spin orbit coupling vanishes at the non-spin-orbit coupled material, both the spin and orbital angular momentum currents drop to zero. The loss of the spin current exactly equals to the gain of the OAM current so that the total angular momentum current or magnetization current is continuous across the interface of the layers; they are both zero. For the same reason, the edge of the sample never develops spin accumulation because the usual boundary condition of zero spin current at the surface is no more valid, instead, the total angular momentum current is zero at the surface for the intrinsic spin Hall effect.

In conclusion, we have constructed a general framework for calculating intrinsic linear response coefficients. We have shown that the intrinsic spin Hall effect is accompanied by the intrinsic orbital-angular-momentum Hall effect so that the magnetization current is zero in a spin-orbit coupled system. The intrinsic spin Hall effect is not a useful source of spin currents because the intrinsic spin current does not enter into the equation of motion for the spin transport. Most of the proposed experimental detections of the intrinsic spin Hall effect are the artifact of the boundary conditions that are not valid for the intrinsic spin Hall current.

A.2 Extrinsic SHE in Rashba bands

Now, we consider the extrinsic spin Hall effect in the presense of Rashba spin-orbit coupling. The extrinsic spin Hall current is the result of spin orbit interaction between electron and impurities. Skew scattering and side jump effect are the most important two contributions. We prove in the following, that the skew scattering will be suppressed in the presense of Rashba spin-orbit coupling unless a spin-flipping scattering is considered.

The Hamiltonian of a two dimensional electron gas system is

$$\vec{H} \;=\; \vec{H}_K + \vec{H}_R = \vec{H}_K + \vec{\sigma}\cdot\vec{B}_R$$

where $\vec{B}_R = \alpha(\hat{z}\times\vec{p})$ can be understood as an effective magnetic field.

We write down non-equilibium distribution function as

$$\hat{f} = g + \vec{\sigma}\cdot\vec{h}$$

Then homogeneous Boltzmann Eq. with skew scattering term can be written as,

$$e\vec{E}\cdot\vec{v}\frac{\partial f_0}{\partial\hat{\epsilon}} = \int W^s_{kk'}\left[\hat{f}(\vec{k}') - \hat{f}(\vec{k})\right]d\vec{k}' + \int W^a_{kk'}\vec{\sigma}\cdot\left(\vec{k}\times\vec{k}'\right)\left[\hat{f}(\vec{k}') + \hat{f}(\vec{k})\right]d\vec{k}' \quad \text{(A.19)}$$

We set $\frac{1}{\tau} = \int W^s_{kk'}d\vec{k}'$; $\frac{1}{\tau_{so}} = \int W^a_{kk'}d\vec{k}'$. If $W^{s(a)}_{kk'}$ weakly depends on k and k', in 2DEG and electric field on x direction, above Eq. becomes

$$eE_x v_x\hat{\delta}(\hat{\epsilon}-\epsilon_f) = -\frac{\hat{f}-\bar{f}}{\tau} - \frac{m(\vec{k}\times\vec{J}^z)_z}{\hbar\tau_{so}} - \sigma_z\frac{m(\vec{k}\times\vec{J})_z}{\hbar\tau_{so}} \quad \text{(A.20)}$$

where $\vec{J}^z$is the spin current in longitudinal or Hall direction. This Eq. give us full information on extrinsic spin Hall Effect (ESHE), as long as there is no spin orbit coupling, i.e. $\alpha = 0$. If we turn on spin orbit coupling, a torque term $\frac{i\left[\hat{H},\hat{f}\right]}{\hbar} = \frac{2\alpha}{\hbar}\vec{\sigma}\cdot(\vec{B}_R\times\vec{h})$ should appear in Eq. (A.19),

$$eE_x k_x\frac{\partial f_0}{\partial\hat{\epsilon}} + \frac{2\alpha}{\hbar}\vec{\sigma}\cdot(\vec{B}_R\times\vec{h}) = -\frac{\hat{f}-\bar{f}}{\tau} - \frac{m(\vec{k}\times\vec{J}^z)_z}{\hbar\tau_{so}} - \sigma_z\frac{m(\vec{k}\times\vec{J})_z}{\hbar\tau_{so}}$$

However, this equation is not correct. If we trace σ_y times the above equation,

$$eE_x\sigma_y v_x\delta(\hat{\epsilon}-\epsilon_f)+2\alpha k_y h_z=-\frac{h_y-\bar{h}_y}{\tau}$$

then integrate over k, first term of left hand side(LHS) is zero, and second term of LHS of above Eq. gives spin Hall current J_y^z, but right hand side(RHS) comes out to be ZERO. Therefore, when we turn on the spin orbit coupling, no matter how small α is, the spin Hall current suddenly becomes zero. This does not make sense. The problem is that when we turn on spin orbit coupling, it will induce an in plane effective magnetic field, which makes out of plane polarization of the transport particles rotating away from their original directions. In the scattering process, this rotation still exists, which leads a spin flip relaxation time $\tau_{sf}(\propto\alpha^{-1})$. So there should be a spin flip scattering term induced by spin orbit coupling on RHS of Boltzmann Eq.

The spin flip scattering term can be written as

$$-\frac{\left(\bar{f}-\frac{I}{2}Tr\bar{f}\right)}{\tau_{sf}}=-\frac{\vec{\sigma}\cdot\bar{\vec{h}}}{\tau_{sf}}$$

and we assume $\bar{h}_y\neq 0$. Now the nonzero torque term is balanced by this term. Note that spin flip exists for many cases. Here we only consider the contribution from the spin orbit coupling band.

Before we continue to solve this problem, we make the following assumptions, which can be proved self-consistently: 1, $\bar{g}=0$; 2, $h_x=h_z=0$; 3, Hall current $J_y=0$; 4, longitudinal spin current $J_x^z=0$. Thus, Boltzmann Eq. becomes

$$\begin{aligned}&ev_xE_x\hat{\delta}(\hat{\epsilon}-\epsilon_f)+2\alpha\left[\left(\sigma_xk_x+\sigma_yk_y\right)h_z-\sigma_z\left(k_xh_x+k_yh_y\right)\right]\\&=-\frac{g+\vec{\sigma}\cdot\vec{h}-\sigma_y\bar{h}_y}{\tau}-\frac{\sigma_y\bar{h}_y}{\tau_{sf}}-\frac{mk_xJ_y^z}{\hbar\tau_{so}}+\frac{\sigma_zmk_yJ_x}{\hbar\tau_{so}}\quad.\end{aligned}\tag{A.21}$$

First, tracing Eq.(A.21), we have

$$Tr\left[ev_xE_x\hat{\delta}(\hat{\epsilon}-\epsilon_f)\right]=-\frac{g}{\tau}-\frac{mk_xJ_y^z}{\hbar\tau_{so}}$$

$$g = -\left\{ Tr\left[ev_x \hat{\delta}(\hat{\epsilon} - \epsilon_f) \right] + \frac{m\tau k_x \sigma_y^z}{\hbar \tau_{so}} \right\} E_x. \tag{A.22}$$

where σ_y^z is the spin Hall conductivity. Integration of Eq.(A.22) gives zero, so that assumption 1 is proved. Charge current is the integration of $k_x g$ over $\vec{k}$, which is proportional to $E_x$and affected by spin Hall Effect. However, charge Hall current $J_y \propto \int k_y g d\vec{k} = 0$, this is consistent with our assumption.

Second, tracing σ_x times Eq.(A.21), we get $2\alpha k_x h_z = -\frac{h_x}{\tau}$. So that

$$h_x = -2\alpha\tau k_x h_z \tag{A.23}$$

Strictly, the driven term $eE_x\sigma_x v_x \delta(\hat{\epsilon} - \epsilon_f)$ should be included in Eq. (A.23). Foutunately, integration of the driven term itself or $k_x(k_y)$ times itself is exactly zero, so that this term is irrelevant to the following derivation. We neglect it for simplicity.

Then, tracing σ_y times Eq.(A.21), neglecting the driven term for the same reason, we obtain

$$2\alpha k_y h_z = -\frac{h_y - \bar{h}_y}{\tau} - \frac{\bar{h}_y}{\tau_{sf}},$$

hence,

$$h_y = -2\alpha\tau k_y h_z + \frac{\tau_{sf} - \tau}{\tau_{sf}} \bar{h}_y. \tag{A.24}$$

Finally, we trace $\sigma_z$times Eq.(A.21). It comes out to be

$$-2\alpha(k_x h_x + k_y h_y) = -\frac{h_z}{\tau} + \frac{k_y J_x}{\tau_{so}}. \tag{A.25}$$

Plug Eqs. (A.23,A.24) into Eq. (A.25),

$$4\alpha^2\tau(k_x^2 + k_y^2)h_z - 2\alpha k_y \frac{\tau_{sf} - \tau}{\tau_{sf}} \bar{h}_y = -\frac{h_z}{\tau} + \frac{\sigma_{xx} k_y E_x}{\tau_{so}}$$

$$(4\alpha^2\tau^2 k^2 + 1)h_z - 2\alpha k_y \frac{\tau}{\tau_{sf}}(\tau_{sf} - \tau)\bar{h}_y = \frac{\tau}{\tau_{so}} \sigma_{xx} k_y E_x$$

$$h_z = \frac{\frac{\tau}{\tau_{so}} \sigma_{xx} k_y E_x + 2\alpha k_y \frac{\tau}{\tau_{sf}}(\tau_{sf} - \tau)\bar{h}_y}{4\alpha^2\tau^2 k^2 + 1} \tag{A.26}$$

Plug Eq. (A.26) into Eq. (A.24),

$$\begin{aligned} h_y &= -\frac{2\alpha\frac{\tau^2}{\tau_{so}}\sigma_{xx}k_y^2E_x + 4\alpha^2k_y^2\tau^2\frac{\tau_{sf}-\tau}{\tau_{sf}}\bar{h}_y}{4\alpha^2\tau^2k^2+1} + \frac{\tau_{sf}-\tau}{\tau_{sf}}\bar{h}_y \\ &= -\frac{2\alpha\frac{\tau^2}{\tau_{so}}\sigma_{xx}k_y^2E_x}{4\alpha^2\tau^2k^2+1} + \frac{\tau_{sf}-\tau}{\tau_{sf}}(\frac{4\alpha^2k_x^2\tau^2+1}{4\alpha^2\tau^2k^2+1})\bar{h}_y \end{aligned}$$

Sum over k,

$$\bar{h}_y = -\frac{\alpha\frac{\tau^2}{\tau_{so}}\sigma_{xx}k_F^2E_x}{4\alpha^2\tau^2k_F^2+1} + \left(\frac{\tau_{sf}-\tau}{\tau_{sf}}\right)\frac{2\alpha^2k_F^2\tau^2+1}{4\alpha^2\tau^2k_F^2+1}\bar{h}_y$$

$$\frac{\left(\frac{\tau_{sf}-\tau}{\tau_{sf}}\right)(2\alpha^2k_F^2\tau^2+1)-(4\alpha^2\tau^2k_F^2+1)}{4\alpha^2\tau^2k_F^2+1}\bar{h}_y = \frac{\alpha\frac{\tau^2}{\tau_{so}}\sigma_{xx}k_F^2E_x}{4\alpha^2\tau^2k_F^2+1}$$

$$\begin{aligned} \bar{h}_y &= \frac{\alpha\frac{\tau^2}{\tau_{so}}\sigma_{xx}k_F^2E_x}{\left(\frac{\tau_{sf}-\tau}{\tau_{sf}}\right)(2\alpha^2k_F^2\tau^2+1)-(4\alpha^2\tau^2k_F^2+1)} \\ &= -\frac{\alpha\frac{\tau\tau_{sf}}{\tau_{so}}\sigma_{xx}k_F^2E_x}{2\alpha^2k_F^2\tau(\tau_{sf}+\tau)+1} \end{aligned} \tag{A.27}$$

Put Eq. (A.27) back into Eq. (A.26),

$$\begin{aligned} h_z &= \frac{\frac{\tau}{\tau_{so}}\sigma_{xx}k_yE_x}{4\alpha^2\tau^2k^2+1} - \frac{2\alpha^2k_F^2\tau^2\left(\frac{\tau_{sf}-\tau}{\tau_{so}}\right)\sigma_{xx}k_yE_x}{(4\alpha^2\tau^2k^2+1)\left[2\alpha^2k_F^2\tau(\tau_{sf}+\tau)+1\right]} \\ &= \frac{\frac{\tau}{\tau_{so}}\sigma_{xx}k_yE_x}{2\alpha^2k_F^2\tau(\tau_{sf}+\tau)+1} \end{aligned} \tag{A.28}$$

Sum over k, we find the assumption $\bar{h}_z = 0$ is satisfied. And since $h_z \propto k_y$, $\bar{h}_x$, $J_x^z \propto \int k_xk_yd\vec{k} = 0$, which are consitent with the assumptions.

According to the general definition, the spin Hall current is

$$J_y^z = \sum_{\vec{k}} Tr(\sigma_z v_y \hat{f})$$

$$
\begin{aligned}
&= \sum_{\vec{k}} Tr\left[\frac{\hbar}{2}\sigma_z\left(\frac{\hbar k_y}{m}-\frac{\alpha}{\hbar}\sigma_x\right)(g+\vec{\sigma}\cdot\vec{h})\right] \\
&= \sum_{\vec{k}} \frac{\hbar^2 k_y h_z}{2m} \\
&= \frac{\frac{\hbar^2}{4m}\frac{\tau}{\tau_{so}}k_F^2 J_x}{2\alpha^2 k_F^2\tau(\tau_{sf}+\tau)+1}
\end{aligned}
$$

Since $\tau_{sf} \propto \alpha^{-1}$, when $\alpha = 0$, i.e., no spin orbit coupling, it goes back to previous theory. Increasing α, spin Hall current will decrease. In strong coupling limit, the induced in-plane effective magnetic field suppresses the out-of-plane polarization.

Therefore, in the presence of Rashba spin-orbit coupling, skew scattering does not contribute to extrinsic spin Hall current unless spin flipping scattering exists. $J_y^z = \frac{\hbar^2 J_x}{8m\alpha^2\tau_{so}(\tau_{sf}+\tau)} \to 0$.

Bibliography

[1] J. Sinova, D. Culcer, Q. Niu, N. A. Sinitsyn, T. Jungwirth, and A. H. MacDonald, Phys. Rev. Lett. **92**, 126603 (2004).

[2] D. Culcer, J. Sinova, N. A. Sinitsyn, T. Jungwirth, A. H. MacDonald, and Q. Niu, Phys. Rev. Lett. **93**, 046602 (2004).

[3] K. Nomura, J. Sinova, T. Jungwirth, Q. Niu, and A. H. MacDonald, Phys. Rev. B**71**, 041304 (2005).

[4] S. Murakami, N. Nagaosa, and S. C. Zhang, Science **301**, 1348 (2003).

[5] E. I. Rashba, Phys. Rev. B **68**, 241315 (2003).

[6] E. I. Rashba, Phys. Rev. B**70**, 161201 (2004).

[7] J. Schliemann and D. Loss, Phys. Rev. B **69**, 165315 (2004).

[8] S. I. Erlingsson, J. Schliemann, and D. Loss, cond-mat/0406531.

[9] O. Chalaev and D. Loss, cond-mat/0407342.

[10] J. Inoue, G. E. W. Bauer, and L. W. Molenkamp, Phys. Rev. B**70**, 041303 (2004).

[11] E. G. Mishchenko, A. V. Shytov, and B. I. Halperin, Phys. Rev. Lett. **93**, 226602 (2004).

[12] O. V. Dimitrova, cond-mat/0405339.

[13] L. Hu, J. Gao, and S. Q. Shen, Phys. Rev. B**70**, 235323 (2004).

[14] X. Ma, L. Hu, R. Tao, and S. Q. Shen, Phys. Rev. B**70**, 195343 (2004).

[15] J. E. Hirsch, Phys. Rev. Lett. **83**, 1834 (1999).

[16] S. Zhang, Phys. Rev. Lett. **85**, 393 (2000).

[17] S. Murakami, N. Nagaosa, and S. C. Zhang, Phys. Rev. Lett. **93**, 156804 (2004).

[18] Y. K. Kato, R. C. Myers, A. C. Gossard, and D. D. Awschalom, Science **306**, 1910 (2004); J. Wunderlich, B. Kaestner, J. Sinova, and T. Jungwirth, Phys. Rev. Lett. **94**, 047204 (2005).

[19] T. Jungwirth, Q. Niu, and A. H. MacDonald, Phys. Rev. Lett. **88**, 207208 (2002).

[20] J. M. Luttinger, Phys. Rev. **102**, 1030 (1956).

[21] T. Valet and A. Fert Phys. Rev. B **48**, 7099(1993).

[22] For the Luttinger Hamiltonian, Culcer *et al.* [2] obtains a spin torque which does not exactly cancel the divergence of the intrinsic spin current. Our approach would produce an exact cancellation. The origin of this discrepancy may be from a different definition in calculating the spin torque.

[23] M. Johnson and R. H. Silsbee, Phys. Rev. Lett. **55**, 1790 (1985).

[24] F. Meier and D. Loss, Phys. Rev. Lett. **90**, 167204 (2004).

[25] Q. -F Sun, H. Guo, J. Wang, Phys. Rev. B **69**, 054409 (2004).

VITA

Zhaoyang Yang was born on March 29th, 1980 in Nanjing, China. He graduated in July, 2001 with a Bachelor of Science degree in Physics from the Southeast University, Nanjing, China. He was then admitted to the graduate school of Southeast University. He was working with Professor Mei Liu on magnetic vortex dynamics in High Tc superconductors. In January, 2003, he transferred to University of Missouri-Columbia in the United States, and joined Department of Physics and Astronomy. Since then, he has been working with Dr. Shufeng Zhang on spin transport theories in metals and semiconductors, as well as magnetization dynamics in magnetic nanostructures. He received his Ph.D. in December, 2007.